INTERMOLECULAR ENERGY AND ELECTRON TRANSFER BY NON-ORTHOGONAL CONFIGURATION INTERACTION

Aitor Maria Sánchez Mansilla

UNIVERSITAT ROVIRA i VIRGILI

Intermolecular energy and electron transfer by Non-Orthogonal Configuration Interaction

AITOR SÁNCHEZ MANSILLA

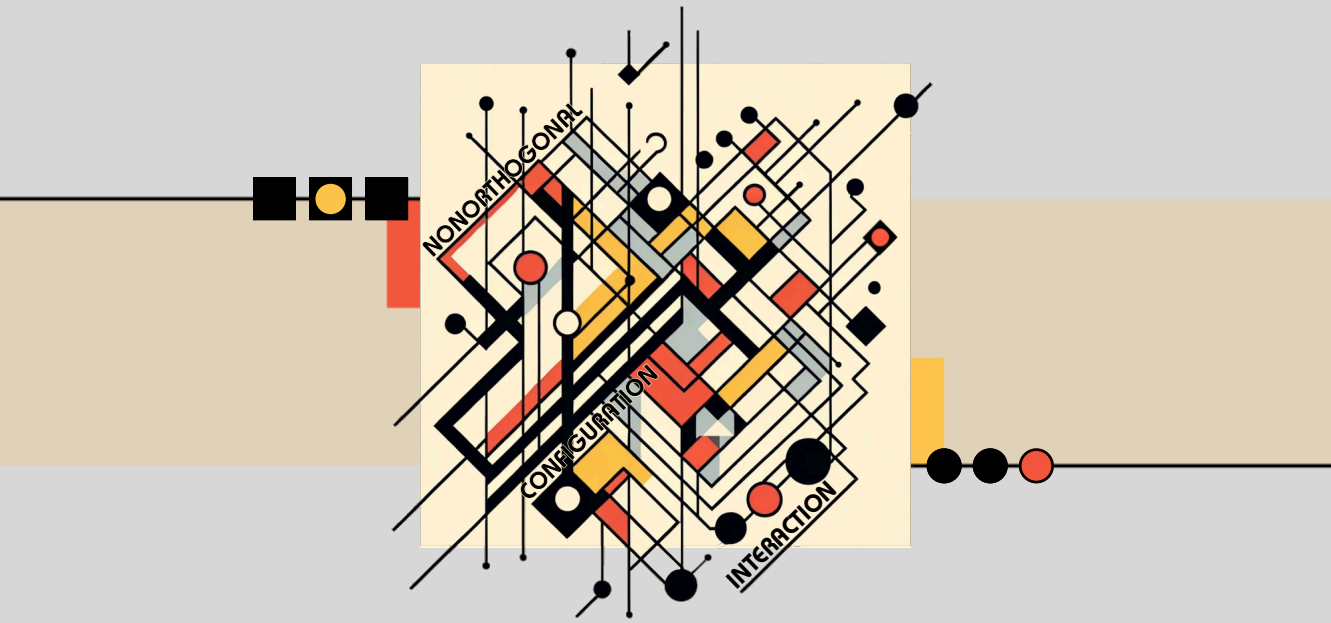

DOCTORAL THESIS
2024

UNIVERSITAT ROVIRA I VIRGILI
INTERMOLECULAR ENERGY AND ELECTRON TRANSFER BY NON-ORTHOGONAL CONFIGURATION INTERACTION
Aitor Maria Sánchez Mansilla

Aitor Sánchez Mansilla

INTERMOLECULAR ENERGY AND ELECTRON TRANSFER BY NON-ORTHOGONAL CONFIGURATION INTERACTION

DOCTORAL THESIS

Supervised by Prof. Coen de Graaf

Departament
de Química Física i Inorgánica

UNIVERSITAT ROVIRA i VIRGILI
Tarragona, 2024

UNIVERSITAT ROVIRA I VIRGILI
INTERMOLECULAR ENERGY AND ELECTRON TRANSFER BY NON-ORTHOGONAL CONFIGURATION INTERACTION
Aitor Maria Sánchez Mansilla

UNIVERSITAT
ROVIRA i VIRGILI

Departament de Química Física i Inorgánica

Prof. Coen Graaf, investigador ICREA en el Departament de Química Física i Inorgánica de la Universitat Rovira i Virgili.

FAIG CONSTAR que aquest treball, titulat

"Intermolecular energy and electron transfer by Non-Orthogonal Configuration Interaction"

que presenta Aitor Sánchez Mansilla per a l'obtenció del títol de Doctor, ha estat realizat sota la meva direcció al Departament de Química Fisica d'aquesta universitat.

Tarragona, 5 de març de 2024

Cornelis De Graaf - DNI X2632706B (TCAT)
Digitally signed by Cornelis De Graaf - DNI X2632706B (TCAT)
Date: 2024.03.11 11:30:27 +01'00'

Prof. Coen de Graaf

UNIVERSITAT ROVIRA I VIRGILI
INTERMOLECULAR ENERGY AND ELECTRON TRANSFER BY NON-ORTHOGONAL CONFIGURATION INTERACTION
Aitor Maria Sánchez Mansilla

Acknowledgements

Me gustaría dar las gracias en primer lugar a mi supervisor, Prof. Coen De Graaf, por su paciencia y esfuerzo, así como por dejarme vía libre para enfocarme en los desafíos que consideraba interesantes en cada momento.

A todos mis compañeros pasados y presentes del Quantum Chemistry Group por todo el conocimiento y las discusiones que hemos compartido todos estos años. A toda la gente del grupo con la que he compartido más tiempo, porque me han ayudado a crecer personalmente y apreciar el lado más humano de la ciencia. También quiero dar créditos a Yannick por ayudarme con la maravillosa portada de este trabajo.

I would like to thank all of the members of the GronOR team, particularly Dr. Tjerk Straatsma for introducing me to the amazing world of High Performance Computing and give me inestimable coding advice.

Gracias a mi familia y amigos de Santalecina, por todo el apoyo que he recibido de ellos a lo largo de mi vida. En especial a mis amigos Antonio y Julio por escucharme y enseñarme a comprender cosas las cuales bajo un filtro racional era incapaz de comprender.

"Sólo es posible conocer en el Presente; en el pasado tan sólo se piensa. Pensar y conocer son dos cosas diferentes."

Sesha

Contents

Overview of the thesis

The overarching goal of this research is to enhance our understanding of electronic structures in molecules and materials, with a specific focus on addressing the challenges posed by the theoretical studies of inter- and intramolecular energy and electron transfer in materials that have the potential to increase the efficiency of photovoltaic cells or photocatalytic reactions. The thesis covers the following topics; 1) Deepening of traditional electronic structure methods to understand their strengths and limitations, particularly in capturing electronic correlations which play a pivotal role in determining properties like magnetic interactions. 2) Exploration of the potential of non-orthogonal approaches, especially the Non-Orthogonal Configuration Interaction (NOCI) method, as an alternative to traditional methods, and assess their ability to provide a more accurate and comprehensive description of electronic structures; 3) Extent, refine, and validate the GronOR computer code to offer a robust and efficient method for electronic structure calculations based on non-orthogonal orbitals. This tool should address some of the challenges posed by existing methods and aim to provide more accurate predictions of molecular and material properties; 4) Apply the developed methods, particularly GronOR, to real-world molecular systems to test their efficiency and reliability. The aim is to demonstrate the practicality and advantages of the proposed methods over traditional ones.

Chapter 1

Introduction

Formulated almost seven decades ago[13], and efficiently implemented in the 1980s[2], Non-Orthogonal Configuration Interaction (NOCI) has not received much attention until recently. However, over the last ten years, several studies have been published in which the orthogonality restriction commonly adopted in electronic structure calculations is lifted[24,16,22,12]. Several reasons can be given for this renewed interest. Firstly, the increasing computer power makes possible calculations with non-orthogonal orbitals for systems beyond small model systems, opening the door to apply these methods to systems that are at the center of current research in chemistry, physics, material science, etc. Secondly, NOCI is very well suited to combine accuracy with interpretability. The compact expression of the many-electron wave function in a few key electronic configurations is ideal to translate the results in terms of concepts that are commonly used in more approximate phenomenological models. Finally, the recent studies have enriched the family of non-orthogonal methods with the possibility to include dynamic electron correlation[27,26,3,19], strategies for orbital optimization[15], more approximate but highly efficient implementations[14,11], massive parallelizations[23] and time propagation[6]. All these new additions indicates that the electronic structure methods based on non-orthogonal orbitals are slowly but steadily becoming mature and are expected to continue to play an important role in the field. It is in this light that the current thesis has been developed, combining further developing existing non-orthogonal configuration interaction

schemes with application of the method to systems of chemical interest, emphasizing the translation of the results of the calculations in straightforward concepts, which makes it possible to reach a more profound of the physical mechanisms underlying the phenomena being studied.
This thesis is divided in five chapters:

1. **Introduction:** A brief discussion on the limits of traditional methods and the objectives of the present work.

2. **Electronic structure methods:** A review of traditional electronic structure methods and context of non-orthogonal approaches.

3. **GronOR:** A description of the GronOR non-orthogonal configuration interaction software with the new features implemented in the scope of this thesis and schemes for future implementations.

4. **Applications:** Case studies in which non-orthogonal configuration interaction is applied for the calculation of chemical properties.

5. **Conclusions:** Conclusions of the work and outline of future work.

1.1 On the limits of traditional methods

This section exposes the major challenges that are currently present in the field which led our group to develop our own implementation of Non Orthogonal Configuration Interaction. The main motivation lies in providing an alternative computational framework to study physical problems that are not well described by commonly applied electronic structure methods.

1.1.1 Exciton transport

An exciton is a bound state of an electron and a positive hole. It is produced when an excitation occurs and the electron and the remaining hole are bound by Coulomb interaction, making them to move together (diffusion) and act as a single uncharged particle. This is why they are often referred to as *quasiparticles*. Excitons[7] play an essential role in energy transport in natural

processes such as photosynthesis as well as in nanostructured optoelectronic devices (photovoltaics, light-emitting diodes ...) based on molecular solids such as organics, colloidal quantum dots, etc.
Most typically, generation of excitons occurs in solids, specially in semiconductor materials. An excitation is induced via photoabsorption, electric field, etc. and an electron is promoted from the Valence Band into the Conduction Band. The remaining hole and electron form an exciton, and they move collectively through the solid. The exciton exists until the excess energy that it "contains" is dissipated. The fate of the exciton can be one of the following

- **Radiative Recombination:** The most common decay process for excitons in direct bandgap semiconductors is radiative recombination. In this process, the electron falls back into the hole it left behind in the Valence Band. This recombination results in the emission of a photon whose energy is approximately equal to the bandgap of the semiconductor. This is the principle behind light-emitting diodes (LEDs).

- **Non-Radiative Recombination:** In this process, the exciton's energy is not emitted as light but is instead transferred to lattice vibrations, known as phonons, or to other electronic states. This process can be dominant in indirect bandgap semiconductors.

- **Exciton Dissociation:** Under certain conditions, the electron and hole comprising the exciton can be separated before they have a chance to recombine. This electron-hole separation is especially desirable in photovoltaic devices, where the goal is to convert the energy of absorbed photons into electrical energy. Once separated, the electron and hole can be collected at electrodes, producing a current.

- **Exciton Diffusion:** Before any of the above processes occur, the exciton can diffuse through the material. This diffusion continues until the exciton encounters a defect, another exciton, or the edge of the material, or until it undergoes one of the recombination processes.

In summary, the fate of an exciton involves either recombination, where its energy is released as light or heat, or separation, where its energy can be harnessed for electrical power.

Excitons are usually classified in Frenkel excitons and Wannier-Mott excitons, as illustrated in figure 1.1). In the first case, the electron and hole are contained in the same cell unit of the crystal, while the Wannier-Mott exciton is much larger and extends over several unit cells. This is related to the material's dielectric constant ϵ; when it is small, the electric Coulombic attraction becomes strong and the electron and hole are closer, and the opposite when it is larger. Frenkel excitons are usually formed in organic molecular crystals in which ϵ is small such as naphthalene or anthracene crystals, Wannier-Mott excitons are found more often in semiconductors.
A third kind of exciton that has been reported in the literature is the Charge Transfer exciton, which is common in organic crystals. It forms when the electron and the hole occupy different molecules. The resulting electron-hole pair could be considered as one of the two types defined above depending on the size of the unit cell. For example, a pair of molecules A and B can be in a charge transfer exciton state $D^+(A)D^-(B)$ where D indicates a doublet state (figure 1.2).
An exciton transfer process occurs when the exciton moves across the material, which means that the excitation energy is transferred through neighboring atoms or molecules. To estimate this transferability, according to the Fermi's Golden Rule, one has to calculate the matrix element between the initial and final states to obtain the transition rate

$$\Gamma_{i\to f} = \frac{2\pi}{\hbar}|\gamma|^2\rho(E_f) \tag{1.1}$$

where $\rho(E_f)$ is the density of states at the energy E_f of the final state and γ is the electronic coupling between the initial and final state, defined as

$$\gamma = \frac{H_{if} - \frac{1}{2}(H_{ii} + H_{ff})}{1 - S_{if}^2} \tag{1.2}$$

This process entails an electron-hole transfer between neighboring atoms or molecules, and therefore, any computational approach to estimate γ requires an accurate description of the ground, excited and charge transfer (ionic) states involved in the process. These states are characterized by different electronic configurations, and hence, the optimal orbital set to express

them may change significantly from state to state. A typical molecular orbital theory approach uses a common orthonormal molecular orbital basis ϕ_j to describe all electronic states involved in the exciton transfer. The same is true for Kohn-Sham DFT approaches, which also rely on one (orthogonal) orbital set. Moreover, it is not straightforward to calculate the matrix element between initial and final state appearing in Fermi's golden rule. Typically additional simplifications need to be made to obtain estimates of γ when using DFT approaches[1].
The problem with electronic structure methods that rely on one set of orthogonal molecular orbitals is that this basis set is not always flexible enough to represent simultaneously all the (excited) states involved in the process, and thus calculate accurately the coupling γ. To illustrate this we take a stack of two chromophores A and B as example. To calculate the propagation of a Frenkel exciton in molecule A to molecule B one would intuitively express the initial and final states, gs(A)–exc(B) and exc(A)–gs(B), both in their own set of optimal orbitals, but this is not possible within standard MO theory in which all electronic states are expressed in one set of (orthogonal) orbitals. Hence, orthogonal MO approaches lead to a neglect of orbital relaxation effects in energy and electron transfer mechanisms. On the contrary, NOCI methods can represent each local excitation with any set of orbitals chosen to describe better the interaction leading to a more rigorous estimation of the electronic coupling.

1.1.2 Interatomic and intermolecular coulombic decay

Interatomic and intermolecular coulombic decay is an electronic decay mechanism principally observed in weakly bound matter. This process allows the emergence of doubly ionized states in monomer couples even when these configurations are not accessible energetically in the isolated monomers. The existence of such process was first suggested theoretically[5] and several years later experimentally confirmed[9]. It was concluded that when a second ionization of the initially excited monomer (that is, the creation of a dication) is not energetically possible, the ionization of a neighboring molecule through intermolecular energy transfer is energetically feasible, leading to monocations on both molecules. This doubly ionization leads rapidly to a

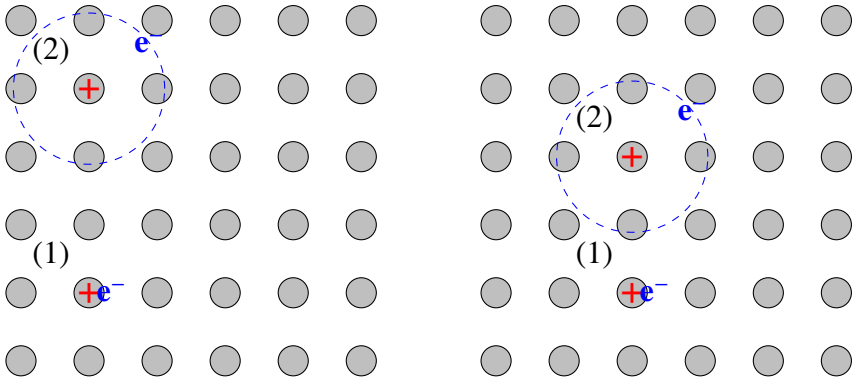

Figure 1.1: Exciton motion across a material (1) Frenkel exciton (2) Wannier-Mott exciton.

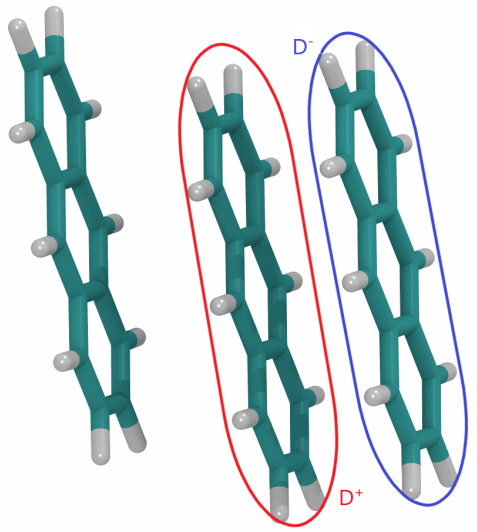

Figure 1.2: Charge Transfer Exciton across two neighboring anthracene molecules.

Coulomb explosion where the two fragments are repelled.
The standard experimental route to induce ICD involves the following three steps:

1. Ionization of an inner-valence electron from one molecule.

2. An outer-valence electron occupies the hole and the excess energy is transferred to the second molecule upon which an outer-valence electron is ionized .

3. Coulomb explosion.

The first two ICD stages are schematically depicted in the left part of Figure 1.3. More recently, a slightly different variant of ICD have garnered attention in biological systems. Harbach and co-workers[8] introduced the first example of ICD as an operating mechanism in a real biological system, taking part in the DNA-reparation process. They showed that the mechanism which is responsible of generating "free" electrons across the photolyases, the enzymes that repair DNA, can also be considered a form of ICD. The two molecules involved in the process are the cofactor reduced flavine nucleotide $NADH^-$ and the chromophore antenna pigment HDF that usually bind to the protein. The three stages of this variant of ICD can be described as:

1. Absorption of the photon by HDF populating an electronically excited state .

2. Excess energy transfer to the neighboring $FADH^-$ inducing ionization and generating a reactive "free" electron.

3. The electron triggers the mechanism for DNA repair by the enzyme.

The right part of Figure 1.3 shows the first two stages of this ICD variant. This illustrates that ICD is not just a scientific curiosity but plays a fundamental role in biological systems. In the same manner as in exciton transfer, the key magnitude to quantify the rate of these processes is the electronic coupling γ defined in equation 1.2. The off-diagonal matrix element needed

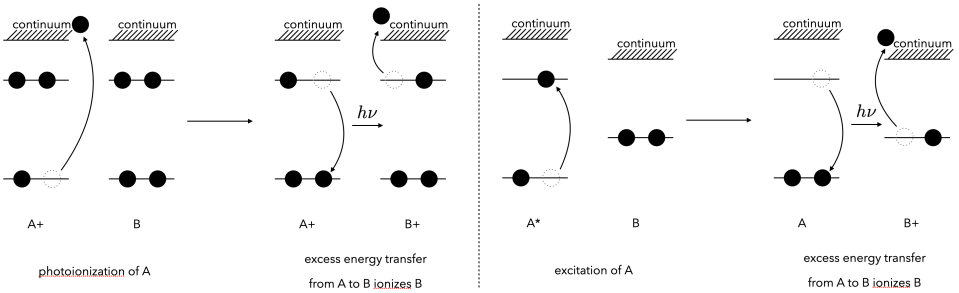

Figure 1.3: Illustration of the two cases of ICD presented in this section; Left: Traditional ICD discovered by Cederbaum et al.[5] Right: Variant of ICD discovered in the DNA rapair process.

to estimate γ that represents the transition between the states involved in ICD is

$$H_{kl,\sigma_1\sigma_2} = |\langle\Phi_{kl}|\hat{H}|\Phi_{\sigma_1\sigma_2}\rangle|^2 = \gamma^2 \tag{1.3}$$

where the initial pair of indices "kl" represent the ionized electron k on the second molecule ($FADH^-$ in the DNA repair process) and the inner-valence electron l in the first molecule, and the final state indices "$\sigma_1\sigma_2$" represent the empty orbitals in both excited and ionized molecules. Treatment of the "free electron" in the continuum requires special treatment, either with increasingly diffuse basis sets or construction of the so-called Dyson orbitals[25].
After the calculation of the electronic coupling via NOCI, the estimation of the transition probability is directly evaluated by Fermi's Golden rule which provides a more direct way to compute the rate.

1.1.3 Singlet fission

Traditional silicon-based solar cells are quite efficient in both solar light conversion and production cost. However, the research in organic photovoltaics shows how these can have potential advantages over the latter, such as portability, lower production costs and lighter weight, implying that they can be used in applications where silicon-based solar cells are impractical. In fact, they can complement current solar cells to increase their efficiency

by mixing layers of the two materials. Simplifying to some extent, commercial silicon-based solar cells consist in a P-N junction that generates one charge carrier (electron-hole pair) per photon absorbed. This implies a theoretical limit in the efficiency of the 33.16% that was estimated by Shockley and Queisser in 1961, also called the Shockey-Queisser limit. Research in multi-junction solar cell technology has managed to break this limit by adding layers of different materials that have different bandgaps and thus respond to different wavelengths, improving the conversion of energy that would be lost otherwise. This has been lead to a record in the efficiency rate of 45% in laboratory conditions and 39% in a real case case scenario, but the expensive production causes them to being non-commercial currently.

Organic materials can improve the efficiency in other way through multiexcitonic generation processes, that is, the generation of several charge carriers per photon absorbed. Singlet fission (SF) is a particular case of multiexcitonic generation process that occurs in organic solids[21], during which two coupled triplets are formed from a singlet photoexcited system in an overall spin-allowed shown in Figure 1.4. SF has been explored as an alternative to break the Shockley-Queisser limit[18] as in principle, two charge carriers are generated by photon absorbed as after singlet fission the phenomenon known as triplet separation happens in which two separated triplets are produced.

Singlet fission processes in materials containing chromophores will occur mostly under two conditions. The first one is that the process must be at least isoergic and preferably slightly exoergic, which means that the energies for the lowest excited singlet state S_1 and the lowest triplet state T_1 must fulfill $E(S_1) \geq 2E(T_1)$. The second one is that the process needs to be fast enough to overcome competing processes such as fluorescence, thermal motion or other ways to dissipate the excess energy. This translates into requiring a sizable electronic coupling γ (equation 1.2) between the local excited singlet S_0S_1 or S_1S_0 and the two coupled triplets ^1TT which is inversely related to the duration of the process. One may also include in the NOCI the charge transfer states D^+ and D^- that can mediate in the process enabling two other possible mechanisms[4]. Finally, although it is not part of the singlet fission mechanism itself, one may also want to characterize the triplet separation mechanism by computing the electronic coupling (and

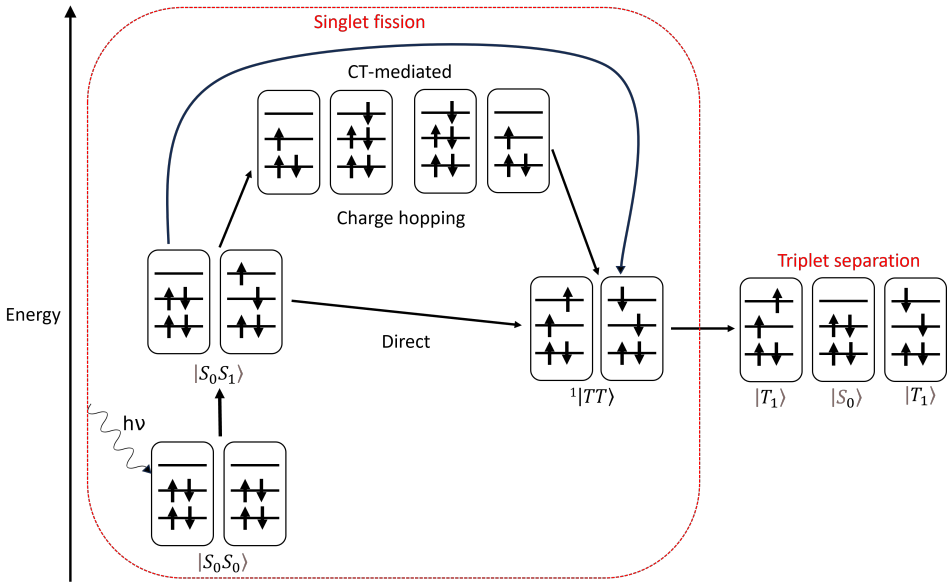

Figure 1.4: Singlet fission plus triplet separation scheme

thus, the mixing) between the coupled and separated triplet states that describes the decoupling of the two charge carriers. The next mechanism of interest after that would be their propagation across the material, known as triplet diffusion.
For these reasons, NOCI is a reliable method to represent local excitations in an ensemble of chromophores and introduce full orbital relaxation to estimate rigorously the electronic coupling and help to find singlet fission candidates for the production of organic photovoltaics.

1.1.4 Magnetic interactions in transition metal compounds

Although not directly related to the generation of charge carriers as the previous two processes, NOCI has also successfully been applied to study the interaction of localized spin angular moments in a variety of materials. Not only it provides a way to obtain accurate estimates of the strength of the coupling, but, and probably more importantly, it also allows to analyze in a relatively straightforward manner the mechanisms that govern the strength

of the coupling. In addition to the above-mentioned orbital relaxation effects, NOCI is designed to include static and dynamic electron correlation in the description of the electronic structure, as will be shown in the next chapter, where more technical details of NOCI are given. The combination of rigorous orbital relaxation and inclusion of electron correlation leads to estimates of the coupling strength in very good agreement with other computational approaches that are considered as benchmark calculations[19]. The big advantage of NOCI is that the final wave function is expressed as a linear combination of a few key electronic configurations, while the corresponding benchmark calculations count with wave functions that require millions (or billions) of determinants to reach the desired accuracy. The compact nature of the NOCI wave functions makes it very easy to (de-)activate certain mechanisms and study the effect on the coupling strength. A similar analysis with wave function based on orthogonal orbitals is not impossible but much more complicated[17], mostly due to the huge amount of determinants. The coupling between spin moments is an essential ingredient to explain many of the (magnetic) properties of a wide variety of materials. Ferro- and antiferromagnetism are essentially the macroscopic manifestation of a net parallel (or anti-parallel) coupling of the local (atomic or molecular) spin moments present in the material. The magnetic susceptibility of a magnetic material reflects the strength of the coupling between the spin moments, and there are many more interesting phenomena that are directly related to the lower part of the energy spectrum of the units that carry unpaired electrons. One aspect that deserves special attention here is the role played by spin-orbit coupling. As long as spin-orbit coupling is neglected the spin moment is completely isotropic because of the non-existence of spatial coordinates in the pure spin operators. By including the spin-orbit operator in the Hamiltonian, the orientation of the spin moment in three-dimensional space becomes important and a much wider spectrum of magnetic phenomena can be studied. One notable example is the existence of single-molecule magnets. For large enough magnetic anisotropy, the spin moment can be trapped in either a 'down' or 'up' state with a sizeable barrier between the two magnetic states. The discovery of this behaviour in a transition metal complex with 12 Mn ions[20] triggered an intense multidisciplinary research effort, including the development of theoretical approaches to include the

effect of spin-orbit coupling in the ab initio description of the electronic structure.

1.2 Objectives

The overarching goal of this research is to enhance our understanding of electronic structures in molecules and materials, with a specific focus on addressing the challenges posed by the theoretical studies of inter- and intramolecular energy and electron transfer in materials that have the potential to increase the efficiency of photovoltaic cells or photocatalytic reactions. The primary objectives of this PhD thesis are:

- **To understand limitations of traditional methods:** Delve deep into traditional electronic structure methods to understand their strengths and limitations, particularly in capturing electronic correlations which play a pivotal role in determining properties like magnetic interactions.

- **To explore non-orthogonal approaches**: Investigate the potential of non-orthogonal approaches, especially the Non-Orthogonal Configuration Interaction (NOCI) method, as an alternative to traditional methods. Assess their ability to provide a more accurate and comprehensive description of electronic structures.

- **Development and enhancement of GronOR**: Extent, refine, and validate the GronOR computer code to offer a robust and efficient method for electronic structure calculations based on non-orthogonal orbitals. This tool should address some of the challenges posed by existing methods and aim to provide more accurate predictions of molecular and material properties.

- **Application to production cases**: Apply the developed methods, particularly GronOR, to real-world molecular systems to test their efficiency and reliability. The aim is to demonstrate the practicality and advantages of the proposed methods over traditional ones.

At the start of this project, a basic implementation of the NOCI approach in GronOR was available. This implementation was very well parallelized and also the GPU off-loading was in an advanced stage. With the introduction of the transformation of the two-electron integrals to a common molecular basis[10], it became possible to perform NOCI calculations with more than 100 atoms. However, the code was completely biased towards applications in the field of singlet fission. It could only handle ensembles of two molecules, the total spin moment of the electronic states was restricted to singlet coupling, and the program only calculated electronic couplings, energies and wave functions. Hence, technically speaking GronOR was a very advanced program, but from an application point-of-view rather limited and not suited to address the applications that could shine a light on the mechanisms of intra- and intermolecular energy and electron transfer.
Therefore, a large effort was made during this thesis project to make the NOCI approach in GronOR more generally applicable, implement new features and also add a few efficiency improvements. It was crucial to generalize the treatment of spin states to go beyond singlet fission applications. It was also compulsory to overcome the limitation to two fragments to study stacks of singlet fission chromophores and understand exciton motion across the ensembles. These challenges were in hand with the implementation of properties such as oscillator strength computations and the design of strategies to overcome the huge size of NOCI calculations. These are the main challenges that have been carried out in this thesis, as well as the propose of future developments in the NOCI approach and strategies to apply it to the phenomena described above.

References

[1] B. Baumeier, J. Kirkpatrick, and D. Andrienko. "Density-functional based determination of intermolecular charge transfer properties for large-scale morphologies". In: *Phys. Chem. Chem. Phys.* 12 (36 2010), pp. 11103–11113.

[2] R. Broer and W. Nieuwpoort. "Broken orbital-symmetry and the description of hole states in the tetrahedral $[CrO_4]^-$ anion. I. Introductory considerations and calculations on oxygen 1s hole states". In: *Chemical Physics* 54.3 (1981), pp. 291–303.

[3] H. G. A. Burton and A. J. W. Thom. "Reaching Full Correlation through Nonorthogonal Configuration Interaction: A Second-Order Perturbative Approach". In: *Journal of Chemical Theory and Computation* 16.9 (2020), pp. 5586–5600.

[4] D. Casanova. "Theoretical Modeling of Singlet Fission". In: *Chemical Reviews* 118.15 (2018). PMID: 29648797, pp. 7164–7207.

[5] L. S. Cederbaum, J. Zobeley, and F. Tarantelli. "Giant Intermolecular Decay and Fragmentation of Clusters". In: *Physical Review Letters* 79 (1997), pp. 4778–4781.

[6] X. Dong and L. M. Thompson. "Time propagation of electronic wavefunctions using nonorthogonal determinant expansions". In: *The Journal of Chemical Physics* 160.2 (2024), p. 024106.

[7] J. Frenkel. "On the transformation of light into heat in solids. I". In: *Physical Review* 37.1 (1931), p. 17.

[8] P. H. P. Harbach et al. "Intermolecular Coulombic Decay in Biology: The Initial Electron Detachment from $FADH^-$ in DNA Photolyases". In: *The Journal of Physical Chemistry Letters* 4.6 (2013). PMID: 26291360, pp. 943–949.

[9] T. Jahnke et al. "Interatomic and Intermolecular Coulombic Decay". In: *Chemical Reviews* 120.20 (2020), pp. 11295–11369.

[10] R. K. Kathir et al. “Reduced Common Molecular Orbital Basis for Nonorthogonal Configuration Interaction”. In: *Journal of Chemical Theory and Computation* 16.5 (2020). PMID: 32279493, pp. 2941–2951.

[11] E. M. Kempfer-Robertson et al. “Nonorthogonal Active Space Decomposition of Wave Functions with Multiple Correlation Mechanisms”. In: *The Journal of Physical Chemistry Letters* 13.51 (2022), pp. 12041–12048.

[12] X. López et al. “Non-orthogonal Configuration Interaction Study on the Effect of Thermal Distortions on the Singlet Fission Process in Photoexcited Pure and B,N-Doped Pentacene Crystals”. In: *The Journal of Physical Chemistry C* 127.33 (2023), pp. 16249–16258.

[13] P. O. Löwdin. “Quantum Theory of Many-Particle Systems. I. Physical Interpretations by Means of Density Matrices, Natural Spin-Orbitals, and Convergence Problems in the Method of Configurational Interaction”. In: *Physical Review* 97.6 (1955), pp. 1474–1489.

[14] A. Morrison, Z.-Q. You, and J. Herbert. “Ab Initio Implementation of the Frenkel-Davydov Exciton Model: A Naturally Parallelizable Approach to Computing Collective Excitations in Crystals and Aggregates”. In: *Journal of Chemical Theory and Computation* 10 (2014), pp. 5366–5376.

[15] J. Olsen. “Novel methods for configuration interaction and orbital optimization for wave functions containing non-orthogonal orbitals with applications to the chromium dimer and trimer”. In: *The Journal of Chemical Physics* 143.11 (2015), p. 114102.

[16] K. J. Oosterbaan, A. F. White, and M. Head-Gordon. “Non-Orthogonal Configuration Interaction with Single Substitutions for Core-Excited States: An Extension to Doublet Radicals”. In: *Journal of Chemical Theory and Computation* 15.5 (2019). PMID: 31017781, pp. 2966–2973.

[17] D. A. Pantazis. "Meeting the Challenge of Magnetic Coupling in a Triply-Bridged Chromium Dimer: Complementary Broken-Symmetry Density Functional Theory and Multireference Density Matrix Renormalization Group Perspectives". In: *Journal of Chemical Theory and Computation* 15.2 (2019). PMID: 30645093, pp. 938–948.

[18] A. Rao and R. H. Friend. "Harnessing singlet exciton fission to break the Shockley-Queisser limit". In: *Nature Reviews Materials* 2.11 (2017), p. 17063.

[19] A. Sánchez-Mansilla et al. "On the role of dynamic electron correlation in non-orthogonal configuration interaction with fragments". In: *Phys. Chem. Chem. Phys.* 24 (19 2022), pp. 11931–11944.

[20] R. Sessoli et al. "High-Spin molecules: $[Mn_{12}O_{12}(O_2CR)_{16}(H_2O)_2]$". In: *Journal of the American Chemical Society* 115.5 (1993), pp. 1804–1816.

[21] M. B. Smith and J. Michl. "Singlet Fission". In: *Chemical Reviews* 110.11 (2010). PMID: 21053979, pp. 6891–6936.

[22] C. Sousa et al. "A Nonorthogonal Configuration Interaction Approach to Singlet Fission in Perylenediimide Compounds". In: *The Journal of Physical Chemistry A* 127.47 (2023). PMID: 37964533, pp. 9944–9958.

[23] T. P. Straatsma et al. "GronOR: Scalable and Accelerated Non-Orthogonal Configuration Interaction for Molecular Fragment Wave Functions". In: *Journal of Chemical Theory and Computation* 18(6) (2022).

[24] E. J. Sundstrom and M. Head-Gordon. "Non-orthogonal configuration interaction for the calculation of multielectron excited states". In: *The Journal of Chemical Physics* 140.11 (2014), p. 114103.

[25] B. N. C. Tenorio et al. "Photoionization Observables from Multi-Reference Dyson Orbitals Coupled to B-Spline DFT and TD-DFT Continuum". In: *Molecules* 27.4 (2022).

[26] S. R. Yost and M. Head-Gordon. “Efficient Implementation of NOCI-MP2 Using the Resolution of the Identity Approximation with Application to Charged Dimers and Long C-C Bonds in Ethane Derivatives”. In: *Journal of Chemical Theory and Computation* 14.9 (2018), pp. 4791–4805.

[27] S. R. Yost and M. Head-Gordon. “Size consistent formulations of the perturb-then-diagonalize Møller-Plesset perturbation theory correction to non-orthogonal configuration interaction”. In: *The Journal of Chemical Physics* 145.5 (2016), p. 054105.

Chapter 2

Electronic Structure Methods

This chapter contains a brief discussion of some of the electronic structure methods that form the basis of Quantum Computational Chemistry. It also contains a brief historical note to give background information about the way in which these methods evolved, enhancing the description of molecules and improving the efficiency of algorithms. This goes hand-to-hand with the birth of Computer Science and the evolution of computers. Its impact on computational chemistry will be shortly discussed here and in Chapter 3. As well as the classic electronic structure methods, I will explain in detail where non-orthogonal methods are to be placed in this context and put special attention to the newest advances in this area of research.

2.1 Notation and further discussion

Before diving into the details of the different electronic structure methods, I will present a list with symbols in an attempt to unify the different notations that are being used in the studies published in the literature dealing with non-orthogonal electronic structure methods. Being a rather new and expanding area of research, it is not surprising that there is no convention (yet) about the notation among theoretical chemists. Head-Gordon and coworkers used the tensor formalism[35] for the description of the method developed to include electron correlation in non-orthogonal approaches. This tensor formalism is equivalent to the Covariant Notation. While this is an

Table 2.1: Symbol list and conventions used in this thesis

Notation	Description
i, j, k, l	occupied spin orbital index
a, b, c, d	virtual spin orbital index
p, q, r, s	any spin orbital index
μ, ν	basis function index
tilde˜	expressed in corresponding orbital basis
hat̂	operator
superscript x, w	orthonormal wave function set
superscript A, B	molecular fragment
$[], []_+$	commutator and anticommutator
Capital greek letters Ψ, Φ, Θ	Many particle wave function
Small greek letters $\psi, \phi, \varphi, \chi$	One particle wave function

important and widely-used notation in the field of general relativity, it remains a rarity in theoretical chemistry papers. The allure of this formalism is its ability to generate expressions that are universally applicable to both orthogonal and non-orthogonal basis sets. However, a caveat exists; it somewhat obfuscates the system's metric (the overlap of basis states). This can lead to ambiguities when transitioning from theoretical formulations to computer program implementations. To illustrate this with an example, consider a pair of non-orthogonal basis vectors of the Hilbert space $\mathcal{H}$

$$S_{\mu\nu} = \langle \phi_\mu | \phi_\nu \rangle \tag{2.1}$$

Expressions involving non-orthogonal orbitals carry a lot of overlap terms, for example, the expression of a two electron operator in second quantization in an orthogonal basis is

$$\hat{g} = \frac{1}{2} \sum_{pqrs} g_{pqrs} \hat{a}_p^\dagger \hat{a}_r^\dagger \hat{a}_s \hat{a}_q \tag{2.2}$$

while in a non-orthogonal basis, overlap terms do appear for each pair of orbitals

$$\hat{g} = \frac{1}{2} \sum_{pqrs} \left(\sum_{ijkl} [S^{-1}]_{pi} [S^{-1}]_{jq} [S^{-1}]_{rk} [S^{-1}]_{ls} g_{pqrs} \right) \hat{a}_p^\dagger \hat{a}_r^\dagger \hat{a}_s \hat{a}_q \tag{2.3}$$

these overlap terms can be hidden in some manner when taking dual basis vectors ϕ^μ, which are contravariant to basis vectors and are a basis of the dual Hilbert space $\mathcal{H}^*$

$$\langle \phi^\mu | = S^{\mu\nu} \langle \phi_\nu | \quad \text{where} \quad S^{\mu\nu} \equiv \left[S^{-1}\right]_{\mu\nu} \tag{2.4}$$

$$\langle \phi^\mu | \phi_\nu \rangle = \delta^\mu{}_\nu \tag{2.5}$$

It is worth noting that some literature, penned by both chemists and physicists, sometimes mislabels these dual vectors as the "contravariant basis" of $\mathcal{H}$. To clarify, these vectors are not a basis of $\mathcal{H}$. In fact, they do not reside within this vector space. The term "contravariant" implies that the object inversely varies as the space's basis, making the phrase "contravariant basis" contradictory. From a purist's perspective, employing these terms with precision is imperative, especially if the aim is to set a benchmark for future non-orthogonal theory researchers. According to this dual basis definition, contravariant creation and annihilation operators that act on these dual vectors are subsequently derived as

$$(\hat{a}^\nu)^\dagger = \sum_\mu \hat{a}^\dagger_\mu S^{\mu\nu} = \sum_\mu \hat{a}^\dagger_\mu \left[S^{-1}\right]_{\mu\nu} \tag{2.6}$$

$$\hat{a}^\nu = \sum_\mu S^{\nu\mu} \hat{a}_\mu = \sum_\mu \left[S^{-1}\right]_{\nu\mu} \hat{a}_\mu \tag{2.7}$$

In terms of these operators, the example 2.3 is re-expressed in the contravariant dual basis in a shorter way

$$\hat{g} = \frac{1}{2} \sum_{pqrs} \left(\sum_{ijkl} \hat{a}^\dagger_p [S^{-1}]_{pi} \; \hat{a}^\dagger_r [S^{-1}]_{rk} \; [S^{-1}]_{ls} \hat{a}_s \; [S^{-1}]_{jq} \hat{a}_q \; g_{pqrs} \right)$$

$$= \frac{1}{2} \sum_{pqrs} g_{pqrs} (\hat{a}^p)^\dagger (\hat{a}^r)^\dagger \hat{a}^s \hat{a}^q \tag{2.8}$$

While the expression is undeniably more concise and applicable to both orthogonal and non-orthogonal, it entails a change of basis of the expression and the dissipated overlap terms have to be taken into account anyways when developing algorithms. I will abstain from using this notation without prior notification in the following pages in order to make non-orthogonal expressions appear more transparent to the reader.

2.2 Overview of Electronic Structure methods

Electronic structure methods emerged in the early 20th century to solve the many-electron problem, that is, to obtain the most accurate description of the ground-state configuration, or equilibrium state, of a system consisting of an arbitrary number N of electrons in presence of nuclei. Even considering the Born-Oppenheimer approximation, in which the movement of the nuclei and electrons is decoupled, the problem is impossible to solve exactly for any system with two or more electrons. The appearance of the electron-electron interaction in the Hamiltonian blocks the separation of variables and leads to the necessity for additional approximations, either in the Hamiltonian or in the solutions of the Schrödinger equation, that is, the many-electron wave function.

The schema of figure 2.1 offers a rough overview of the current landscape of Electronic Structure Methods. In an attempt to describe many body quantum systems (and hence solve the many-electron problem), three main approaches arose. One of the first attempts was made by Thomas and Fermi who treated molecules semi-classically (neglecting the exchange interactions) to describe the electron density. The addition of an exchange term by Dirac only slightly improved the results, but the Thomas-Fermi-Dirac approach does not lead to chemical bonding. It took about thirty years before electronic structure calculations based on the electron density regained popularity when Hohenberg and Kohn put this approach on a firm basis and Kohn and Sham provided a simple scheme to obtain meaningful results.

A distinct and directly from the start more successful path was opened by Heitler and London, who presented a quantum mechanical description of the chemical bond in H_2 based on a two-electron wave function. The Heitler-London description evolved into two distinct approaches for electronic structure studies: Valence Bond Theory (VBT) and Molecular Orbital Theory (MOT). Both models, although equivalent in the limit of full Configuration Interaction (see Sec. 2.5.2), excel in different areas. VBT is very well suited to delivering human-interpretable results and the large advantage of MOT lies in the easiness when programming faster Computational Chemistry software. This is why, due to the birth of Computer Science, MOT surpassed VBT in popularity and became the main source of new Electronic

Structure Methods. However, in the recent days with the advent of the most powerful supercomputers, the line which separates the two models is thinner than ever.

On this increasingly thinner line is where the Non-Orthogonal Configuration Interaction method is located. It is a flexible approach that can give the precision of the most powerful MOT methods without losing the flexibility typical of VBT to describe the results in terms of meaningful chemical concepts such as lone pairs, two- or three center bonds, charge-transfer configurations, etc. These concepts can be translated in an almost one-to-one correspondence into Lewis structures, which have a long-standing history in explaining all kinds of chemical phenomena.

The remainder of this chapter will first shortly point out the main characteristics of the three different approaches: density functional theory, molecular orbital theory and valence bond theory. This is followed by a more detailed account of non-orthogonal configuration interaction, including the most recent developments in the field.

2.3 Quantum description of molecules

The discoveries in Quantum Theory and the failure of previous semi-classical models urged to build a new full quantum description of the electronic structure. Molecules, as neutral groups of atoms held by chemical bonds, can be viewed as composed only of positively charged nuclei and negatively charged electrons.

In a full quantum description, a system of K nuclei and N electrons is described by the Hamiltonian operator:

$$\begin{aligned}\hat{H} &= \hat{T}_{\mathrm{n}}(\boldsymbol{R}_1, \ldots, \boldsymbol{R}_K) + \hat{T}_{\mathrm{e}}(\boldsymbol{r}_1, \ldots, \boldsymbol{r}_N) \\ &+ \hat{V}_{\mathrm{ne}}(\boldsymbol{r}_1, \ldots, \boldsymbol{r}_N, \boldsymbol{R}_1, \ldots, \boldsymbol{R}_K) + \hat{V}_{\mathrm{ee}}(\boldsymbol{r}_1, \ldots, \boldsymbol{r}_N) + \hat{V}_{\mathrm{nn}}(\boldsymbol{R}_1, \ldots, \boldsymbol{R}_K)\end{aligned} \quad (2.9)$$

The first two terms are the kinetic energies of nuclei and electrons and the rest are Coulomb interaction potentials between the two types of particles.

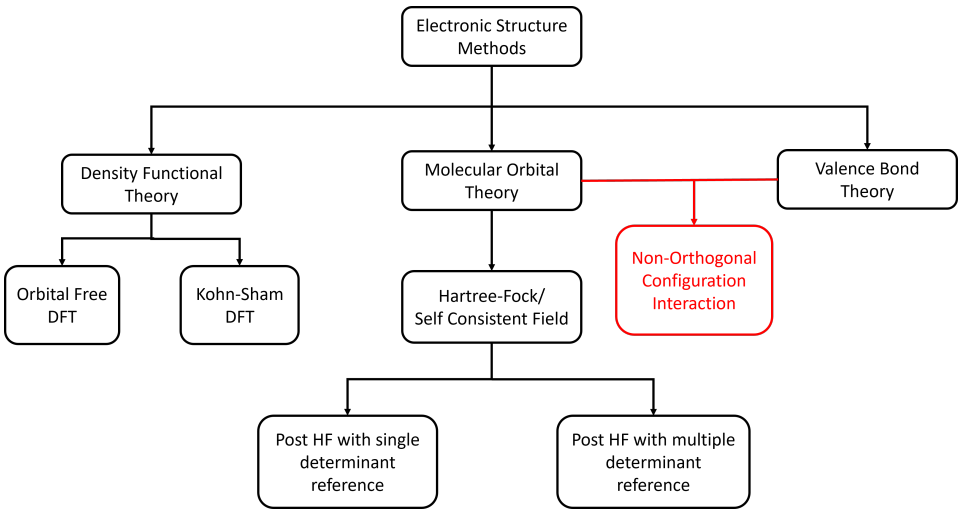

Figure 2.1: General schema of Electronic Structure Methods

These are defined as, with α and β running over the K nuclei:

$$\hat{T}_{\mathrm{n}} = \sum_{\alpha}^{K} \frac{1}{2M_{\alpha}} \nabla_{\alpha}^{2} \qquad \hat{T}_{\mathrm{e}} = -\frac{1}{2} \sum_{i}^{N} \nabla_{i}^{2} \tag{2.10}$$

$$\hat{V}_{\mathrm{ne}} = \sum_{i}^{N} \sum_{\alpha}^{K} \frac{-Z_{\alpha}}{|\boldsymbol{r}_i - \boldsymbol{R}_{\alpha}|} = \sum_{i}^{N} v_{\mathrm{nuc}}(\boldsymbol{r}_i) \tag{2.11}$$

$$\hat{V}_{\mathrm{ee}} = \frac{1}{2} \sum_{i} \sum_{j \neq i} \frac{1}{|\boldsymbol{r}_i - \boldsymbol{r}_j|} \tag{2.12}$$

$$\hat{V}_{\mathrm{nn}} = \sum_{\alpha \neq \beta} \frac{Z_{\alpha} Z_{\beta}}{|\boldsymbol{R}_{\alpha} - \boldsymbol{R}_{\beta}|} \tag{2.13}$$

where $\boldsymbol{r}_i$ are the positions of electrons and $\boldsymbol{R}_i$ are the positions of nuclei. The expressions are written using atomic units in which constants (m_{e}, $\hbar$, etc.) are equal to one. From this point until the end of this chapter we will use $r \equiv (\boldsymbol{r}_1, \ldots, \boldsymbol{r}_N)$ and $\boldsymbol{R} \equiv (\boldsymbol{R}_1, \ldots, \boldsymbol{R}_K)$ when possible in order to use a lighter notation. The eigenstates of the system are the wave functions of well-defined energy, obtained from the time-independent Schrödinger

equation[51]:

$$\hat{H}\Psi(\boldsymbol{r},\boldsymbol{R}) = E_{\text{total}}\Psi(\boldsymbol{r},\boldsymbol{R}) \tag{2.14}$$

which is an eigenvalue problem whose solution is a set of wave functions Ψ_j corresponding to each one of the energy levels E_j that describe electronic and nuclear motion.

2.3.1 The Born-Oppenheimer approximation

The Born-Oppenheimer approximation[5] states that the degrees of freedom of nuclei and electrons can be separated. Thus, the molecular wave function (or molecular quantum state) can be broken into its electronic and nuclear components, related by the product ansatz:

$$\Psi_{\text{total}}(\boldsymbol{r},\boldsymbol{R}) = \psi_{\text{e}}(\boldsymbol{r};\boldsymbol{R}) \otimes \chi_{\text{n}}(\boldsymbol{R}) = \psi(\boldsymbol{r};\boldsymbol{R})\chi(\boldsymbol{R}) \tag{2.15}$$

where the ";" indicates that, though the electronic wave function ψ is a function of the electron positions $\boldsymbol{r}_i$, depends parametrically —through the Coulomb interaction potential— on the positions of nuclei $\boldsymbol{R}_i$. This approximation is based on the assumption that electrons move much faster than the heavier nuclei, adapting instantly to changes in the nuclear conformation without requiring a finite relaxation time. This approximation makes that the problem, though still purely quantum in nature, can be solved first electronically in a fixed nuclear frame. Substitution of the wave function 2.15 into Schrödinger equation yields

$$\begin{aligned}
&\left[\hat{T}_{\text{n}}(\boldsymbol{R}) + \hat{T}_{\text{e}}(\boldsymbol{r}) + \hat{V}_{\text{ne}}(\boldsymbol{r};\boldsymbol{R}) + \hat{V}_{\text{ee}}(\boldsymbol{r}) + \hat{V}_{\text{nn}}(R)\right]\psi(\boldsymbol{r};\boldsymbol{R}) \otimes \chi(\boldsymbol{R}) \\
&\quad = \psi(\boldsymbol{r};\boldsymbol{R}) \otimes \left[\hat{T}_{\text{n}}(\boldsymbol{R})\chi(\boldsymbol{R})\right] + \left[\hat{T}_{\text{e}}(r)\psi(\boldsymbol{r};\boldsymbol{R})\right] \otimes \chi(\boldsymbol{R}) \\
&\quad + \left[\hat{V}_{\text{ne}}(\boldsymbol{r};\boldsymbol{R})\psi(\boldsymbol{r};\boldsymbol{R})\right] \otimes \chi(\boldsymbol{R}) + \psi(\boldsymbol{r};\boldsymbol{R})\left[\hat{V}_{\text{ne}}(\boldsymbol{r};\boldsymbol{R})\chi(\boldsymbol{R})\right] \\
&\quad + \left[\hat{V}_{\text{ee}}(\boldsymbol{r})\psi(\boldsymbol{r};\boldsymbol{R})\right] \otimes \chi(\boldsymbol{r}) + \psi(\boldsymbol{r};\boldsymbol{R}) \otimes \left[\hat{V}_{\text{nn}}(\boldsymbol{R})\chi(\boldsymbol{R})\right] \\
&\quad = E_{\text{total}}\psi(\boldsymbol{r};\boldsymbol{R}) \otimes \chi(\boldsymbol{R})
\end{aligned} \tag{2.16}$$

Through simplification by removing ψ from both sides the equation for the nuclei is obtained, leading to the following system:

$$\left[\hat{T}_{\text{e}}(\boldsymbol{r}) + \hat{V}_{\text{ne}}(\boldsymbol{r};\boldsymbol{R}) + \hat{V}_{\text{ee}}(\boldsymbol{r})\right]\psi(\boldsymbol{r};\boldsymbol{R}) = E_{\text{e}}(\boldsymbol{R})\psi(\boldsymbol{r};\boldsymbol{R}) \tag{2.17}$$

$$\left[\hat{T}_{\text{n}}(\boldsymbol{R}) + \hat{V}_{\text{nn}}(\boldsymbol{R}) + E_e(\boldsymbol{R})\right]\chi(\boldsymbol{R}) = E_{\text{total}}\chi(\boldsymbol{R}) \tag{2.18}$$

where the following Hamiltonian separation is identified

$$\hat{H}_{\mathrm{e}} = \hat{T}_{\mathrm{e}}(\boldsymbol{r}) + \hat{V}_{\mathrm{ne}}(\boldsymbol{r};\boldsymbol{R}) + \hat{V}_{\mathrm{ee}}(\boldsymbol{r}) \tag{2.19}$$

$$\hat{H}_{\mathrm{n}} = \hat{T}_{\mathrm{n}}(\boldsymbol{R}) + \hat{V}_{\mathrm{nn}}(\boldsymbol{R}) + E_{\mathrm{e}}(\boldsymbol{R}) \tag{2.20}$$

where the electronic energy $E_{\mathrm{e}}(\boldsymbol{R})$ plays the role of potential energy surface for the nuclear motion. In particular, the nuclear wave functions belonging to the potential energy surface (PES) are determined as eigenfunctions of the nuclear Hamiltonian $\hat{H}_{\mathrm{n}}$.
The step of BO approximation takes care of *separation* in general depends on the quotient of masses of both types of particles. The heavier the nuclei are compared to electrons, the better the approximation works. However, there are some cases in which the BO approximation breaks down. For example, there are cases in which the electronic wave function changes rapidly with nuclear coordinates and the term $\hat{T}_n$ applied to the electronic wave function cannot be neglected despite the factor $1/M_\alpha$. Some phenomena in which BO does not work are related to photochemistry such as conical intersection, charge transfer, internal conversion and singlet-fission. Most of them deal with excited states that are well handled by novel non-orthogonal methods such as NOCI due to the proper calculations of electronic couplings which are precisely the terms neglected in the derivation of the BO approximation.

2.3.2 Slater determinants

As nuclei are considered to have fixed positions in the BO approximation, from now we can restrict ourselves to the electronic contribution. Solving the eigenvalue problem for the electronic part we arrive at a set of states $\Psi_1, \Psi_2, \ldots, \Psi_n$ whose energies are the eigenvalues of the Hamiltonian

$$\hat{H}\Psi_k(\boldsymbol{r}_1\sigma_1, \boldsymbol{r}_2\sigma_2, \ldots, \boldsymbol{r}_N\sigma_N) = E_k\Psi_k(\boldsymbol{r}_1\sigma_1, \boldsymbol{r}_2\sigma_2, \ldots, \boldsymbol{r}_N\sigma_N) \tag{2.21}$$

where σ_i is the spin of the electron i and the index k runs over the set of many-electron eigenstates. Dealing with fermions, the solution Ψ_k can only be an antisymmetric function under the exchange of two electron labels[44]

$$\Psi_k(\boldsymbol{r}_1\sigma_1, \boldsymbol{r}_2\sigma_2, \ldots, \boldsymbol{r}_i\sigma_i, \ldots, \boldsymbol{r}_j\sigma_j, \ldots, \boldsymbol{r}_N\sigma_N) = -\Psi_k(\boldsymbol{r}_1\sigma_1, \boldsymbol{r}_2\sigma_2, \ldots, \boldsymbol{r}_j\sigma_j, \ldots, \boldsymbol{r}_i\sigma_i, \ldots, \boldsymbol{r}_N\sigma_N) \quad (2.22)$$

The simplest many-electron wave function that fulfills this condition is a single Slater determinant[53] built from all the mono-electronic wave functions $\chi_i(\mathbf{r}_i\sigma_i)$:

$$\Psi_k(\boldsymbol{r}_1\sigma_1, \ldots, \boldsymbol{r}_N\sigma_N) = \frac{1}{\sqrt{N!}} \begin{vmatrix} \chi_1(\boldsymbol{r}_1\sigma_1) & \chi_2(\boldsymbol{r}_1\sigma_1) & \cdots & \chi_N(\boldsymbol{r}_1\sigma_1) \\ \chi_1(\boldsymbol{r}_2\sigma_2) & \chi_2(\boldsymbol{r}_2\sigma_2) & \cdots & \chi_N(\boldsymbol{r}_2\sigma_2) \\ \vdots & \vdots & \ddots & \vdots \\ \chi_1(\boldsymbol{r}_N\sigma_N) & \chi_2(\boldsymbol{r}_N\sigma_N) & \cdots & \chi_N(\boldsymbol{r}_N\sigma_N) \end{vmatrix}$$

In some cases, the many-electron state cannot be described accurately by a single Slater determinant but rather requires a linear combination of them. A method that describes the many-electron wave function as a single Slater determinant is the Hartree-Fock method whose underlying approximation will be described later in this chapter.

2.3.3 Configuration State Functions

The Hamiltonian commutes with the total and projected spin operators:

$$\left[\hat{H}, \hat{S}^2\right] = 0 \quad (2.23)$$

$$\left[\hat{H}, \hat{S}_z\right] = 0 \quad (2.24)$$

Therefore, a set of common eigenfunctions to all three operators exists. Slater determinants are eigenstates of the $\hat{H}$ and the operator $\hat{S}_z$ but not necessarily of $\hat{S}^2$. Using them as a basis for the electronic wave function (eigenstate of $\hat{H}$) will not guarantee the approximate solution to be an eigenfunction of $\hat{S}^2$, thus, the result may not have a well defined spin multiplicity (a pure Singlet, Doublet, Triplet, etc). This is easily shown considering a Slater determinant for a two electron system occupying different spatial orbitals. The situation with the same spin for both electrons can be represented as the Slater determinant

$$|\chi_1\chi_2| = \frac{1}{\sqrt{2}}[\chi_1(\boldsymbol{r}_1)\chi_2(\boldsymbol{r}_2) - \chi_1(\boldsymbol{r}_2)\chi_2(\boldsymbol{r}_1)] \quad (2.25)$$

Applying $\hat{S}_z$ and $\hat{S}^2$

$$\hat{S}_z|\chi_1\chi_2| = M_S|\chi_1\chi_2| = 1|\chi_1\chi_2| \tag{2.26}$$
$$\hat{S}^2|\chi_1\chi_2| = S(S+1)|\chi_1\chi_2| = 2|\chi_1\chi_2| \tag{2.27}$$

so the spin multiplicity is $2S + 1 = 3$ and the Slater determinant represents a triplet spin state. On the contrary, if we take the opposite spin for both electrons, the result of applying the operators is

$$\hat{S}_z|\chi_1\bar{\chi}_2| = 0|\chi_1\bar{\chi}_2| \tag{2.28}$$
$$\hat{S}^2|\chi_1\bar{\chi}_2| = |\chi_1\bar{\chi}_2| + |\bar{\chi}_1\chi_2| \tag{2.29}$$

where $\bar{\chi}_i = \chi_i(\sigma_i = \downarrow)$, showing that this second Slater determinant is not an eigenstate of $\hat{S}^2$. In order to fix it we can take a Configuration State Function (CSF)

$$|S = 0, M_S = 0\rangle = |\chi_1\bar{\chi}_2| = \frac{1}{\sqrt{2}}[\chi_1(\boldsymbol{r}_1)\bar{\chi}_2(\boldsymbol{r}_2) - \bar{\chi}_1(\boldsymbol{r}_2)\chi_2(\boldsymbol{r}_1)] \tag{2.30}$$

that is a linear combination of Slater determinants which is an eigenstate of $\hat{H}$, $\hat{S}_z$ and $\hat{S}^2$

$$\hat{S}_z\,|S = 0, M_S = 0\rangle = 0\,|S = 0, M_S = 0\rangle \tag{2.31}$$
$$\hat{S}^2\,|S = 0, M_S = 0\rangle = 1\,|S = 0, M_S = 0\rangle \tag{2.32}$$

Most of modern Electronic Structure methods use combinations of CSFs instead of Slater determinants.

2.4 Valence Bond Theory

Valence Bond Theory was developed, together with Molecular Orbital Theory, under the quantum mechanics paradigm arisen from Heisenberg and Schrödinger developments. The origin of this method dates back to 1916 when G. N. Lewis published the paper *The Atom and the Molecule*[31] which introduced the notions of electron-pair bonding and the octet rule, explaining how atoms tend to bond in order to have eight electrons in their valence

shell. This is schematically explained by Lewis Structures, where each atom is represented together with its valence shell electrons as dots, for example the formation of lithium fluoride (LiF) from lithium and fluoride ions.

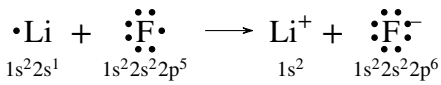

This presented an insight to the mechanism by which an electron pair could constitute a bond, which was demonstrated in 1927 by W. H. Heitler and F. W. London when they published the seminal paper *Interaction Between Neural Atoms and Homopolar Binding*[20] in which they showed that the covalent bond present in the H_2 molecule originates in the quantum mechanical *resonance* interaction when the two electrons present are allowed to exchange their positions. As electrons are indistinguishable particles, there are two possible wave functions that describe the system for spatial and spin parts. For the spatial part we have electrons 1 and 2 in $\varphi_1(1)\varphi_2(2)$ or $\varphi_1(2)\varphi_2(1)$, where φ_1 and φ_2 are the exact ground-state wave functions of the hydrogen atom 1 and 2, respectively. The spin part of the wave function can be written as $\alpha(1)\beta(2)$ or $\alpha(2)\beta(1)$. The spatial and spin parts can be combined to give an antisymmetric wave function in two different ways:

$$\Psi_{HL,1} = N_1\big(\varphi_1(1)\varphi_2(2) + \varphi_1(2)\varphi_2(1)\big)\big(\alpha(1)\beta(2) - \alpha(2)\beta(1)\big) \quad (2.33)$$

$$\Psi_{HL,2} = N_2\big(\varphi_1(1)\varphi_2(2) - \varphi_1(2)\varphi_2(1))(\alpha(1)\beta(2) + \alpha(2)\beta(1)\big) \quad (2.34)$$

Ψ_1 corresponds to a spin singlet function, and Ψ_2 is a spin triplet. Whereas the energy of the triplet function is higher than the sum of two isolated hydrogen atoms ($2E_H$) for all interatomic distances, the singlet shows a minimum around 0.71 Å, with an energy that is 5.2 eV lower than $2E_H$, demonstrating bond formation. Analysis of the energy expression shows that the largest contribution to the energy lowering arises from the resonance integral β:

$$\beta = \langle\varphi_1|\hat{h}|\varphi_2\rangle = \langle\varphi_2|\hat{h}|\varphi_1\rangle$$

This integral parametrizes the movement of an electron from site 1 to site 2 and vice-versa, and therefore, bond formation is predicted to find its origin in the interchange of electrons between the two atoms. Therefore, there is a mixing of the states, that is, the *resonance* between the two situations in

which one electron has spin up, while the other has spin down and vice-versa, as well as the interchange in the spatial part

$$\underset{\uparrow\ \downarrow}{H\bullet\bullet H} \longleftrightarrow \underset{\downarrow\ \uparrow}{H\bullet\bullet H}$$

is called the Heitler-London (HL) wave function. In their paper, they showed that the resonance energy supposes a 75% of the total bonding energy of the molecule, therefore that the HL wave function can describe satisfactorily the chemical bonding. In 1928, London extended this result and established the general principles of the covalent bonding in terms of the resonance interaction, which can be interpreted as a quantum version of the Lewis structures. In the 1930s, Pauling and Slater extended the model to a general quantum chemical theory for polyatomic molecules, introducing concepts such as hybridization of orbitals (for example, the hybrid sp orbitals in carbon), superposition of the covalent and ionic bonds and the description of the resonating structure of benzene. All of these works enabled the description of many bond types in a large variety of molecules.

The main feature of Valence Bond Theory is that it expresses the molecular wave functions as linear combinations of chemically meaningful structures built from electron pairs representing bonds between two atoms (like in the HL wave function), lone pairs, ionic structures (electron pairs formed on one atom after transfer from a neighboring atom), etc. In order to be recognizable as such, the structure used in the Valence Bond approach must be built from localized, basically atomic, orbitals. In the standard VB approach these atomic orbitals are in general non-orthogonal when located on different atoms, although a branch emerged recently applying orthogonalized atomic orbitals to construct the VB wave function[19,10,38]. Because these VB basis functions are non-orthogonal in general, it follows that the covalent bonds between atoms are typically formed by the sharing of these overlapping regions. Therefore, Valence Bond Theory can be used to explain how covalent bonds are formed by the maximum overlap condition, or in other words, the maximum overlap region between two atoms.

This intuitive description of the electronic structure of molecules (or extended systems), although convenient for understanding, is also the major drawback of the method and the reason the theory lacks popularity nowadays. Due to the non-orthogonality between the basis functions, Valence

Bond Theory implementations in computer codes are relatively slow compared to methods based on orthogonal (but delocalized) orbitals. The later approaches have been chosen much more frequently to calculate electronic structure properties although losing the intuitive description Valence Bond Theory can provide. In the recent years, increasing computation power has triggered a renewed interest in Valence Bond Theory, allowing the use at some extent of non-orthogonal basis sets and thus the flexibility in the global picture. Some examples of these new advances include the programs CRUNCH (2002) by Gordon A. Gallup and his group[18], TURTLE (2002) by J.H. van Lenthe, F. Dijkstra and R. W. A. Havenith[29], VB2000 (released in 2014) by J. Li, B. Duke and R. McWeeny[32] and XMVB (1969, version 2.0 released in 2015) by S. Lingchung and co-workers[11].

2.5 Molecular Orbital Theory

Molecular Orbital Theory was proposed shortly after Valence Bond Theory. Its origin can be traced back to 1928 when Hund and Mülliken made spectral and quantum number assignments of electrons in molecules, connecting the energies from separated to united atoms. Studying the band spectra of diatomic molecules they assigned electrons to states that extend over the entire molecule instead of being attached to a particular atom. Molecular Orbital Theory uses the linear combination of atomic orbitals (LCAO) to construct molecular orbitals[28] that are used as the one-electron basis functions to approximate the many-electron wave function. The use of delocalized molecular orbitals leads to an immediate interpretation of the electronic transitions observed for the diatomic molecules considered in the study.
The use of delocalized orbitals leaves behind the intuitive interpretation of the electronic structure characteristic of VB methods and was therefore not immediately accepted as a usual alternative upon its introduction, but gradually found its place in the community. Already in 1929, Lennard-Jones used a Linear Combination of Atomic Orbitals wave function for the treatment of the O_2 molecule, successfully explaining the paramagnetic character of the molecule before Valence Bond Theory, which came with its own explanation in 1931. Many more successes of Molecular Orbital Theory in

the early years of Quantum Chemistry can be mentioned (Walsh diagrams, bonding properties of ferrocene, among others), but the real breakthrough of MO theory lies in the fact that the orbitals are mutually orthogonal which greatly enhances its ability to be implemented in efficient algorithms. The first method developed to variationally determine the coefficients c_{ij} of the LCAOs was the Hartree-Fock method, whose main characteristics will be outlined in the next section.

2.5.1 The Hartree-Fock method

The Hartree-Fock (HF) method, was published by D. Hartree and improved by V. Fock. It was an essential step in the development of Electronic Structure Methods and is in general a starting point for all future developments in the discipline. Its original version consists in applying the variational principle to the Molecular Orbital Theory approach making an assumption of the many-electron wave function as a single Slater determinant Ψ, as defined in section 2.3.
The optimal choice for the many-electron wave function minimizes the energy expectation value with respect to infinitesimal changes in the wave function

$$\delta \langle \Psi | \hat{H} | \Psi \rangle = \delta \langle \psi_1 \psi_2 \dots \psi_N | \hat{H} | \psi_1 \psi_2 \dots \psi_N \rangle = 0 \tag{2.35}$$

Furthermore, the orthogonality and the norm of the orbitals are forced to be conserved during the optimization procedure through the Lagrange multipliers ϵ_{ij}, leading to the condition that needs to be satisfied

$$\begin{aligned} &\delta_\psi \mathcal{L}[\Psi] \\ &\quad = \delta \left[\langle \psi_1 \psi_2 \dots \psi_N | \hat{H} | \psi_1 \psi_2 \dots \psi_N \rangle - \sum_{ij}^{N} \epsilon_{ij} \left(\langle \psi_i | \psi_j \rangle - \delta_{ij} \right) \right] = 0 \end{aligned} \tag{2.36}$$

The Hamiltonian reads

$$\hat{H} = \sum_{i}^{N} \hat{h}(i) + \frac{1}{2} \sum_{ij}^{N} \frac{1 - \hat{P}_{ij}}{r_{ij}} \tag{2.37}$$

where the permutation operator emerges due to the antisymmetric character of the many-electron wave function. The variation of the first term is

$$\begin{aligned}
\delta\left[\langle\psi_1\psi_2\dots\psi_N|\hat{H}|\psi_1\psi_2\dots\psi_N\rangle\right] &= \delta\left[\langle\psi_1\psi_2\dots\psi_N|\sum_i^N \hat{h}(i)|\psi_1\psi_2\dots\psi_N\rangle\right. \\
&\left. + \frac{1}{2}\langle\psi_1\psi_2\dots\psi_N|\sum_{ij}^N \frac{1-\hat{P}_{ij}}{r_{ij}}|\psi_1\psi_2\dots\psi_N\rangle\right] \\
&= \sum_i^N \langle\psi_1\psi_2\dots\delta\psi_i\dots\psi_N|\hat{h}(i)|\psi_1\psi_2\dots\psi_i\dots\psi_N\rangle \\
&+ \frac{1}{2}\sum_{ij}^N \langle\psi_1\psi_2\dots\delta\psi_i\psi_j\dots\psi_N|\frac{1-\hat{P}_{ij}}{r_{ij}}|\psi_1\psi_2\dots\psi_i\psi_j\psi_N\rangle \\
&+ \frac{1}{2}\sum_{ij}^N \langle\psi_1\psi_2\dots\psi_i\delta\psi_j\dots\psi_N|\frac{1-\hat{P}_{ij}}{r_{ij}}|\psi_1\psi_2\dots\psi_i\psi_j\dots\psi_N\rangle + \text{c.c}
\end{aligned} \tag{2.38}$$

where "c.c" indicates the complex conjugate of the three terms. The second term of Eq. 2.36 can be written as

$$\delta\left[\sum_{ij}^N \epsilon_{ij}\left(\langle\psi_i|\psi_j\rangle - \delta_{ij}\right)\right] = \sum_{ij}^N \epsilon_{ij}\langle\delta\psi_i|\psi_j\rangle + \text{c.c} \tag{2.39}$$

After some rearrangements the variation of the Lagrangian functional can be expressed as

$$\delta_\psi \mathcal{L}[\Psi] = \sum_i^N \langle \delta\psi_i | \Big[\langle \psi_1\psi_2 \dots \psi_N | \psi_1\psi_2 \dots \psi_N \rangle \, \hat{h}(i) \, |\psi_i\rangle + \sum_j^N \langle \psi_1\psi_2 \dots \psi_j \dots \psi_N | \frac{1}{r_{ij}} | \psi_1\psi_2 \dots \psi_j \dots \psi_N \rangle \, |\psi_i\rangle - \sum_j^N \langle \psi_1\psi_2 \dots \psi_j \dots \psi_N | \frac{\hat{P}_{ij}}{r_{ij}} | \psi_1\psi_2 \dots \psi_i \dots \psi_N \rangle \, |\psi_i\rangle - \sum_j^N \epsilon_{ij} \, |\psi_j\rangle \Big] + \text{c.c} = 0 \quad (2.40)$$

Since the variation $\delta\psi_i^*$ is arbitrary, the term inside the brackets must be zero for all values of i. This leads directly to the Hartree-Fock equation after applying a unitary transformation to the orbitals such that the Lagrange-multipliers become diagonal.

$$\hat{f}_i(\boldsymbol{r}_i)\psi_i(\boldsymbol{r}_i) = \epsilon_i \psi_i(\boldsymbol{r}_i) \quad (2.41)$$

where $\hat{f}$ is the Fock operator, an effective one-electron operator

$$\hat{f}_i(\boldsymbol{r}_i) = \hat{h}_i(\boldsymbol{r}_i) + \sum_j^N \left[\hat{J}_j(\boldsymbol{r}_i) - \hat{K}_j(\boldsymbol{r}_i) \right] \quad (2.42)$$

with $\hat{J}_j$ and $\hat{K}_j$ the Coulomb and exchange operators, respectively.

$$\hat{J}_j = \langle \psi_j | \frac{1}{\boldsymbol{r}_{ij}} | \psi_j \rangle \qquad \hat{K}_j = \langle \psi_j | \frac{\hat{P}_{ij}}{\boldsymbol{r}_{ij}} | \psi_j \rangle \quad (2.43)$$

Next, we can substitute the expression of the molecular orbitals in the atomic basis

$$\hat{f}_i(\boldsymbol{r}_i) \sum_\nu^N c_{\nu i} \chi_\nu(\boldsymbol{r}_i) = \epsilon_i \sum_\nu^N c_{\nu i} \chi_\nu(\boldsymbol{r}_i) \quad (2.44)$$

and multiplying by χ_μ we can express the result as

$$\sum_\nu^N c_{\nu i} \langle \chi_\mu | \hat{f}_i | \chi_\nu \rangle = \epsilon_i \sum_\nu^N c_{\nu i} \langle \chi_\mu | \chi_\nu \rangle \quad (2.45)$$

or

$$Fc_i = \epsilon_i S c_i \tag{2.46}$$

If we consider the $i = 1, \ldots, N$ orbitals as columns of the matrix $\mathbb{C}$ we arrive to the matrix form of the equation

$$F\mathbb{C} = \epsilon_i S\mathbb{C} \tag{2.47}$$

The Self Consistent Field procedure consists in calculating the Fock matrix F and then compute a new set $\mathbb{C}'$ with it. Then we use the new set to compute again the Fock operator and so on until the convergence is reached by fulfilling some convergence criterion.
The Hartree-Fock method has several weaknesses. It is a mean-field approach: the electron-electron interaction does not depend on the instantaneous positions of the electrons but rather on the average distribution of the electrons and hence the electrons move uncorrelated. We can introduce the electron correlation term as the difference between the mean-field HF solution and the exact solution; electrons are capable of avoiding each other in a more efficient way than predicted by a mean-field approach. Electronic correlation is usually divided between non-dynamic (static) and dynamic electron correlation. Static correlation originates form the lacking of one dominant electron configuration in the description of the state, but not necessarily the ground state; and dynamic correlation accounts for the instantaneous electron-electron interaction. Electronic correlation takes its name on the fact that electrons, as they can coexist with each other in the same point of space, must move to avoid each other, i.e. their motion must be correlated. The method makes key assumptions that lead to an underestimation of this energy even if a complete orbital basis set is used

- It assumes that the wave function of the system can be written as a single Slater determinant. This is an approximation as there are multiple Slater determinants that can satisfy the antisymmetry condition such as excited configurations.

- The Fock matrix is actually an approximation of the true Hamiltonian operator, because it includes the effect of electron-electron repulsion in an average way, as if each electron was immerse in a mean field.

Post HF methods take care of generalizing HF assumptions and including static and dynamic correlation properly. We can group post HF methods into two main clusters: Single determinant reference and multi-determinant reference methods.

2.5.2 Post Hartree-Fock methods

In cases where the single Slater determinant approximation for the many-electron wave function is a reasonable starting point, dynamic electron correlation can be accounted for by a variety of computational methods that all share the common feature of using the HF wave function as reference wave function. Here, three flavors of including the correlation are shortly reviewed: Configuration interaction, perturbation theory and coupled cluster.

Configuration Interaction

One way to add dynamic correlation is the *Configuration Interaction* (CI) method. The CI wave function (both orthogonal and non-orthogonal) is expanded in terms of (normally orthogonal) many electron basis functions (MEBFs). A MEBF can be a single Slater determinant or a CSF.

$$\Psi_{\mathrm{CI}} = \sum_i C_i \Phi_i \tag{2.48}$$

where Φ_i are determinants or CSFs . The expansion coefficients C_i can be determined variationally. A *full-CI* calculation includes all possible Slater determinants or CSFs and includes all correlation effects within the limits of the one-electron basis set that is used, but the computational cost of a full CI calculation becomes rapidly prohibitive. The size of the full CI space for a system with N electrons in M orbitals with a total spin S scales with the Weyl's formula

$$D(N, M, S) = \frac{2S+1}{M+1} \binom{M+1}{N/2-S} \binom{M+1}{N/2+S+1} \tag{2.49}$$

For a small system such as a Li_2 molecule with 6 electrons in 30 orbitals the number of CSF scales up to $5 \cdot 10^6$. With this factorial scaling of the CI space,

a full CI calculation that yields the exact energy for a system with a finite basis set is impractical for any but the smallest model systems. Usually, the CI expression is truncated to some excitation level. *CI Singles* (CIS) takes only single excitations, *CI Singles and Doubles* (CISD) includes also double excitations, etc. Truncated CI methods are neither size consistent nor size extensive. A method is called size consistent if the total energy of two fragments equals the sum of the energies for well-separated fragments A and B,

$$E_{AB} = E_A + E_B \tag{2.50}$$

A method is called size extensive if the calculated energy scales linearly with the number of (interacting or non-interacting) particles in a given system. As the size of a given system increases, the percentage of correlation energy recovered by the truncated CI methods will diminish, leading to unbalanced comparisons. Some efforts have been made to correct this problem depending on whether the correction applies to the modification of the original CI equation or only to the CI energy. The former is known as coupled electron pair approximation while an example of the latter is the Davidson correction[26].

As mentioned above, solving the CI problem requires the calculation of matrix elements between Slater determinants. Non-contributing matrix elements are determined beforehand by the Slater-Condon Rules[13], which show that matrix elements between determinant pairs differing by more than two spin orbitals are zero. For one electron operators $\hat{F}$ the rules are

$$\langle \Psi | \hat{F} | \Psi \rangle = \sum_{i}^{N} \langle \phi_i | \hat{f} | \phi_i \rangle \tag{2.51}$$

$$\langle \Psi | \hat{F} | \Psi_i^a \rangle = \langle \phi_i | \hat{f} | \phi_a \rangle \tag{2.52}$$

$$\langle \Psi | \hat{F} | \Psi_{ij}^{ab} \rangle = 0 \tag{2.53}$$

so any matrix element between states differing in two or more orbitals are

zero. For two electron operators $\hat{G}$

$$\langle\Psi|\hat{G}|\Psi\rangle = \frac{1}{2}\sum_{p}^{N}\sum_{q\neq p}^{N}\Big(\langle\phi_p\phi_q|\hat{g}|\phi_p\phi_q\rangle - \langle\phi_p\phi_q|\hat{g}|\phi_q\phi_p\rangle\Big) \tag{2.54}$$

$$\langle\Psi|\hat{G}|\Psi_i^a\rangle = \sum_{p}^{N}\Big(\langle\phi_i\phi_p|\hat{g}|\phi_a\phi_p\rangle - \langle\phi_i\phi_p|\hat{g}|\phi_p\phi_a\rangle\Big) \tag{2.55}$$

$$\langle\Psi|\hat{G}|\Psi_{ij}^{ab}\rangle = \langle\phi_i\phi_j|\hat{g}|\phi_a\phi_b\rangle - \langle\phi_i\phi_j|\hat{g}|\phi_b\phi_a\rangle \tag{2.56}$$

$$\langle\Psi|\hat{G}|\Psi_{ijk}^{abc}\rangle = 0 \tag{2.57}$$

matrix elements between states differing in three or more orbitals are zero. Slater-Condon Rules only apply when the basis of molecular orbitals is orthogonal, which is not fulfilled in non-orthogonal methods such as NOCI. The non-orthogonal general expression of matrix elements is known as the general Löwdin formula or the Löwdin rules[34].

Perturbation Theory

Another way to improve the Hartree-Fock solution with dynamic correlation is by using the Rayleigh-Schrödinger Perturbation Theory (RSPT)[52,48]. The Hamiltonian is divided into two hermitian operators, i.e., the unperturbed Hamiltonian $\hat{H}^{(0)}$ for which solution is known and a small perturbation $\hat{V}$ that depends on a parameter $\lambda \in [0,1]$

$$\hat{H} = \hat{H}^{(0)} + \lambda\hat{V} \tag{2.58}$$

As λ rises, a small perturbation is introduced in the expressions of the energy and wave function. The energy and wave function now depend on the parameter λ, so we can expand them in power series

$$E(\lambda) = E^{(0)} + \lambda E^{(1)} + \lambda^2 E^{(2)} + \lambda^3 E^{(3)} \tag{2.59}$$

$$\Psi(\lambda) = \Psi^{(0)} + \lambda\Psi^{(1)} + \lambda^2\Psi^{(2)} + \lambda^3\Psi^{(3)} \tag{2.60}$$

where $E^{(0)}$ is the eigenvalue of the non perturbed wave function $\Psi^{(0)}$ and the other terms are the first order, second order, third order, etc, corrections to the energy and wave functions. A particular many-body version of RSPT

is Møller-Plesset Perturbation Theory (MPPT)[39] in which the unperturbed Hamiltonian $\hat{H}^{(0)}$ is the sum of all one electron Fock operators $\sum_i \hat{f}_i(\boldsymbol{r}_i)$ and the Hartree-Fock solution is taken as the unperturbed wave function $\Psi^{(0)}$. The MPPT includes electron correlation by means of the perturbation operator. The perturbation operator in MPPT is the difference between the mean-field treatment of the electron-electron interaction in HF and the exact electron-electron interaction. The MPPT method is size extensive as the total energy for every perturbation order scales linearly with the number of particles in a given system. It is also size consistent in it single-reference version. Usually, the perturbation is only applied to a certain order denoted as MPn, where $n = 2, 3, 4$. The MP2 method is the most widely used and it recovers more than 80% of the dynamic correlation energy. In most cases, higher orders of perturbation only slightly improve the result but vastly increase the computational demand.

Coupled Cluster

Instead of the linear expansion of the many-electron wave function characteristic for Configuration Interaction methods, Coupled cluster (CC)[12] adopts an exponential expansion in terms of many-electron basis functions using the Hartree-Fock solution as reference.

$$\Psi_{\mathrm{CC}} = \exp\left(\hat{T}\right)\Psi_0 \tag{2.61}$$

where $\exp\left(\hat{T}\right)$ is given by a Taylor series expansion

$$\exp\left(\hat{T}\right) = \left(1 + \hat{T} + \frac{1}{2!}\hat{T}^2 + \frac{1}{3!}\hat{T}^3 + \cdots\right) \tag{2.62}$$

The cluster operator $\hat{T}$ is defined as the sum up to N-particle excitations

$$\hat{T} = \hat{T}_1 + \hat{T}_2 + \hat{T}_3 + \cdots + \hat{T}_N \tag{2.63}$$

As in the CI method, this series is truncated at a certain level of excitations. The most common choice is to do it up to two-particle excitations so $\hat{T} =$

$\hat{T}_1 + \hat{T}_2$ where

$$\hat{T}_1 = \sum_i \sum_a t_a^i \hat{a}_a^\dagger \hat{a}_i \tag{2.64}$$

$$\hat{T}_2 = \frac{1}{4} \sum_{ij} \sum_{ab} t_{ab}^{ij} \hat{a}_a^\dagger \hat{a}_b^\dagger \hat{a}_j \hat{a}_i \tag{2.65}$$

which is referred as the Coupled Cluster Singles and Doubles method (CCSD). The expanded formula is obtained substituting the expression of $\hat{T}$ in the Taylor expansion

$$\begin{aligned} \exp(T) &= 1 + \hat{T} + \frac{1}{2!}\hat{T}^2 + \cdots \\ &= 1 + \hat{T}_1 + \hat{T}_2 + \frac{1}{2}\hat{T}_1^2 + \frac{1}{2}\hat{T}_1\hat{T}_2 + \frac{1}{2}\hat{T}_2\hat{T}_1 + \frac{1}{2}\hat{T}_2^2 + \cdots \end{aligned} \tag{2.66}$$

Due to applying various powers of $\hat{T}_1$ and $\hat{T}_2$, one can generate more than doubly excited determinants. This makes the CC method size extensive. A very successful extension of CCSD is the CCSD(T) method, in which the effect of the triple excitations is estimated through perturbation theory.

2.5.3 Multi-Configurational electronic structure methods

The above described post-HF methods efficiently incorporate the effect of electron correlation as long as the HF solution is a reasonable starting point. If this is not the case then a multi-configurational reference wave function must be used to include static electron correlation from the start. Usually, but not exclusively, this multi-configurational reference is obtained from the variational procedure given by some variant of the Multi-Configurational Self-Consistent-Field method (MCSCF) approach, which is similar to CI but optimizes the orbitals. As in single-determinant post-HF methods, we can apply CI, MP2 or CC to the multi-configurational solution giving rise to the multi-reference generalization of these methods.

Multi-Configurational Self-Consistent-Field

The Multi-Configurational Self-Consistent-Field method is the equivalent to Hartree-Fock without the single determinant restriction. Similarly to CI,

the MCSCF wave-function is written as linear combination of CSFs where the MOs are those that minimize the CI energy with respect to the MCSCF wave function and the CI coefficients are determined variationally.

In practice, it is quite common to select all possible CSFs in a set of “active" orbitals called the *active space* and keep the remaining orbitals either double occupied (core) or empty (virtual), called the inactive orbitals. This method is called Complete Active Space Self-Consistent-Field (CASSCF) popularized by Roos *et al.*[37]. A more flexible approach is to use the Restrictive Active Space (RASSCF) approach by Malmqvist *et al*. In this method, the active space is divided into three sub-spaces named RAS1, RAS2 and RAS3. While all CSFs are allowed in RAS2, only a limited number of holes and particles are allowed in RAS1 and RAS3 respectively. The most general and flexible approach is the General Active Space (GASSCF) in which the user can create an arbitrary number of sub-spaces GAS*n* specifying the accumulated minimum and maximum numbers of electrons for each one. All of these methods are not black-boxes, the user has to leverage chemical knowledge to include the most important orbitals that are involved in the process into the active space.

As it is said above, all multi-configurational reference methods are built on top MCSCF solution.

Multi-Configurational Reference Configuration Interaction

Multi-Configurational Reference CI (MRCI) generates excited Slater determinants with respect to the MCSCF solution to form the MRCI wavefunction. As a result of a MRCI calculation one gets a more balanced description of the ground and excited states than in a post HF approach using a single Slater determinant as reference. This is because static correlation is usually more important for excited states. There exist two approaches to construct the MRCI wave function that are the so-called contracted and uncontracted MRCI expansions. Consider the following MCSCF solution

$$\Psi_{\mathrm{REF}} = c_1\Phi_1 + c_2\Phi_2 + c_3\Phi_3 + c_4\Phi_4 \tag{2.67}$$

as a reference to form a Singles and Doubles MRCI wave function. The contracted representation considers SD excitations in the reference as a whole

$$\Psi_{\text{MRCI(C)}} = \hat{E}_{pqrs}\Psi_{\text{REF}} \tag{2.68}$$

where $\hat{E}_{pqrs}$ is the two-electron excitation operators which represents excitations from orbitals p, q to orbitals r, s. In this representation the only way to optimize variationally is to change the coefficients c_1, c_2, c_3, c_4 so if one of the configurations is under- or over-represented in the reference is difficult to fix it in the optimization process. On the other hand, the uncontracted representation takes excitations separately on each configuration of the reference

$$\Psi_{\text{MRCI(U)}} = \hat{E}_{pqrs}\Phi_1 + \hat{E}_{pqrs}\Phi_2 + \hat{E}_{pqrs}\Phi_3 + \hat{E}_{pqrs}\Phi_4 \tag{2.69}$$

which results in c_n coefficients with n the number of excitations which allows more freedom degrees in the optimization with the drawback of being more expensive computationally. Both MRCI approaches are, although highly accurate, not often applied nowadays. The main reason is that the computational cost is so large that the method can only be applied to relatively small systems.

Multi-Configurational Reference Perturbation theory

A more versatile alternative is provided by multi-configurational reference perturbation theory. There are several implementations of MRPT, among which the complete active space second order perturbation theory (CASPT2)[2] and N-electron valence state second-order perturbation theory (NEVPT2) are two of the most widely applied approaches. CASPT2 is a generalization of standard Møller-Plesset perturbation theory for multi-configurational references, more specifically a CAS wave function. Its zeroth-order Hamiltonian is a sum of Fock-like one electron operators that reduces to MP2 in the limit of a single determinant reference wave function. NEVPT2 also takes the CAS wave function as reference, but defines the zeroth-order Hamiltonian differently. The method uses the Dyall Hamiltonian[14], which contains two-electron terms for the active orbitals, and hence, should in principle give more accurate results than the purely one-electron operator adopted in the CASPT2 approach.

Multi-Configurational Reference Coupled Cluster

The coupled cluster method can be also generalized to take a multiconfigurational reference (MRCC) in an attempt to go beyond MRPT and MRCI. There are several ways to generalize the single-reference coupled cluster wave function to the case of a multi-determinantal reference. The first ansatz proposed for the exact MRCC wave function was

$$|\Psi_{\text{ic}}\rangle = \exp\left(\hat{T}\right)|\Psi_0\rangle = \exp\left(\hat{T}\right)\sum_{\mu}^{d} c_\mu |\Phi_\mu\rangle \tag{2.70}$$

Methods based on this ansatz are referred to as internally contracted MRCC (ic-MRCC) approaches since the $\hat{T}$ operator is applied to a linear combination of determinants, that is, to the reference wave function as a whole. An alternative MRCC ansatz was later introduced by Jerzioski and Monkhorst (JM):

$$|\Psi_{\text{ic}}\rangle = \exp\left(\hat{T}\right)|\Psi_0\rangle = \sum_{i=\mu}^{d} c_i \exp\left(\hat{T}^\mu\right)|\Phi_\mu\rangle \tag{2.71}$$

where $\hat{T}^i$ is a reference-specific excitation operator that annihilates or creates electrons in occupied or unoccupied orbitals, respectively, of the reference determinant Φ_μ. The JM ansatz may be viewed as a linear combination of coupled cluster wave functions, with each cluster operator optimized for a different determinant. Both families of methods (ic-MRCC and JM-based MRCC) are in continuous development and present different strengths and weaknesses.

2.6 Density Functional Theory

Density functional theory refers to a series of methods that formulate the many-electron problem in terms of an electronic density ρ instead of using the wave function as its central object.

2.6.1 Origins of Density Functional Theory

For introducing Density Functional Theory we first refer to the two Hohenberg-Kohn theorems (H-K)[24] introduced in 1964, which state that the ground state electronic energy of a N electron system is completely determined by the electron density (H-K 1) and that there is a energy functional that is minimized by the exact ground state density (H-K 2).
The advantage of this formulation in terms of the density instead of the many electron wave function is that, for minimizing the energy E one has to vary the electronic density which only depends on 3 degrees of freedom (x,y,z) instead of $3N$ of the wave function. The exact energy functional $E[\rho]$, which assigns a real number energy E to the electronic density function ρ is unknown, but must include the same information as the energy functional of the wave function

$$E[\Psi] = \int \Psi^* \left\{ \sum_i \left(-\nabla_i^2 + \sum_\alpha \frac{-eZ_\alpha}{r_{i\alpha}} + \sum_{j>i} \frac{e^2}{r_{ij}} \right) \right\} \Psi d\tau \qquad (2.72)$$

The general expression of the density functional is written as

$$E[\rho] = T[\rho] + E_{\mathrm{ne}}[\rho] + J[\rho] + K[\rho] \qquad (2.73)$$

where the kinetic energy $T[\rho]$ and the exchange $K[\rho]$ are unknown. The nuclear-electron and Coulomb interactions are

$$E_{\mathrm{ne}}[\rho] = -\sum_\alpha \int \frac{Z_\alpha(\boldsymbol{r}_\alpha)\rho(\boldsymbol{r})}{\boldsymbol{r}_\alpha - r} d^3r \qquad (2.74)$$

$$J[\rho] = \frac{1}{2} \int \frac{\rho(\boldsymbol{r})\rho(\boldsymbol{r}')}{|\boldsymbol{r} - \boldsymbol{r}'|} d^3r d^3r' \qquad (2.75)$$

The first attempt to fill in the unknown contributions had been already proposed by Thomas, Fermi and Dirac in 1927[55,16] by using the exact expressions of the uniform electron gas.

$$T[\rho] = \frac{3}{10}(3\pi^2)^{2/3} \int \rho^{5/3}(\boldsymbol{r}) d^3r \qquad (2.76)$$

$$K[\rho] = \frac{3}{4}\left(\frac{3}{\pi}\right)^{1/3} \int \rho^{4/3}(\boldsymbol{r}) d^3r \qquad (2.77)$$

However, this attempt was unsuccessful, as proved by Teller, due to the incapacity of the model to stabilize molecules[54], because the energy of the molecule obtained by this method is greater than the sum of the energies of each atom. In 1965, Kohn and Sham developed the DFT as we know today[25] (also called Kohn-Sham DFT or KS-DFT) in which they re-introduced orbitals to get a better approximation of the energy functional. First, the kinetic energy functional is separated as follows

$$T[\rho] = T_{\mathrm{S}}[\rho] + T_{\mathrm{c}}[\rho] \tag{2.78}$$

where T_{S} is the kinetic energy of independent electrons (around 99%) and T_{c} is the remainder, due to the correlated nature of the electrons. T_{S} can be calculated exactly with these so-called Kohn-Sham orbitals.

$$\rho = \sum_{i}^{N} |\phi_i|^2 \quad \longrightarrow \quad T_{\mathrm{S}}[\rho] = \sum_{i}^{N} \langle \phi_i | -\frac{1}{2}\nabla^2 | \phi_i \rangle \tag{2.79}$$

The unknown terms are collected in what is known as the exchange correlation functional $E_{\mathrm{xc}} = T_{\mathrm{c}}[\rho] + K[\rho]$

$$E[\rho] = \underbrace{T_{\mathrm{S}}[\rho] + E_{\mathrm{ne}}[\rho] + J[\rho]}_{\text{Exact}} + \underbrace{E_{\mathrm{xc}}[\rho]}_{\text{Unknown}} \tag{2.80}$$

This approach gives a much better account of the kinetic energy, but has again 3N degrees of freedom due to the re-introduction of orbitals. The exchange correlation functional has to be approximated, and there are plenty of options. Some popular types of exchange-correlation functional approximations are Local Spin Density Approximation (LSDA), Generalized Gradient Approximation (GGA), Higher-Order gradient approximations and Hybrid functionals. In general the choice of the functional employed depends on the material to study.

The idea of getting a density functional depending only on coordinates x, y, z to avoid the $\mathcal{O}\left(N^3\right)$ scaling of KS-DFT is an active area of research called Orbital-Free Density Functional Theory (OF-DFT). Methods of this family try of finding a good kinetic energy functional T_{S} without depending on KS-orbitals (as in expression 2.79) but solely on the electronic density[30,27,15,22].

2.6.2 Time dependent Density Functional Theory

The extension to time-dependent systems to study the dynamics of many-body quantum systems is called Time-Dependent Density Functional Theory (TD-DFT) and it was introduced in 1984 in the article of Runge and Gross[49] which shows that the external potential uniquely determines the density. The first approach to TD-DFT, also called real-time TD-DFT was proposed by propagating the time-dependent Kohn-Sham equations. However, the most important application of TD-DFT nowadays is its formulation in terms of linear response theory when studying excited states, that is, the response of the density with respect to the irradiation that is treated as a small external pertirbing potential over time. Consider a system in its ground state with ground-state density $\rho^{(0)}$ subject to a nuclear potential $v^{(0)}$. At t_0 an external perturbation $v^{(1)}$ is turned on, so that the total external potential now is

$$v_{\text{ext}} = v^{(0)} + v^{(1)} \tag{2.81}$$

The perturbation $v^{(1)}$ will induce a change in the density. Assuming than the perturbing potential is well-behaved (continuous, differentiable, etc), the density can be expanded in a perturbative series.

$$\rho(\boldsymbol{r}, t) = \rho^{(0)}(\boldsymbol{r}) + \rho^{(1)}(\boldsymbol{r}, t) + \rho^{(2)}(\boldsymbol{r}, t) + \cdots \tag{2.82}$$

where $\rho^{(1)}$ depends linearly on $v^{(1)}$, $\rho^{(2)}$ depends quadratically, etc. As the perturbation is weak, only the linear term $\rho^{(1)}$ is taken, which in frequency space reads

$$\rho^{(1)}(\boldsymbol{r}, \omega) = \int \chi(\boldsymbol{r}, \omega, \boldsymbol{r}', \omega) v^{(1)}(\boldsymbol{r}, \omega) d^3 r' \tag{2.83}$$

where χ_{KS} is the linear density-density response function of the system. In the time-dependent Kohn-Sham framework, the density of the interacting system of electrons is obtained from the fictitious system of non-interacting electrons. Clearly, the linear change of density can be calculated using the Kohn-Sham system

$$\rho^{(1)}(\boldsymbol{r}, \omega) = \int \chi_{\text{KS}}(\boldsymbol{r}, \omega, \boldsymbol{r}', \omega) v^{(1)}_{\text{KS}}(\boldsymbol{r}, \omega) d^3 r' \tag{2.84}$$

and is calculated in terms of the unperturbed stationary orbitals of the non-interacting system

$$\chi_{\mathrm{KS}}(\boldsymbol{r},\boldsymbol{r}',\omega)=\lim_{\eta\to 0^{+}}\sum_{jk}^{\infty}(f_k-f_j)\frac{\phi_j(\boldsymbol{r})\phi_j^{*}(\boldsymbol{r}')\phi_k(\boldsymbol{r}')\phi_k^{*}(\boldsymbol{r})}{\omega-(\epsilon_j-\epsilon_k)+i\eta} \tag{2.85}$$

where f_m is the occupation number of the mth orbital in the Kohn-Sham ground-state. The variation in the effective potential $v_{\mathrm{KS}}^{(1)}$ is

$$v_{\mathrm{KS}}^{(1)}(\boldsymbol{r},t)=v^{(1)}(\boldsymbol{r},t)+v_{\mathrm{Hartree}}^{(1)}(\boldsymbol{r},t)+v_{\mathrm{xc}}^{(1)}(\boldsymbol{r},t) \tag{2.86}$$

where the variation of the external potential is simply $v^{(1)}$ while the change in the Hartree potential is

$$v_{\mathrm{Hartree}}^{(1)}(\boldsymbol{r},t)=\int\frac{\rho^{(1)}(\boldsymbol{r}',t)}{|\boldsymbol{r}-\boldsymbol{r}'|}d^3r' \tag{2.87}$$

Finally $v_{\mathrm{xc}}^{(1)}$ is the linear part in $\rho^{(1)}$ of the functional $v_{\mathrm{xc}}[\rho]$,

$$v_{\mathrm{xc}}^{(1)}(\boldsymbol{r},t)=\int\rho^{(1)}\frac{\delta v_{\mathrm{xc}}(\boldsymbol{r},t)}{\delta\rho(\boldsymbol{r}',t')}d^3r'dt' \tag{2.88}$$

where

$$f_{\mathrm{xc}}(\boldsymbol{r}t,\boldsymbol{r}'t')=\frac{\delta v_{\mathrm{xc}}(\boldsymbol{r},t)}{\delta\rho(\boldsymbol{r}',t')} \tag{2.89}$$

is called the exchange-correlation kernel. These quantities yield the expression of the change in the density in the frequency space

$$\begin{aligned}\rho^{(1)}(\boldsymbol{r},\omega)=&\int\chi(\boldsymbol{r},\omega,\boldsymbol{r}',\omega)v^{(1)}(\boldsymbol{r},\omega)d^3r'\\&+\int\chi_{\mathrm{KS}}(\boldsymbol{r},\boldsymbol{x},\omega)\left[\frac{1}{|\boldsymbol{x}-\boldsymbol{r}'|}+f_{\mathrm{xc}}(\boldsymbol{x},\boldsymbol{r}',\omega)\right]\rho^{(1)}(\boldsymbol{r}',\omega)d^3r'd^3x\end{aligned} \tag{2.90}$$

and for the linear density response

$$\chi(\boldsymbol{r},\boldsymbol{r}',\omega) = \chi_{\mathrm{KS}}(\boldsymbol{r},\boldsymbol{r}',\omega) + \int \chi(\boldsymbol{r},\boldsymbol{x},\omega)v^{(1)}(\boldsymbol{r}',\omega)\left[\frac{1}{|\boldsymbol{x}-\boldsymbol{x}'|} + f_{\mathrm{xc}}(\boldsymbol{x},\boldsymbol{x}',\omega)\right]\chi_{\mathrm{KS}}(\boldsymbol{x},\boldsymbol{r}',\omega)d^3r'd^3x \tag{2.91}$$

This equations is a exact representation of a linear response in the sense that, if having the exact Kohn-Sham potential, a self consistent solution of 2.91 would yield the response function χ of the interacting system.
In this formulation, the main ingredient is the xc kernel f_{xc} that includes all non trivial many-body effects. Many approximate xc kernels have been proposed in the literature. Commonly used examples of these kernels are the ALDA and PGG[46] kernels (see[17] for a detailed explanation about these kernels and more)

2.6.3 Corrections to KS-DTF

The most prominent shortcoming of KS-DFT is the appearance of the self-interaction error (SIE). It is named after the fact that one electron interacts with its own mean field. Consider a system containing a single electron in orbital ϕ_1. In the Hartree-Fock picture, the interaction of the electron with itself cancels as expected

$$\Delta E_{\mathrm{HF}}(N=1) = \frac{1}{2}\langle\phi_1(\boldsymbol{r}_1)\phi_1(\boldsymbol{r}_1')|\frac{1-\hat{P}_{11}}{|\boldsymbol{r}_1-\boldsymbol{r}_1'|}|\phi_1(\boldsymbol{r}_1)\phi_1(\boldsymbol{r}_1')\rangle \tag{2.92}$$

In the DFT picture, the state of the electron is described by density $\rho_1 = |\phi_1|^2$, then the Coulomb $J[\rho_1]$ and the exchange-correlation $E_{\mathrm{xc}}[\rho_1]$ functionals should exactly cancel.

$$\Delta E_{\mathrm{DFT}}(N=1) = \frac{1}{2}\int \frac{\rho_1(\boldsymbol{r}_1)\rho_1(\boldsymbol{r}_1')}{|\boldsymbol{r}_1-\boldsymbol{r}_1'|} + E_{\mathrm{xc}}[\rho] \neq 0 \tag{2.93}$$

for a system of N electrons this error becomes

$$\Delta E_{\mathrm{SIE}} = \sum_i^N \left(J_{ii} + E_{\mathrm{xc}}[\rho]\right) \tag{2.94}$$

Depending of the choice of functional E_{xc} and the material this error varies. This is specially important in solids where the predicted gaps from band structure calculations are underestimated, that is known as the band gap problem. There are multiple solutions proposed to this problem, such as the Perdew-Zunger (PZ) correction[45] which simply removes the self-interaction error, so for system of n electrons the correction is

$$E_{\mathrm{PZ}} = E_{\mathrm{KS}} - \sum_{i}^{N} \left(\hat{J}_{ii} + E_{\mathrm{xc}}[\rho_i] \right) \tag{2.95}$$

and also for the exchange potential

$$V_{\mathrm{x,PZ}}(\boldsymbol{r}) = \frac{\delta E_{\mathrm{x}}}{\delta \rho} - \sum_{i}^{N} \left(\hat{J}_i + \frac{\delta E_{\mathrm{x}}}{\delta \rho}[\rho_i(\boldsymbol{r})] \right) \tag{2.96}$$

which has a problem in that the KS equations for the non-interacting electron system is not invariant when making a unitary transformation in contrast to the Hartree-Fock equation. So, the self-interaction energies are not compensated in the Kohn-Sham equation even after the correction, leading to instabilities.

A method that is used widely to overcome the band gap problem in solid state calculations is the GW approximation (GW). The GW approximation, approximates the self-energy of a system as the product of a Green's function (G) and the screened Coulomb interaction (W). The description in detail of this method requires an introduction to Green's functions and solid state physics so it will not be described here, but the reader can refer to[3] for mode details.

2.7 Advantages and disadvantages of traditional methods

Each one of the methods described above has advantages and disadvantages. Depending on the type of problem to deal with, one may choose between one method or another.

2.7.1 On Kohn-Sham Density Functional Theory

Advantages

- **Accurate, yet computationally cheap.** The main reason for its popularity is the fact that it offers excellent effort-to-insight and cost-to-accuracy ratios compared to related approaches such as Semi-empirical quantum chemical methods (faster and cheaper but less robust) and post Hartree-Fock wave function methods (more accurate but slower and expensive). As a consequence, it is the quickest way to study complex systems and get meaningful results.

Disadvantages

- **Functionals can be material dependent.** Functionals must be chosen carefully based on the particularities of the chemical system under investigation. They usually compensate accuracy by adding much more parametrization to the table which could not extend well to all types of materials.

- **No multi-configurational treatment.** Standard KS-DFT is a single configuration method, so it does not always work well for multi-configurational systems, although several attempts have been made to create a MR-DFT[33].

- **No straightforward way to improve the results.** The lack of a clear hierarchy among the different functionals makes it sometimes difficult to systematically improve the results of a DFT calculation. A trial-and-error strategy of using functionals until the 'correct' result is obtained should be avoided.

2.7.2 On post Hartree-Fock methods

Advantages

- **Suitable for all chemical problems.** Methods such as CI, CC or MR-approaches are accurate and suitable for all chemical problems, being

usually the high computational cost the only reason they are discarded as first option in benefit of DFT.

- **Straightforward way to improve the results.**In contrast to KS-DFT, there is a strict hierarchy in the post HF methods, more accuracy usually implies a larger computational effort. One can either increase the length of a CI expansion, use a multi-reference approach or, if that is insufficient, increase the size of the basis set. Eventually, all approaches converge to a full CI treatment.

Disadvantages

- **Computationally expensive.** As it is said, one can achieve the most accurate results through full CI calculations. However, this is only affordable for very small systems. Calculations with relatively complex systems such as large organic molecules and small proteins (600 atoms) have been carried out with DLPNO-CCSD(T) but they do not achieve the scaling of DFT (up to 2 million atoms) and semi-empirical methods.
- **Analysis of the results can be complicated.** The long wave function expansion typical for multiconfigurational approaches are not directly ideal for a detailed analysis of the electronic structure. The expansion of the wave function in CSFs does not only add electron correlation to the description of the electron structure, but also contains determinants that account for orbital relaxation. Only by mapping the whole wave function on a small model space spanned by a conveniently chosen set of configurations, one can properly assign relative weights to chemically meaningful electronic configurations.

2.7.3 On Valence Bond methods

Advantages

- **Intuitive chemical interpretation.** The length of the expansion is short and no further action is required to determine the relative importance of the different structures.

Disadvantages

- **Computationally costly.** Valence Bond approaches are more complex than most post Hartree-Fock techniques because VB because VB does not impose orthogonality restrictions on the orbitals. This makes these methods difficult to apply for larger system in a routine fashion.

2.8 NOCI as an alternative

Non-Orthogonal Configuration Interaction (NOCI) is a wide term which includes several non-orthogonal methods developed in the last years. As stated above, a CI wave function is a linear combination of configurations (determinants or CSFs) that not only adds electron correlation effects to the description of the electron structure, but also accounts for orbital relaxation effects. The (basically) mean-field description of the reference wave function, in most cases a HF or a small CASSCF wave function, can lead to a set of orbitals that is not optimal for a correlated wave function. Since orbital optimization can be seen as the mixing of the occupied orbitals with the virtual ones, the appearance of singly excited determinants in the CI expansion contribute to the orbital optimization beyond the mean-field treatment of the reference calculation. Orbital relaxation effects are even stronger when the reference wave function was optimized for an average of different electronic states. It is obvious that in this case the orbitals are not optimal for any of the states and that the CI expansion acts as an orbital optimizer to an even larger extent.
In order to reduce the length of the CI expansion when dealing with several states, each electronic state of the system can be described in its own optimal set of orbitals and account therewith for the full orbital relaxation effects. The resulting orbitals and hence the configurations describing each state become non-orthogonal to each other. The resulting CI in this non-orthogonal basis is a Non-Orthogonal CI (NOCI). The NOCI wave function can be defined as a CI of configurations expressed in non-orthogonal orbitals

$$\Psi_{\text{NOCI}} = \sum_i C_i \Theta_i \tag{2.97}$$

where the Φ_i can be called Many-Electron Basis Functions (MEBFs) and they often correspond to distinct electronic configurations . The MEBFs can be multiconfigurational functions of any type, typically CASSCF wave functions, but simpler wave functions such as Hartree-Fock or short MCSCF can also be used.

$$^x\Theta_i = \sum_k {}^x b_k {}^x\Phi_k \tag{2.98}$$

where the $^x\Theta_k$ are Slater determinants. All determinants of the MEBF $^x\Theta_i$ are expressed in the same set of optimized orbitals $^x\phi_1, \ldots, {}^x\phi_n$ related by the superscripted x as they are the result of the same electronic structure calculation. Hence the determinants in eq. 2.98 can be expressed in the usual way as an antisymmetrized product of the one-electron functions with an extra index (the superscript 'x') to distinguish the different orbital sets used in each MEBF

$$^x\Phi_k = |{}^x\phi_1 {}^x\phi_2 \ldots {}^x\phi_n| \tag{2.99}$$

To obtain the NOCI energies and wave function the generalized eigenvalue problem given by the secular equation

$$\mathbf{H}\mathbb{C} = \epsilon\mathbf{S}\mathbb{C} \tag{2.100}$$

must be solved. Here $\mathbf{S}$ is the overlap matrix between the many-electron basis functions $\langle {}^x\Theta | {}^w\Theta \rangle$. Resolution of the secular equation implies the calculation of the overlap and Hamiltonian matrix elements between determinants belonging to different MEBFs. The overlap of the MEBFs corresponds to the determinant of the overlap matrix of the different sets of molecular orbitals. Note that in the orthogonal case, $\mathbf{S}$ is reduced to the identity matrix, but this is not the case with a non-orthogonal basis of many-electron functions. The matrix elements of the Hermitian one- and two-electron operators $\hat{h}_1 =$ and $\hat{g}_{12} = \hat{J}_{12} - \hat{K}_{12}$ between non-orthogonal determinants $^x\Phi$ and $^w\Phi$ can be written as

$$I_1 = \sum_p^N \sum_q^N \langle {}^x\phi_p | \hat{h}_1 | {}^w\phi_q \rangle \, S(p,q) \tag{2.101}$$

$$I_2 = \sum_{pr}^N \sum_{qs}^N \langle {}^x\phi_p {}^x\phi_r | \hat{g}_{12}(1 - \hat{p}_{qs}) | {}^w\phi_q^w\phi_s \rangle \, S(pr,qs) \tag{2.102}$$

$S(i,j)$ denotes the first order cofactor of the element $S_{ij} = \left\langle \phi_i \middle| \phi_j \right\rangle$ of the square matrix of overlap integrals. The second order cofactor $S(ik,jl)$ is defined as the determinant of the matrix obtained by deleting in **S** the rows i and k, and the columns j and l, multiplied by a factor $(-1)^{i+j+k+l}$.
The calculation of the determinant of a non-diagonal matrix is computationally expensive and therefore it is common practice to apply the corresponding orbital transformation introduced by Amos and Hall[1] to the original spin orbital sets

$$ {}^{x}\tilde{\phi}_p = \sum_{q}^{N} {}^{x}\phi_q \, {}^{x}U_{qp} \tag{2.103} $$

$$ {}^{w}\tilde{\phi}_p = \sum_{q}^{N} {}^{w}\phi_q \, {}^{w}V_{qp} \tag{2.104} $$

As it is a unitary transformation it does not change the determinantal wave functions.

$$ {}^{x}\Phi = |{}^{x}\tilde{\phi}_1 \, {}^{x}\tilde{\phi}_2 \ldots {}^{x}\tilde{\phi}_N| \tag{2.105} $$

$$ {}^{w}\Phi = |{}^{w}\tilde{\phi}_1 \, {}^{w}\tilde{\phi}_2 \ldots {}^{w}\tilde{\phi}_N| \tag{2.106} $$

$$ {}^{xw}\tilde{S}_{pq} = \langle {}^{x}\phi_p | {}^{w}\tilde{\phi}_q \rangle = \delta_{pq}\lambda_p \tag{2.107} $$

A corresponding orbital transformation maximizes the overlap of pairs of orbitals in the two sets, making them orthogonal to all the others, that is done computationally by performing a Singular Value Decomposition of the overlap matrix between the two sets. The result is a diagonal matrix of singular values λ_i whose determinant, the overlap between the two configurations, is simplified as the product $\prod_i \lambda_i$ and the one- and two-electron parts of the Hamiltonian matrix elements become

$$ I_1 = \sum_{p}^{N} \langle {}^{x}\tilde{\phi}_p | \hat{h}_1 | {}^{w}\tilde{\phi}_p \rangle \prod_{\alpha \neq p}^{N} \lambda_\alpha \tag{2.108} $$

$$ I_2 = \sum_{r>p}^{N} \langle {}^{x}\tilde{\phi}_p \, {}^{x}\tilde{\phi}_r | \hat{g}_{12} | {}^{w}\tilde{\phi}_p \, {}^{w}\tilde{\phi}_r \rangle \prod_{\alpha \neq p,r}^{N} \lambda_\alpha \tag{2.109} $$

The expansion of the corresponding orbitals in terms of two not necessarily identical sets of basis functions $\{\chi\}$ and $\{\chi'\}$ of dimensions m and n ($m, n \geq N$)

$$ {}^{x}\tilde{\phi}_i = \sum_{p}^{m} \chi_p C_{pi} \tag{2.110} $$

$$ {}^{w}\tilde{\phi}_i = \sum_{p}^{n} \chi'_p C_{pi} \tag{2.111} $$

leads to

$$ I_1 = \sum_{p}^{m}\sum_{q}^{n} \langle \chi_p | \hat{h}_1 | \chi'_q \rangle \sum_{i}^{N} C^{\dagger}_{ip} D_{qi} \prod_{\alpha \neq i} \lambda_\alpha \tag{2.112} $$

$$ I_2 = \sum_{pr}^{m}\sum_{qs}^{n} \langle \chi_p \chi_r | \hat{g}_{12} | \chi'_q \chi'_s \rangle \sum_{k>i}^{N} C^{\dagger}_{ip} C^{\dagger}_{kr} D_{qi} D_{sk} \prod_{\alpha \neq i,k}^{N} \lambda_\alpha \tag{2.113} $$

Rearranging the terms of I_2 leads to

$$ I_2 = \sum_{r>p}^{m}\sum_{s>q}^{n} \langle \chi_p \chi_r | \hat{g}_{12} | \chi'_q \chi'_s \rangle \, B(pq, rs) \tag{2.114} $$

with

$$ B(pq, rs) = \frac{1}{2}(1 - \hat{p}_{pr})(1 - \hat{p}_{qs}) \sum_{ki}^{N} C^{\dagger}_{ip} C^{\dagger}_{kr} D_{qi} D_{sk} \prod_{\alpha \neq i,k}^{N} \lambda_\alpha \tag{2.115} $$

Van Monfort showed[40] that the second order cofactor $A(pr, qs)$ of a square matrix $\mathbf{A}$ can always be written in a factorized form:

$$ A(pr, qs) = (1 - \hat{p}_{pq})(1 - \hat{p}_{rs}) X_{pq} Y_{rs} \tag{2.116} $$

The explicit form of $\mathbf{X}$ and $\mathbf{Y}$ will be specified below, but it must be noted that their dimension is N^2 whereas the super matrix of second order cofactors contains $\approx 1/8N^4$ elements, so the two electron matrix element can now be written in terms of a factorized second order cofactor $B(pr, qs)$

$$ I_2 = \sum_{r>p}^{m}\sum_{s>q}^{n} \langle \chi_p \chi_r | \hat{g}_{12} | \chi'_q \chi'_s \rangle \, (1 - \hat{p}_{pr})(1 - \hat{p}_{qs}) F(\omega)_{pq} G(\omega)_{rs} \tag{2.117} $$

where F and G are co-densities of the kind $C^{\dagger}D$ and ω corresponds to the number of singularities in S, that is, the number of zero diagonal elements in B or the number of pairs of zero-overlap orbitals. There are three possibilities for I_2 to be non-zero

- $\omega = 0$ (No singularities in S), then $\lambda_\alpha \neq 0; \alpha = 1, \ldots, N$ so, the co-densities in this case take the form

$$F(0)_{pq} = \frac{1}{2} \sum_i C^{\dagger}_{ip} D_{qi} \lambda_i^{-1} \tag{2.118}$$

$$G(0)_{pq} = 2F(0)_{pq} \prod_\alpha^N \lambda_\alpha = 2|S|\, F(0)_{pq} \tag{2.119}$$

  that yields the expression 2.117 for I_2 .

- $\omega = 1$ (One singularity in S). $\lambda_\mu = 0$; $\lambda_\alpha \neq 0$ ($\alpha \neq \mu$) which reduces the expression of $B(pr, qs)$ to

$$B(pr, qs) = (1 - \hat{p}_{pr})(1 - \hat{p}_{qs}) C^{\dagger}_{p\mu} D_{\mu q} \sum_{i \neq \mu}^{N} C^{\dagger}_{ir} D_{si} \sum_{\alpha \neq \mu, i}^{N} \lambda_\alpha \tag{2.120}$$

  with

$$F(1)_{pq} = \sum_i^N C^{\dagger}_{ip} D_{qi} \lambda_i^{-1} \tag{2.121}$$

$$G(1)_{pq} = C^{\dagger}_{\mu p} D_{q\mu} \prod_{\alpha \neq \mu}^{N} \lambda_\alpha \tag{2.122}$$

- Two singularities in S, then $\lambda_\mu = \lambda_\nu = 0$; $\lambda_\alpha \neq 0$ ($\alpha \neq \mu, \nu$), then

$$B(pr, qs) = (1 - \hat{p}_{pr})(1 - \hat{p}_{qs}) F_{pq} G_{rs} \tag{2.123}$$

  with

$$F(2)_{pq} = C^{\dagger}_{\nu p} D_{q\nu} \tag{2.124}$$

$$G(2)_{pq} = C^{\dagger}_{\mu p} D_{q\mu} \prod_{\alpha \neq \mu \neq \nu}^{N} \lambda_\alpha \tag{2.125}$$

Summarizing this set of rules, the one-electron integral is only non-zero if there is at most one singularity in S

$$I_1 = \begin{cases} \sum_{p}^{m}\sum_{q}^{n} \langle \chi_p|\hat{h}_1|\chi'_q\rangle \sum_{i}^{N} C^{\dagger}_{ip} D_{qi} \prod_{\alpha\neq i}^{N} \lambda_\alpha, & \text{if } \omega = 0 \\ \sum_{p}^{m}\sum_{q}^{n} \langle \chi_p|\hat{h}_1|\chi'_q\rangle C^{\dagger}_{ip} D_{qi} \prod_{\alpha\neq i}^{N} \lambda_\alpha, & \text{if } \omega = 1 \\ 0, & \text{if } \omega \geq 2 \end{cases} \tag{2.126}$$

whereas more than two singularities yields a zero two-electron integral

$$I_2 = \begin{cases} \sum_{r>p}^{m}\sum_{s>q}^{n} \langle \chi_p\chi_r|\hat{g}_{12}|\chi'_q\chi'_s\rangle \sum_{ik}^{N} C^{\dagger}_{ip} C^{\dagger}_{kr} D_{qi} D_{sk} \prod_{\alpha\neq i,k}^{N} \lambda_\alpha, & \text{if } \omega = 0 \\ \sum_{r>p}^{m}\sum_{s>q}^{n} \langle \chi_p\chi_r|\hat{g}_{12}|\chi'_q\chi'_s\rangle C^{\dagger}_{p\mu} D_{\mu q} \sum_{i\neq\mu}^{N} C^{\dagger}_{ir} D_{si} \prod_{\alpha\neq\mu,i}^{N} \lambda_\alpha, & \text{if } \omega = 1 \\ \sum_{r>p}^{m}\sum_{s>q}^{n} \langle \chi_p\chi_r|\hat{g}_{12}|\chi'_q\chi'_s\rangle C^{\dagger}_{\nu p} D_{q\nu} C^{\dagger}_{\mu p} D_{q\mu} \prod_{\alpha\neq\mu\neq\nu}^{N} \lambda_\alpha, & \text{if } \omega = 2 \\ 0, & \text{if } \omega \geq 3 \end{cases} \tag{2.127}$$

This factorization and derivation of rules was implemented for the first time in the General Non-Orthogonal Matrix Elements (GNOME) algorithm[6] described by Broer and Nieuwport in 1981 and can be considered to some as extent as"generalized Slater-Condon rules", an extension of the orthogonal case. In the case of non-orthogonal determinants one cannot discard matrix element based on the number of differences in orbital occupations but the calculation can be simplified using the number of singularities as guideline. These rules have been revisited recently by various authors[41,36,43,42,8,7,23] in an attempt to make NOCI calculations even more efficient. An example is the Extended Wick's Theorem described at the end of this chapter.

Despite the high computational cost, NOCI possesses other advantages rather than the rigorous treatment of the orbital relaxation. The NOCI wave function expansion is much more compact than the corresponding wave function expansion of multi-configurational approaches based on orthogonal orbitals. Hence, it can recover to some extent the flexibility and intuitive

chemical description of Valence Bond methods as one can expand the NOCI in terms of the Lewis Structures or other meaningful configurations. This capacity for analysis and the advancements in computer hardware and software (more powerful CPUs, GPU offloading, massively parallelized algorithms) explain the resurgence of non-orthogonal methods. The focus of this thesis relies on our implementation of NOCI called NOCI-Fragments, but also other recent implementations will be discussed.

2.8.1 NOCI-Fragments

The NOCI-Fragments (NOCI-F) approach is the one we are following in the development of the GronOR software. This method was introduced to describe the electronic structure of (i) an ensemble of molecules as they can be found in molecular solids or (ii) an assembly fragments of an extended structure. The basis of the description of the electronic structure is in terms of individual molecular states. The advantage of this fragment approach is that the electronic states obtained in this basis can be directly interpreted in terms of these molecular states (like Valence Bond picture) but at the same time also give an accurate description of processes that occur locally such as local excitations on one of the molecules in the ensemble. For example, in the exciton transfer across a stack of molecules discussed in the previous chapter, NOCI-F uses individual fragment states to describe the process instead of delocalizing the orbitals across all the ensemble and then determines the delocalization of the exciton over all fragments. Thus, one can specifically select and optimize the S_0, S_1 on one particular molecule in the ensemble (say molecule A) and add charge transfer states D^+, D^- in which one electron is transferred from molecule A to a neighboring molecule B and subsequently calculate the diabatic coupling γ between MEBFs

$$\gamma = \langle S_1^A S_0^B | \hat{H} | S_0^A S_1^B \rangle \tag{2.128}$$

where the MEBFs are formed by coupling the states of A and B

$$S_0^A S_1^B \equiv S_0^A \otimes S_1^B \tag{2.129}$$

$$(D^+)^A (D^+)^B \equiv (D^+)^A \otimes (D^-)^B \tag{2.130}$$

To further illustrate this kind of calculation we will describe chemical processes such as singlet-fission in molecular ensembles using the NOCI-Fragments approach in chapter 4. The computational implementation with technical details in GronOR will be discussed in the next chapter.

2.8.2 Other Non-Orthogonal implementations

Many other non-orthogonal implementations have been developed in the last years. This section shortly reviews the essential features of four of them, namely the Ab Initio Frenkel-Davydov Exciton Model[41], Non-Orthogonal Orbital Optimization[42], Extended Wick's Theorem[8,7] and Non Orthogonal Active Space Decomposition[23].

Ab Initio Frenkel Davydov Exciton Model

The Ab Initio Frenkel-Davydov Exciton Model (AIFDEM) is an approximate NOCI fragment-based method, and it is capable of calculating exactly the same magnitudes (vertical excitation energies, diabatic couplings) with much lower computational requirements. It was introduced by Morrison and coworkers[41] and implemented in QCHEM software. It is based on the exclusive use of singly excited monomer basis states in order to construct the NOCI wave function instead of using long multiconfigurational expansions as in NOCI-F.
An AIFDEM-NOCI calculation consists in two steps: Calculation of excited monomer basis states and a regular NOCI calculation of Hamiltonian matrix elements. For the first part, the monomer ground state is the SCF wave function

$$|\Theta_{\text{gs}}\rangle = |\Phi_0\rangle = \frac{1}{\sqrt{n}}|\phi_1\phi_2 \dots \phi_n| \tag{2.131}$$

corresponding to a single Slater determinant, and the monomer excited states are written as a linear combination of singly substituted determinants, whose expansion coefficients are determined in a CIS calculation.

$$|\Theta_{\text{exc}}\rangle = C_0\,|\Phi_0\rangle + \sum_{ia} C_i^a\,|\Phi_i^a\rangle \tag{2.132}$$

This already rather short (and necessarily approximate) expansion is further compacted by transforming the canonical Hartree-Fock orbitals to the Natural Transition Orbital (NTO) basis. Natural Transition Orbitals are by construction the orbitals that lead to the shortest wave function expansion to describe singly excited states. In order to obtain NTOs first we must compute the single particle Transition Density Matrix (1-TDM)

$$T_{pq} = \sum_{pq} \langle \Theta_{\text{exc}} | \hat{a}^{\dagger}_{p\alpha} \hat{a}_{q\alpha} + \hat{a}^{\dagger}_{p\beta} \hat{a}_{q\beta} | \Theta_{\text{gs}} \rangle \tag{2.133}$$

of dimension $n_{\text{occ}} \times n_{\text{vir}}$ the number of occupied times number of virtual orbitals in the ground state.
In the case of a CIS description of the excited state, the 1-TDM matrix element T_{ai} corresponds to the CI coefficient C_i^a of the excited determinant in which one electron in orbital i (occupied in the ground state) is deleted and an electron in orbital a (empty in the ground state) is created. Performing a singular value decomposition of the 1-TDM

$$T = U \Lambda V^{\dagger} \tag{2.134}$$

yields two separate unitary transformation matrices (U, V) to transform the canonical occupied and virtual MOs to state-specific paired hole and particle NTOs. Expressing the excited state in this transformed orbitals reduces the CI expansion to no more than n_{occ} particle-hole excitations, the smallest dimension of the 1-TDM, to be compared with the $n_{\text{occ}} \times n_{\text{vir}}$ terms before the transformation. Λ is a diagonal $n_{\text{occ}} \times n_{\text{occ}}$ matrix containing the coefficients of these excitations in the NTO basis and can be used to further reduce the CI expansion in a controlled manner, leaving out the excitations for which Λ_i is smaller than a certain threshold.

$$h = U \phi \tag{2.135}$$

$$p = V \phi \tag{2.136}$$

After expressing the excited states in the NTO basis specific for each different excited state under consideration, and therefore introducing nonorthogonality, one can follow the same procedure as in NOCI or NOCI-Fragments if we deal with an ensemble of molecules. A detailed comparison and implementation in GronOR is given in Chapter 3 along with a generalization for multiple reference and higher order excitations.

NOCI implementation in OpenMolcas

Malmqvist developed a very efficient but more restrictive variant of NOCI in the 1990s[36,43], implemented in the module RASSI of OpenMolcas. This Restricted Active Space State Interaction (RASSI) calculates the Hamiltonian and overlap matrix elements between two or more RASSCF states (among many other properties such as the transition dipole moments and spin-orbit coupling). The key restriction in this approach is that the overlap matrix between the orbitals of two different states has to be block-diagonal, with the active space block being unitary and the inactive and virtual space blocks being orthogonal to the active space block and to themselves. Ordering the orbital spaces as inactive (first-column), active (second-column) and virtual (third-column), the matrix takes the form:

$$S = \left(\begin{array}{c|c|c} 1 & 0 & 0 \\ \hline 0 & S_{AA} & 0 \\ \hline 0 & 0 & 1 \end{array}\right) \tag{2.137}$$

The advantage is that a unique corresponding orbital transformation for all determinant pairs can be defined which makes the two configurations bi-orthogonal. Thus, as all determinants of one multi-configurational expansion are bi-orthogonal to those in the other. The only difference with the Slater-Condon rules is that the overlap is given by the product of all singular values instead of one. The consequence here is a loss of flexibility due to the fact that the dimension of inactive, active and virtual spaces of both configurations must be equal. Furthermore, the overlap matrix cannot have singularities, meaning that the character of the orbitals in the different subblocks cannot be too different in the two nonorthogonal states

Non-orthogonal Orbital Optimization

The Non-Orthogonal Orbital Optimization (NOO) method, is a method introduced by Olsen[42] for optimizing wave functions containing nonorthogonal orbitals. It is closely related to the RASSI method, described above. It is based on the idea of optimizing the wave function while maintaining the metric given by 2.137. The presence of non-zero terms in the off-diagonal

blocks of the metric lead to undesired changes the wave function. To illustrate that, consider a three electron system with one inactive and two active orbitals. Let ϕ_i be the inactive orbital, non-orthogonal to the active orbitals ϕ_a and ϕ_b, for example:

$$|\phi_i\rangle = \frac{1}{\sqrt{2}}\left(|\phi_a\rangle + |\phi_b\rangle\right) \tag{2.138}$$

Let the three electron wave function be a Slater determinant that reads

$$\Psi = |\phi_i\bar{\phi}_i\phi_a\rangle \tag{2.139}$$

that can be rewritten in terms of orthogonal orbitals as

$$\Psi = \frac{1}{2}\left(|\phi_b\bar{\phi}_b\phi_a\rangle - |\phi_a\bar{\phi}_a\phi_b\rangle\right) \tag{2.140}$$

Consider an orthogonalization of ϕ_i on ϕ_a, which gives $\phi_i^{\perp} = \phi_b$, the three electron wave function expressed in orthogonal orbitals becomes

$$\Psi' = |\phi_b\bar{\phi}_b\phi_a\rangle \neq \frac{1}{2}\left(|\phi_b\bar{\phi}_b\phi_a\rangle - |\phi_a\bar{\phi}_a\phi_b\rangle\right) \tag{2.141}$$

so the wave function has changed.
In the general algorithm for orthogonal orbital optimization all possible transformations of the MO set must be unitary to keep the orthonormality between MOs, that is, to keep $\boldsymbol{S} = \boldsymbol{I}$. Unitary transformations can be parametrized in terms of a general anti-symmetric one electron operator $\hat{\kappa}$[21]

$$\boldsymbol{U} = \exp(-\hat{\kappa}) \tag{2.142}$$

where

$$\hat{\kappa} = \sum_{pq} \kappa_{pq}\left(\hat{E}_{pq} - \hat{E}_{qp}\right) \tag{2.143}$$

$$\kappa_{pq} = -\kappa_{qp} \tag{2.144}$$

where κ_{rs} are the elements of the anti-Hermitian matrix $\boldsymbol{\kappa}$ and the singlet excitation operators have been introduced as

$$\hat{E}_{rs} = \hat{a}^{\dagger}_{r\alpha}\hat{a}_{s\alpha} + \hat{a}^{\dagger}_{r\beta}\hat{a}_{s\beta} \tag{2.145}$$

After a rotation, these creation and annihilation operators are

$$\tilde{a}^{\dagger}_{p\sigma} = \exp(-\hat{\kappa})\hat{a}^{\dagger}_{p\sigma}\exp(\hat{\kappa}) \tag{2.146}$$

with $\sigma = \alpha, \beta$. Considering the separation into inactive, active and virtual orbital, rotations are taken between the three subsets of orbitals. Internal rotations of inactive and virtual sub spaces do not change the wave function as they are redundant, so the form of the matrix $\boldsymbol{\kappa}$ that represents the operator $\hat{\kappa}$ in the MO basis set is

$$\boldsymbol{\kappa} = \left(\begin{array}{c|c|c} 0 & -(\boldsymbol{\kappa}_{AI})^T & -(\boldsymbol{\kappa}_{SI})^T \\ \hline \boldsymbol{\kappa}_{AI} & \boldsymbol{\kappa}_{AA} & -(\boldsymbol{\kappa}_{SA})^T \\ \hline \boldsymbol{\kappa}_{SI} & \boldsymbol{\kappa}_{SA} & 0 \end{array}\right) \tag{2.147}$$

Assuming an initial CI wave function $|0\rangle = \sum_I \boldsymbol{C}_I |I\rangle$ whose configurations are defined in a given set of orthonormal orbitals, all allowed wave functions are now obtained by varying the orbitals and CI coefficients with the orthonormality constraint. The optimal orbitals and CI coefficients are those that minimize the energy. An ansatz for the wave function allowing changes of the orbitals and CI-coefficients is

$$|\tilde{0}\rangle = \exp(-\hat{\kappa})\,|0(\delta)\rangle \tag{2.148}$$

where $|0(\delta)\rangle$ is a wave function containing the initial orbitals and the CI-coefficients that are parametrized in terms of a set of variations δ

$$|0(\delta)\rangle = |0\rangle + \hat{P}\sum_i \delta_i |i\rangle \tag{2.149}$$

where $\hat{P}$ is the projection operator

$$\hat{P} = \hat{I} - |0\rangle\langle 0| \tag{2.150}$$

The optimal orbitals and CI-coefficients minimize the energy for the wave function 2.148

$$E = E(\kappa, \delta) = \frac{\langle\tilde{0}|\hat{H}|\tilde{0}\rangle}{\langle\tilde{0}|\tilde{0}\rangle} = \frac{\langle 0(\delta)|\exp(\hat{\kappa})\hat{H}\exp(-\hat{\kappa})|0(\delta)\rangle}{\langle 0(\delta)|0(\delta)\rangle} \tag{2.151}$$

Considering both Taylor and BCH expansions around $\kappa = 0$ and assuming that the wave function is real and normalized at the expansion point, thus $\langle 0|0\rangle = 1$

$$E(\kappa) = E^{(0)} + \kappa^T + k^T E^{(1)} + \frac{1}{2}\kappa^T E^{(2)}\kappa + \cdots \tag{2.152}$$

$$E(\kappa) = \langle 0|\hat{H}|0\rangle + \langle 0|\left[\hat{\kappa}, \hat{H}\right]|0\rangle + \langle \left[\hat{\kappa}, \left[\hat{\kappa}, \hat{H}\right]\right]\rangle + \cdots \tag{2.153}$$

an identifying terms, the expressions for the electronic energy, the electronic gradient the electronic Hessian at $\boldsymbol{\kappa} = 0$ are obtained

$$E^{(0)} = E(0) = \langle 0|\hat{H}|0\rangle \tag{2.154}$$

$$E^{(1)} = 2\langle 0|(\hat{H} - E^{(0)}\hat{I})C^{(0)}|0\rangle \tag{2.155}$$

$$E^{(2)} = 2\langle 0|\hat{P}(\hat{H} - E^{(0)}\hat{I})\hat{P}|0\rangle \tag{2.156}$$

Once arrived to this point there are two options for the optimization procedure. The first is to carry out a first order optimization procedure that is the SCF method described in 2.5.1, in which imposing the condition of vanishing gradient

$$E^{(1)} = 2\langle 0|\hat{H} - E^{(0)}\hat{I}|0\rangle = 0 \tag{2.157}$$

we optimize orbitals by subsequent diagonalization of the Fock matrix, that involves itself a unitary transformation on the orbitals. The second option is to carry out a second order optimization algorithm such as the Newton's method in which the equation to solve is the Newton step

$$\Delta\kappa = -E^{(1)}\left(E^{(2)}\right)^{-1} \tag{2.158}$$

where the Hessian is needed, so the calculation becomes more expensive. The NOO procedure is similar to the previous one but now the orthogonality restriction in the active space is removed. Assume the same initial CI wave function $|0\rangle = \sum_I C_I |I\rangle$, but now the orbitals have an overlap matrix with the block structure as 2.137. All allowed wave functions are now obtained by varying the orbitals and CI coefficients with the constraint that the overlap matrix preserves its structure and the optimal orbitals and CI coefficients

are those that minimize the energy. This optimization is realized by separating the orbital transformation into a metric conserving part acting on all the space and a metric changing part acting only on the active space. The metric conserving part consists in a unitary transformation operator $\exp(-\hat{\kappa}^a)$ described in 2.143 and the matrix changing part is a transformation operator $\exp(-\hat{\kappa}^s)$ expressed in terms of a general symmetric one electron operator $\hat{\kappa}^s$:

$$\hat{\kappa}^s = \sum_{rs} \kappa^s_{rs} \hat{E}_{rs} \tag{2.159}$$

$$\kappa^s_{rs} = \kappa^s_{sr} \tag{2.160}$$

The combined transformation

$$\tilde{a}^\dagger_{p\sigma} = \exp(-\hat{\kappa}^a)\exp(-\hat{\kappa}^s)\hat{a}^\dagger_{p\sigma}\exp(\hat{\kappa}^s)\exp(\hat{\kappa}^a) \tag{2.161}$$

can be rewritten using the BCH expansion as:

$$\tilde{a}^\dagger_{p\sigma} = \sum_r \hat{a}^\dagger_{r\sigma}\left(\exp(-\boldsymbol{\kappa}^a \boldsymbol{S})\exp(-\boldsymbol{\kappa}^s \boldsymbol{S})\right)_{rp} \tag{2.162}$$

with $\mathbf{S}$ the overlap matrix. The exponential operator using the anti-symmetric one-electron operator 2.143 allows the generation of all sets of orbitals with the overlap matrix 2.137. The matrix $\boldsymbol{\kappa}^a$ is identical to that present in the orthogonal algorithm

$$\boldsymbol{\kappa}^a = \left(\begin{array}{c|c|c} 0 & -(\boldsymbol{\kappa}^a_{AI})^T & -(\boldsymbol{\kappa}^a_{SI})^T \\ \hline \boldsymbol{\kappa}^a_{AI} & \boldsymbol{\kappa}^a_{AA} & -(\boldsymbol{\kappa}^a_{SA})^T \\ \hline \boldsymbol{\kappa}^a_{SI} & \boldsymbol{\kappa}^a_{SA} & 0 \end{array}\right) \tag{2.163}$$

with the parameters below the diagonal being the independent parameters of this antisymmetric matrix. On the other hand, symmetric rotations, as they do not preserve the metric, are restricted to preserve the block-form of the overlap matrix 2.137. Therefore, the parameters of the symmetric rotations do only act on the active-active sub-block:

$$\boldsymbol{\kappa}^s = \left(\begin{array}{c|c|c} 0 & 0 & 0 \\ \hline 0 & \boldsymbol{\kappa}^s_{AA} & 0 \\ \hline 0 & 0 & 0 \end{array}\right) \tag{2.164}$$

This choice ensures that the overlap between the various spaces and the overlap of the inactive and of the secondary orbitals are kept of the form of 2.137, that is, non-orthogonality is restricted to the active orbitals. The parameters below the diagonal are again chosen as the independent parameters. An ansatz for the wave function allowing these changes of the orbitals and CI-coefficients is

$$|\tilde{0}\rangle = \exp(-\hat{\kappa}^a)\exp(-\hat{\kappa}^s)\,|0(\delta)\rangle \tag{2.165}$$

The optimal orbitals and CI-coefficients minimize the energy for the wave function 2.148

$$\begin{aligned} E = E(\boldsymbol{\kappa}^a, \boldsymbol{\kappa}^s, \delta) &= \frac{\langle\tilde{0}|\hat{H}|\tilde{0}\rangle}{\langle\tilde{0}|\tilde{0}\rangle} \\ &= \frac{\langle 0(\delta)|\exp(\hat{\kappa}^s)\exp(\hat{\kappa}^a)\hat{H}\exp(-\hat{\kappa}^a)\exp(-\hat{\kappa}^s)|0(\delta)\rangle}{\langle 0(\delta)|\exp(-2\hat{\kappa}^s)|0(\delta)\rangle} \end{aligned} \tag{2.166}$$

From this expression the gradient is readily obtained by first derivatives with respect to the parameters κ^a, κ^s and δ.

$$\frac{\partial E}{\partial \kappa^a_{pq}} = 2\,\langle 0|\left[\hat{E}_{pq}, \hat{H}\right]|0\rangle \tag{2.167}$$

$$\frac{\partial E}{\partial \kappa^s_{pq}} = -2\,\langle 0|\left(\hat{E}_{pq} + \hat{E}_{qp}\right)\left(\hat{H} - E_0\hat{I}\right)|0\rangle \tag{2.168}$$

$$\frac{\partial E}{\partial \delta_i} = 2\,\langle i|\hat{P}\left(\hat{H} - E_0\hat{I}\right)|0\rangle \tag{2.169}$$

and so on. In the algorithm described in[42], the second derivative terms with respect to the CI-coefficients are neglected, so only the orbitals are optimized using a second-order method. At the moment, the NOO method is implemented in the author's code LUCIA.

Extended non-orthogonal Wick's Theorem

This approach was introduced in 2021 by Burton[8,7]. It presents a generalization of the non-orthogonal Wick's theorem to any pair of non-orthogonal

determinants. The existing formulation of the Wick's theorem for non-orthogonal orbitals was only applicable for determinant pairs that do not show singularities in the overlap matrix of the corresponding orbitals and therefore of limited use for NOCI calculations. Let's introduce a set of molecular orbital creation and annihilation operators $\hat{b}_p$ and $\hat{b}_q^\dagger$ in terms of atomic orbital operators

$$\hat{b}_p^\dagger = \sum_\mu \hat{a}_\mu^\dagger C_{\mu p} \tag{2.170}$$

$$\hat{b}_p = \sum_\mu C_{p\mu}^\dagger \hat{a}_\mu \tag{2.171}$$

where C are the molecular orbital coefficients. The atomic orbital operators, thus, are defined as the inverse of these operators

$$\hat{a}_\mu^\dagger = \sum_{p\sigma} C_{\sigma p}^\dagger \hat{b}_p^\dagger S_{\sigma\mu} \tag{2.172}$$

$$\hat{a}_\mu = \sum_{p\sigma} \hat{b}_p C_{p\sigma} S_{\sigma\mu} \tag{2.173}$$

where $S_{\sigma\mu}$ is the overlap of the atomic orbitals, yielded by the anticommutator of the atomic orbital operators

$$\left[\hat{a}_\nu^\dagger, \hat{a}_\mu\right]_+ = \hat{a}_\nu^\dagger \hat{a}_\mu + \hat{a}_\mu \hat{a}_\nu^\dagger = S_{\mu\nu} \tag{2.174}$$

Let's introduce the one- and two-body operators in the atomic basis. In the second quantization formalism they take the form of products of operators 2.170 (see[21] for the proof of this)

$$\hat{f} = \sum_{\mu\nu} f_{\mu\nu} \hat{a}_\mu^\dagger \hat{a}_\nu \tag{2.175}$$

$$\hat{g} = \sum_{\mu\nu\sigma\tau} g_{\mu\nu\sigma\tau} \hat{a}_\mu^\dagger \hat{a}_\nu^\dagger \hat{a}_\sigma \hat{a}_\tau \tag{2.176}$$

To calculate the matrix elements of these operators between a pair of determinants ${}^x\Phi$ and ${}^w\Phi$ defined in mutually non-orthogonal orbital sets x an w

but orthogonal among themselves, let express the operators in the molecular orbital set x

$$\hat{f} = \sum_{pq} {}^{x}f_{pq}\, {}^{x}\hat{b}_{p}^{\dagger}\, {}^{x}\hat{b}_{q} \tag{2.177}$$

$$\hat{g} = \sum_{pqrs} {}^{x}g_{pqrs}\, {}^{x}\hat{b}_{p}^{\dagger}\, {}^{x}\hat{b}_{q}^{\dagger}\, {}^{x}\hat{b}_{r}\hat{b}_{s} \tag{2.178}$$

with

$${}^{x}f_{pq} = \sum_{\mu\nu} {}^{x}C_{p\mu}^{\dagger} f_{\mu\nu}\, {}^{x}C_{\nu q} \tag{2.179}$$

$${}^{x}g_{pqrs} = \sum_{\mu\nu\sigma\tau} {}^{x}C_{p\mu}^{\dagger} C_{q\nu}^{\dagger} g_{\mu\nu\sigma\tau}\, {}^{x}C_{\sigma r}\, {}^{x}C_{\tau s} \tag{2.180}$$

so the matrix elements can be expressed as

$$\langle {}^{x}\Phi|\hat{f}|{}^{w}\Phi\rangle = \sum_{pq} {}^{x}f_{pq} \langle {}^{x}\Phi|{}^{x}\hat{b}_{p}^{\dagger}\, {}^{x}\hat{b}_{q}|\Phi\rangle \tag{2.181}$$

$$\langle {}^{x}\Phi|\hat{g}|{}^{w}\Phi\rangle = \sum_{pqrs} {}^{x}g_{pqrs} \langle \Phi|{}^{x}\hat{b}_{p}^{\dagger}\, {}^{x}\hat{b}_{q}^{\dagger}\, {}^{x}\hat{b}_{r}\, {}^{x}\hat{b}_{s}|{}^{w}\Phi\rangle \tag{2.182}$$

that of course fulfill the non-orthogonal generalized Slater-Condon rules 2.126 to 2.127. In the same way, the overlap between two excited configurations can be expressed using these creation and annihilation MO operators

$$\langle {}^{x}\Phi|{}^{w}\Phi_{i}^{a}\rangle = \langle {}^{x}\Phi|{}^{w}\hat{b}_{a}^{\dagger}\, {}^{w}\hat{b}_{i}|{}^{w}\Phi\rangle \tag{2.183}$$

Now add this excitation to the one- and two-electron integrals,

$$\langle {}^{x}\Phi|\hat{f}|{}^{w}\Phi_{i}^{a}\rangle = \sum_{pq} {}^{x}f_{pq} \langle {}^{x}\Phi|{}^{x}\hat{b}_{p}^{\dagger}\, {}^{x}\hat{b}_{q}\, {}^{w}\hat{b}_{a}^{\dagger}\, {}^{w}\hat{b}_{i}|{}^{w}\Phi\rangle \tag{2.184}$$

$$\langle {}^{x}\Phi|\hat{g}|{}^{w}\Phi_{i}^{a}\rangle = \sum_{pqrs} {}^{x}g_{pqrs} \langle {}^{x}\Phi|{}^{x}\hat{b}_{p}^{\dagger}\, {}^{x}\hat{b}_{q}^{\dagger}\, {}^{x}\hat{b}_{r}\, {}^{x}\hat{b}_{s}\, {}^{w}\hat{b}_{a}^{\dagger}\, {}^{w}\hat{b}_{i}|{}^{w}\Phi\rangle \tag{2.185}$$

The one electron now involves a two electron transition density calculation and the two-electron term involves a three electron density calculation between two non-orthogonal sets. This can be extended further up to an

arbitrary number of excitation on both configurations, so for a given pair of configurations ${}^{x}\Phi$ and ${}^{w}\Phi$ one could in principle compute $\hat{f}$ and $\hat{g}$ evaluations on arbitrary excited configurations obtained from these two determinants. Unfortunately a set of generalized extension of Slater-Condon rules for more than two-electron transitions does not exists for such task. Generalized non-orthogonal Wick's theorem deals with this problem. To proceed with the method it is compulsory to introduce the contraction of two operators $\hat{A}$ and $\hat{B}$ denoted as $\hat{A}\hat{B}$

$$\hat{A}\hat{B} = \hat{A}\hat{B} - \mathcal{N}\left(\hat{A}\hat{B}\right) \tag{2.186}$$

where $\mathcal{N}(\hat{b}_p\hat{b}_q)$ represents a normal ordered product which depends on which reference vacuum one is working. In this case the reference vacuum is the Fermi vacuum, which is either the symmetric Fermi vacuum $\langle {}^{x}\Phi|\ldots|{}^{x}\Phi\rangle$, orthogonal in this case, or the antisymmetric Fermi vacuum $\langle {}^{x}\Phi|\ldots|{}^{w}\Phi\rangle$ that is non-orthogonal. Recovering the convention to use indices $i, j, k, \ldots$ for occupied orbitals, $a, b, c, \ldots$ for virtual orbitals and $p, q, r, \ldots$ for general orbitals, a hole is created by the operator b_i while a particle is created by $b_a^\dagger$. The normal order when working on a Fermi vacuum is given by placing all annihilation operators, hole and particle, to the right of the creation operators and multiplying by a factor $(-1)^P$ where P is the number of permutations. Applying this definition the only non-zero contractions within the symmetric Fermi vacuum is

$$\begin{aligned} {}^{x}\hat{b}_a\,{}^{x}\hat{b}_b^\dagger &= {}^{x}\hat{b}_a\,{}^{x}\hat{b}_b^\dagger + {}^{x}\hat{b}_b^\dagger\,{}^{x}\hat{b}_a = \delta_{ab} \\ {}^{x}\hat{b}_i^\dagger\,{}^{x}\hat{b}_j &= {}^{x}\hat{b}_i^\dagger\,{}^{x}\hat{b}_j + {}^{x}\hat{b}_j\,{}^{x}\hat{b}_i^\dagger = \delta_{ij} \end{aligned}$$

Wick's theorem, used extensively in Quantum Field Theory, proves that the expectation value of a product of any number of operators $\hat{b}_p\hat{b}_q^\dagger\hat{b}_r\ldots$ can be decomposed as the sum of products of pairs of operator, e.g

$$\langle {}^{x}\Phi_i^a|{}^{x}\Phi_j^b\rangle = \langle {}^{x}\Phi|{}^{x}\hat{b}_i^\dagger\,{}^{x}\hat{b}_a\,{}^{x}\hat{b}_b^\dagger\,{}^{x}\hat{b}_j|{}^{x}\Phi\rangle = \delta_{ij}\delta_{ab} \tag{2.187}$$

and the second quantized operators; in first place the one-electron matrix element between a reference and a excited configuration

$$\begin{aligned}&\langle {}^{x}\Phi|\hat{f}|{}^{w}\Phi_i^a\rangle \\ &= \sum_{pq} {}^{x}f_{pq}\left(\langle {}^{x}\Phi|\hat{b}_p^{\dagger x}\hat{b}_q\,{}^{w}\hat{b}_a^{\dagger w}\hat{b}_i|{}^{w}\Phi\rangle + \langle {}^{x}\Phi|\hat{b}_p^{\dagger x}\hat{b}_q\,{}^{w}\hat{b}_a^{\dagger w}\hat{b}_i|{}^{w}\Phi\rangle\right) \quad (2.188)\end{aligned}$$

and second the corresponding two-electron matrix element

$$\begin{aligned}\langle {}^{x}\Phi|\hat{g}|{}^{w}\Phi_i^a\rangle = \sum_{pqrs} {}^{x}g_{pqrs}\Big(&\langle {}^{x}\Phi|\hat{b}_p^{\dagger x}\hat{b}_q^{\dagger x}\hat{b}_s\,{}^{x}\hat{b}_r\,{}^{w}\hat{b}_a^{\dagger w}\hat{b}_i|{}^{w}\Phi\rangle\Big) \\ &+ \langle {}^{x}\Phi|\hat{b}_p^{\dagger x}\hat{b}_q^{\dagger x}\hat{b}_s\,{}^{x}\hat{b}_r\,{}^{w}\hat{b}_a^{\dagger w}\hat{b}_i|{}^{w}\Phi\rangle + \langle {}^{x}\Phi|\hat{b}_p^{\dagger x}\hat{b}_q^{\dagger x}\hat{b}_s\,{}^{x}\hat{b}_r\,{}^{w}\hat{b}_a^{\dagger w}\hat{b}_i|{}^{w}\Phi\rangle \\ &+ \langle {}^{x}\Phi|\hat{b}_p^{\dagger x}\hat{b}_q^{\dagger x}\hat{b}_s\,{}^{x}\hat{b}_r\,{}^{w}\hat{b}_a^{\dagger w}\hat{b}_i|{}^{w}\Phi\rangle + \langle {}^{x}\Phi|\hat{b}_p^{\dagger x}\hat{b}_q^{\dagger x}\hat{b}_s\,{}^{x}\hat{b}_r\,{}^{w}\hat{b}_a^{\dagger w}\hat{b}_i|{}^{w}\Phi\rangle \\ &+ \langle {}^{x}\Phi|\hat{b}_p^{\dagger x}\hat{b}_q^{\dagger x}\hat{b}_s\,{}^{x}\hat{b}_r\,{}^{w}\hat{b}_a^{\dagger w}\hat{b}_i|{}^{w}\Phi\rangle\Big)\end{aligned}$$

and so on, up to a general expression involving an arbitrary number of operator products and excitations

$$\begin{aligned}&\langle {}^{x}\Phi|{}^{x}\hat{b}_i^{\dagger x}\hat{b}_a\cdots{}^{x}\hat{b}_p^{\dagger x}\hat{b}_q\cdots{}^{w}\hat{b}_b^{\dagger w}\hat{b}_j|{}^{w}\Phi\rangle \\ &\qquad = \langle {}^{x}\Phi|{}^{x}\hat{b}_i^{\dagger x}\hat{b}_a\cdots{}^{x}\hat{b}_p^{\dagger x}\hat{b}_q\cdots{}^{w}\hat{b}_b^{\dagger w}\hat{b}_j|{}^{w}\Phi\rangle \\ &\qquad\quad + \langle {}^{x}\Phi|{}^{x}\hat{b}_i^{\dagger x}\hat{b}_a\cdots{}^{x}\hat{b}_p^{\dagger x}\hat{b}_q\cdots{}^{w}\hat{b}_b^{\dagger w}\hat{b}_j|{}^{w}\Phi\rangle + \cdots\end{aligned}$$

The non-orthogonal version of Wick's Theorem can in principle compute all of these terms considering only the biorthogonalization of the reference configuration, that is, doing only one corresponding orbital transformation for configurations ${}^{x}\Phi$ and ${}^{w}\Phi$, as it will be shown below, that the mixed contractions such as involving different orbital sets does not require any additional biorthogonalization apart from the one that was needed already. Unfortunately its original statement does not handle zero-overlap determinant pairs where singularities are present. The author presents an extension to the non-orthogonal Wick's theorem that handles singularities. Consider the overlap matrix between the two sets

$${}^{xw}S_{ij} = \sum_{\mu\nu} {}^{x}C_{i\mu}^{\dagger}S_{\mu\nu}\,{}^{w}C_{\nu j} \quad (2.189)$$

where $S_{\mu\nu}$ is the overlap of the atomic basis. The corresponding orbital transformation is carried out yielding the modified occupied orbital coefficients ${}^{\mu}\tilde{C}_{\mu i}$ and ${}^{\nu}\tilde{C}_{\mu i}$ that satisfy

$$\sum_{\mu\nu} {}^{x}\tilde{C}^{\dagger}_{i\mu} S_{\mu\nu} {}^{w}\tilde{C}_{\nu j} = {}^{xw}\tilde{S}_i \delta_{ij} \tag{2.190}$$

where there can be present singularities denoted as the integer ω that is the number of zero diagonal overlap terms ${}^{xw}\tilde{S}_i$ appearing also in the generalized Slater-Condon rules. It is shown in[8] that the fundamental contractions that involve operators defined on both orbital sets are given by

$${}^{x}\hat{b}^{\dagger}_{p}\,\overbrace{{}^{w}\hat{b}_{q}} = {}^{wx}X_{qp} \tag{2.191}$$

$${}^{x}\hat{b}_{p}\,\overbrace{{}^{w}\hat{b}^{\dagger}_{q}} = -{}^{wx}Y_{pq} \tag{2.192}$$

where ${}^{wx}X_{qp}$ and ${}^{wx}Y_{pq}$ are intermediate values defined for a given pair of determinants, If there are zero-overlap orbital pairs in the biorthogonal basis ($\omega > 0$), then a sum must be taken over every possible way to assign the ω zeros to the contractions in each product. This distribution is denoted by indices ω_k assigned to each contraction (i.e ${}^{wx}X^{(\omega_k)}_{qp}$ and ${}^{wx}Y^{(\omega_k)}_{pq}$), which take values of 0 or 1 and satisfy $\sum_k \omega_k = \omega$. The individual contractions represented in the original orbital basis

$${}^{wx}X^{(\omega)}_{qp} = \begin{cases} \sum_{\mu\nu\sigma\tau} {}^{w}C^{\dagger}_{q\mu} S_{\mu\sigma} {}^{xw}M_{\sigma\tau} S_{\tau\mu} {}^{x}C_{\nu p} & \omega = 0 \\ \sum_{\mu\nu\sigma\tau} {}^{w}C^{\dagger}_{q\mu} S_{\mu\sigma} {}^{xw}P_{\sigma\tau} S_{\tau\mu} {}^{x}C_{\nu p} & \omega = 1, \end{cases} \tag{2.193}$$

$${}^{wx}Y^{(\omega)}_{pq} = \begin{cases} {}^{wx}X^{(\omega)}_{pq} - {}^{xw}S_{pq} & \omega = 0 \\ {}^{wx}X^{(\omega)}_{pq} & \omega = 1, \end{cases} \tag{2.194}$$

where

$${}^{wx}P_{\sigma\tau k} = {}^{w}\tilde{C}_{\sigma k} {}^{x}\tilde{C}^{\dagger}_{k\tau} \tag{2.195}$$

$${}^{wx}W_{\sigma\tau} = \sum_{\{i|{}^{xw}\tilde{S}_i \neq 0\}} {}^{w}\tilde{C}_{\sigma i} \frac{1}{{}^{xw}\tilde{S}_i} {}^{x}\tilde{C}^{\dagger}_{i\tau} \tag{2.196}$$

$${}^{wx}P_{\sigma\tau} = \sum_{\{k|{}^{xw}\tilde{S}_k = 0\}} {}^{xw}P_{\sigma\tau k} \tag{2.197}$$

$${}^{wx}M_{\sigma\tau} = {}^{xx}P_{\sigma\tau} + {}^{xw}P_{\sigma\tau} + {}^{xw}W_{\sigma\tau} \tag{2.198}$$

As it can be seen, contractions 2.191 and 2.192 are defined with respect to the original orbital coefficients such that the definition of excited configurations is not affected by the biorthogonal transformations which confirms that biorthogonalizing with respect to the references is enough to compute the excited terms. Furthermore, the intermediates ${}^{wx}X_{qp}^{(\omega_k)}$ and ${}^{wx}Y_{pq}^{(\omega_k)}$ intermediates can be evaluated and stored once for each pair of nonorthogonal reference determinants. Regarding the number of singularities, if ω is greater than the total number of contractions, then the corresponding matrix element is strictly zero. The process to compute an arbitrary non-orthogonal matrix element is summarized in the following steps

- Assemble all fully contracted combinations of the second-quantized operator and excitations, and calculate the corresponding phase factors.
- Sum, for each term, every possible way to distribute ω zeros among the contractions $\{\omega_k\}$ such that $\sum_k \omega_k = \omega$.
- For every set of $\{\omega_k\}$ in each term , compute the contribution as a product of fundamental contractions 2.191 and 2.192.
- Multiply the combined expression by the reduced overlap cofactor ${}^{xw}\tilde{S}$.

As an example, consider the matrix element

$$\langle {}^{x}\Phi_i^a | {}^{w}\Phi_j^b \rangle = \langle {}^{x}\Phi | {}^{x}\hat{b}_i^{\dagger x}\hat{b}_a \, {}^{x}\hat{b}_b^{\dagger x}\hat{b}_j | {}^{w}\Phi \rangle \tag{2.199}$$

Applying the first steps yields two contributions

$$\langle {}^{x}\Phi_i^a | {}^{w}\Phi_j^b \rangle = \langle {}^{x}\Phi | {}^{x}\hat{b}_i^{\dagger x}\hat{b}_a \, {}^{w}\hat{b}_b^{\dagger w}\hat{b}_j | {}^{w}\Phi \rangle + \langle {}^{x}\Phi | {}^{x}\hat{b}_i^{\dagger x}\hat{b}_a \, {}^{w}\hat{b}_b^{\dagger w}\hat{b}_j | {}^{w}\Phi \rangle \tag{2.200}$$

Each term corresponds to a product of two fundamental contractions with a phase +1. Taking a sum over all ω_1, ω_2 such that $\omega_1 + \omega_2 = \omega$ and multiplying by the overlap

$$\langle {}^{x}\Phi_i^a | {}^{w}\Phi_j^b \rangle = {}^{xw}\tilde{S} \sum_{\substack{\omega_1\omega_2 \\ \omega_1+\omega_2=\omega}} \left({}^{xx}X_{ai}^{(\omega_1)} {}^{ww}X_{jb}^{(\omega_2)} - {}^{wx}X_{ji}^{(\omega_1)} {}^{xw}X_{ab}^{(\omega_2)} \right)$$

$$= {}^{xw}\tilde{S} \sum_{\substack{\omega_1\omega_2 \\ \omega_1+\omega_2=\omega}} \begin{vmatrix} {}^{xx}X_{ai}^{(\omega_1)} & {}^{xw}X_{ab}^{(\omega_2)} \\ {}^{wx}X_{ji}^{(\omega_1)} & {}^{ww}X_{jb}^{(\omega_2)} \end{vmatrix} \quad (2.201)$$

that reduces to zero if $\omega > 2$. References[8] and[7] demonstrate the explicit derivation of matrix elements for the overlap, one-body and two-body operators between excited configurations. The author shows a scaling $\mathcal{O}(1)$ with respect to the number of basis functions instead of the $\mathcal{O}\left(n^4\right)$ of the two-body terms.

Non Orthogonal Active Space Decomposition

The Non Orthogonal Active Space Decomposition (NO-ASD) method was formulated by Kempfer-Robertson and coworkers[23]. As the name suggest, the method aims at decomposing a complete active space in smaller pieces in order to reduce the computational cost and make easier the analysis of the outcomes. The first step involves a series of Unrestricted Hartree-Fock calculations describing different stationary states to disentangle different electron correlations mechanisms. Subsequently, the canonical spin-orbitals of each state are transformed to a set of Unrestricted Natural Orbitals (UNO) to identify the minimal active space that correctly describes the correlation mechanism of the corresponding UHF solution. This is done by selecting a set of partially occupied natural orbitals based on the deviation from 0 (empty) and 2 (doubly occupied) of the eigenvalue of the $\alpha + \beta$ density operator. This procedure is known as UNO-CAS[4,47].
In the second step of the NO-ASD approach a Hamiltonian is constructed with the previously constructed CAS Hamiltonians as diagonal blocks and non-orthogonal matrix elements between the determinants of the different active spaces as off-diagonal blocks.

$$\mathcal{H} = \oplus_I^{N_{CM}} \left(\otimes_i^{N_I} | {}^{I}\psi_i \rangle \right) \quad (2.202)$$

$$S = \left(\begin{array}{c|c} \hat{I}_1 & S_{12} \\ \hline S_{12} & \hat{I}_2 \end{array} \right) \quad H = \left(\begin{array}{c|c} \hat{H}_1 & NO \\ \hline NO & \hat{H}_2 \end{array} \right) \quad (2.203)$$

where I indicates the correlation mechanism and N_{CM} the number of correlation mechanisms (or in other words, UHF solutions) that are being considered. This blocked Hamiltonian leads to much smaller wave function expansions than the full active space with little loss of accuracy. One of the examples discussed by Kempfer-Robertson *et al.* deals with the correlation mechanisms in ozone. The UNO analysis of the two UHF solutions shows that the static correlation can be divided in an $n \rightarrow \pi^*$ contribution and an $\sigma \rightarrow \pi^*$ contribution, both reasonably accurate described with an active space containing 2 orbitals and 2 electrons. The resulting NO-ASD Hamiltonian has 64 matrix elements and is comparable in accuracy to a standard CASCI(8,7) calculation with $1.5 \cdot 10^6$ matrix elements. This procedure is to some extent similar to a NOCI-F calculation with two MEBFs.

Dynamic correlation with a NOCI reference

Most of the discussion so far focused on orbital relaxation and static electron correlation, whereas dynamic electron correlation also plays an important role, especially in the relative energies of the different electronic states. This effect can also be included in post-NOCI techniques, dynamic correlation methods with a NOCI reference that aim to capture dynamic correlation via perturbative approximation from a NOCI reference.

There are two basic perturbative approaches. The first one is a perturb-then-diagonalize strategy: dynamic correlation is estimated for each state separately and after including this correction, the NOCI wave function is obtained by solving the generalized eigenvalue problem with the modified Hamiltonian matrix. The second strategy, diagonalize-then-perturb, solves the NOCI problem and then modifies the NOCI wave functions and energies with the perturbative effect of the (non-orthogonal) determinants that can be generated by applying single- and double excitations on the determinants spanning the different NOCI wave functions.

The NOCI-F approach applies a simple perturb then diagonalize strategy[50] in which the diagonal elements of the NOCI matrix are shifted by a previously calculated correlation energy correction (usually with CASPT2) for the particular fragment states. Incorporating the dynamic correlation into NOCI-F leads to significant changes in the electronic coupling relevant to

singlet fission and gives remarkably accurate results for the magnetic coupling strength.
The NOCI-MP2 method developed by Yost and Head-Gordon[57,56] is also a perturb-then-diagonalize approach. Given a set of HF non-orthogonal determinants, each one can be expanded in the Møller-Plesset perturbation theory fashion $|{}^x\Phi\rangle = \left|{}^x\Phi^{(0)}\right\rangle + \left|{}^x\Phi^{(1)}\right\rangle$. Then, the overlap is

$$\langle {}^x\Phi|{}^w\Phi\rangle = \langle {}^x\Phi^{(0)}|{}^w\Phi^{(0)}\rangle + \langle {}^x\Phi^{(0)}|{}^w\Phi^{(1)}\rangle + \langle {}^x\Phi^{(1)}|{}^w\Phi^{(0)}\rangle + \langle {}^x\Phi^{(1)}|{}^w\Phi^{(1)}\rangle \quad (2.204)$$

and the Hamiltonian

$$\langle {}^x\Phi|\hat{H}|{}^w\Phi\rangle = \langle {}^x\Phi^{(0)}|\hat{H}|{}^w\Phi^{(0)}\rangle + \langle {}^x\Phi^{(0)}|\hat{H}|{}^w\Phi^{(1)}\rangle + \langle {}^x\Phi^{(1)}|\hat{H}|{}^w\Phi^{(0)}\rangle + \langle {}^x\Phi^{(1)}|\hat{H}|{}^w\Phi^{(1)}\rangle \quad (2.205)$$

where the overlap and interaction between the first order corrections (the last terms in the equations) were originally dropped to keep the computational cost of conventional MP2, but had to be introduced again to achieve size consistency. The final set of working equations for the MP2-like terms is

$$H_{\mathrm{MP2}} = \langle {}^x\Phi^{(0)}|\hat{H}|{}^w\Phi^{(1)}\rangle = \frac{1}{4}t_{ij}^{ab}E_x^{\mathrm{HF}}\langle {}^x\Phi^{(0)}|{}^w\Phi_{ij}^{ab}\rangle + \frac{1}{16}g_{klcd}t_{ij}^{ab}\langle {}^x\Phi_{kl}^{cd}|{}^w\Phi_{ij}^{ab}\rangle \quad (2.206)$$

$$S_{\mathrm{MP2}} = \langle {}^x\Phi^{(0)}|{}^w\Phi^{(1)}\rangle = \frac{1}{4}t_{ij}^{ab}\langle {}^x\Phi^{(0)}|{}^w\Phi_{ij}^{ab}\rangle \quad \text{where} \quad t_{ij}^{ab} = \frac{g_{ijab}}{\epsilon_i + \epsilon_j - \epsilon_a - \epsilon_b} \quad (2.207)$$

and the additional term between first order corrections is

$$\langle {}^x\Phi^{(1)}|\hat{H}|{}^w\Phi^{(1)}\rangle = \langle {}^x\Phi^{(1)}|\hat{H}|{}^x\Phi\rangle\langle {}^x\Phi|{}^w\Phi^{(1)}\rangle + \langle {}^x\Phi^{(1)}|\hat{H}|{}^x\Phi_k^c\rangle\langle {}^x\Phi_k^c|{}^w\Phi^{(1)}\rangle + \langle {}^x\Phi^{(1)}|\hat{H}|{}^x\Phi_{kl}^{cd}\rangle\langle {}^x\Phi_{kl}^{cd}|{}^w\Phi^{(1)}\rangle + \cdots \quad (2.208)$$

which is approximated by cutting of the RHF calculation after the first term

$$\langle {}^x\Phi^{(1)}|\hat{H}|{}^w\Phi^{(1)}\rangle \approxeq t_{kl}^{cd} t_{ij}^{ab} \langle {}^x\Phi_{kl}^{cd}|\hat{H}|{}^x\Phi\rangle \langle {}^x\Phi|{}^w\Phi_{ij}^{ab}\rangle = E_{\mathrm{MP2}}^{x} t_{ij}^{ab} \langle {}^x\Phi|{}^w\Phi_{ij}^{ab}\rangle \quad (2.209)$$

A perturbative method which adds a diagonalize-then-perturb correction is the NOCI-PT2 method[9] by Burton and Thom. The proposed method tries to avoid the reliance on the existence of well-behaved MP2 or CISD expansions for the NOCI basis states, that is achieved by directly perturbing the NOCI wave function after diagonalization.

References

[1] A. T. Amos, G. G. Hall, and H. Jones. “Single determinant wave functions”. In: *Proceedings of the Royal Society of London. Series A. Mathematical and Physical Sciences* 263.1315 (1961), pp. 483–493.

[2] K. Andersson et al. “Second-order perturbation theory with a CASSCF reference function”. In: *The Journal of Physical Chemistry* 94.14 (1990), pp. 5483–5488.

[3] F. Aryasetiawan. “Correlation effects in solids from first principles”. In: *Bussei Kenkyu* 75.3 (2000).

[4] J. M. Bofill and P. Pulay. “The unrestricted natural orbital-complete active space (UNO–CAS) method: An inexpensive alternative to the complete active space-self-consistent-field (CAS–SCF) method”. In: *The Journal of Chemical Physics* 90.7 (1989), pp. 3637–3646.

[5] M. Born and R. Oppenheimer. “Zur Quantentheorie der Molekeln”. In: *Annalen der Physik* 389.20 (1927), pp. 457–484.

[6] R. Broer and W. Nieuwpoort. “Broken orbital-symmetry and the description of hole states in the tetrahedral $[CrO_4]^-$ anion. I. Introductory considerations and calculations on oxygen 1s hole states”. In: *Chemical Physics* 54.3 (1981), pp. 291–303.

[7] H. G. A. Burton. “Generalized nonorthogonal matrix elements for arbitrary excitations”. In: *arXiv e-prints*, arXiv:2208.10208 (2022), arXiv:2208.10208.

[8] H. G. A. Burton. “Generalized nonorthogonal matrix elements: Unifying Wick’s theorem and the Slater-Condon rules”. In: *The Journal of Chemical Physics* 154.14 (2021), p. 144109.

[9] H. G. A. Burton and A. J. W. Thom. “Reaching Full Correlation through Nonorthogonal Configuration Interaction: A Second-Order Perturbative Approach”. In: *Journal of Chemical Theory and Computation* 16.9 (2020), pp. 5586–5600.

[10] R. C. C. Angeli and J.-P. Malrieu. “Non-orthogonal and orthogonal valence bond wavefunctions in the hydrogen molecule: the diabatic view”. In: *Molecular Physics* 111.9-11 (2013), pp. 1069–1077.

[11] Z. Chen et al. “XMVB 2.0: A new version of Xiamen valence bond program”. In: *International Journal of Quantum Chemistry* 115.11 (2015), pp. 731–737.

[12] J. Čížek. “On the Correlation Problem in Atomic and Molecular Systems. Calculation of Wavefunction Components in Ursell-Type Expansion Using Quantum-Field Theoretical Methods”. In: *JCP* 45.11 (1966), pp. 4256–4266.

[13] E. Condon. “The Theory of Complex Spectra”. In: *Physical Review* 36.7 (1930), pp. 1121–1133.

[14] K. G. Dyall. “The choice of a zeroth-order Hamiltonian for second-order perturbation theory with a complete active space self-consistent-field reference function”. In: *The Journal of Chemical Physics* 102.12 (1995), pp. 4909–4918.

[15] L. A. Espinosa-Leal et al. “Optimizing a parametrized Thomas-Fermi-Dirac-Weizsäcker density functional for atoms”. In: *Phys. Chem. Chem. Phys.* 17 (47 2015), pp. 31463–31471.

[16] E. Fermi. “Un metodo statistico per la determinazione di alcune priorieta dell’atome”. In: *Rend. Accad. Naz. Lincei* 6.602-607 (1927), p. 32.

[17] F. Furche and D. Rappoport. “III - Density Functional Methods for Excited States: Equilibrium Structure and Electronic Spectra”. In: *Computational Photochemistry*. Ed. by M. Olivucci. Vol. 16. Theoretical and Computational Chemistry. Elsevier, 2005, pp. 93–128.

[18] G. A. Gallup. *Valence Bond Methods: Theory and Applications*. 2002.

[19] E. Giner et al. “Orthogonal Valence Bond Hamiltonians incorporating dynamical correlation effects”. In: *Computational and Theoretical Chemistry* 1116 (2017). Understanding Chemistry and Biochemistry Using Computational Valence Bond Theory, pp. 134–140.

[20] W. Heitler and F. London. “Interaction between Neutral Atoms and Homopolar Binding according to Quantum Mechanics”. In: *Quantum Chemistry*, pp. 140–155.

[21] T. Helgaker and J. O. P. Jørgensen. *Molecular Electronic Structure Theory*. Chichester: John Wiley & Sons, LTD, 2000.

[22] V. V. Karasiev and S. B. Trickey. “Issues and challenges in orbital-free density functional calculations”. In: *Computer Physics Communications* 183.12 (2012), pp. 2519–2527.

[23] E. M. Kempfer-Robertson et al. “Nonorthogonal Active Space Decomposition of Wave Functions with Multiple Correlation Mechanisms”. In: *The Journal of Physical Chemistry Letters* 13.51 (2022), pp. 12041–12048.

[24] P. H. W. Kohn. “Inhomogeneous electron gas”. In: *Physical review* 136.3B (1964), B864.

[25] W. Kohn and L. J. Sham. “Self-consistent equations including exchange and correlation effects”. In: *Physical review* 140.4A (1965), A1133.

[26] S. R. Langhoff and E. R. Davidson. “Configuration interaction calculations on the nitrogen molecule”. In: *International Journal of Quantum Chemistry* 8.1 (1974), pp. 61–72.

[27] J. Lehtomäki et al. “Orbital-free density functional theory implementation with the projector augmented-wave method”. In: *The Journal of Chemical Physics* 141.23 (2014), p. 234102.

[28] J. E. Lennard-Jones. “The electronic structure of some diatomic molecules”. In: *Faraday Transactions* 25 (1929), pp. 668–686.

[29] J. Lenthe, F. Dijkstra, and R. Havenith. “Chapter 4 TURTLE-A gradient VBSCF program theory and studies of aromaticity”. In: *Theoretical and Computational Chemistry* 10 (2002), pp. 79–116.

[30] M. Levy, J. P. Perdew, and V. Sahni. “Exact differential equation for the density and ionization energy of a many-particle system”. In: *Phys. Rev. A* 30 (5 1984), pp. 2745–2748.

[31] G. N. Lewis. "The atom and the molecule." In: *Journal of the American Chemical Society* 38.4 (1916), pp. 762–785.

[32] J. Li and R. McWeeny. "VB2000: Pushing valence bond theory to new limits". In: *International Journal of Quantum Chemistry* 89.4 (2002), pp. 208–216.

[33] G. Li Manni et al. "Multiconfiguration Pair-Density Functional Theory". In: *Journal of Chemical Theory and Computation* 10.9 (2014). PMID: 26588512, pp. 3669–3680.

[34] P. O. Löwdin. "Quantum Theory of Many-Particle Systems. I. Physical Interpretations by Means of Density Matrices, Natural Spin-Orbitals, and Convergence Problems in the Method of Configurational Interaction". In: *Physical Review* 97.6 (1955), pp. 1474–1489.

[35] P. E. M. M. Head-Gordon and C. A. White. "A tensor formulation of many-electron theory in a nonorthogonal single-particle basis". In: *The Journal of Chemical Physics* 108.2 (1998), pp. 616–625.

[36] P. A. Malmqvist. "Calculation of transition density matrices by nonunitary orbital transformations". In: *International Journal of Quantum Chemistry* 30.4 (1986), pp. 479–494.

[37] P. A. Malmqvist and B. O. Roos. "The CASSCF state interaction method". In: *Chemical Physics Letters* 155.2 (1989), pp. 189–194.

[38] J.-P. Malrieu, C. Angeli, and R. Cimiraglia. "On the Relative Merits of Non-Orthogonal and Orthogonal Valence Bond Methods Illustrated on the Hydrogen Molecule". In: *Journal of Chemical Education* 85.1 (2008), p. 150.

[39] C. Møller and M. Plesset. "Note on an Approximation Treatment for Many-Electron Systems". In: *Physical Review* 46.7 (1934), pp. 618–622.

[40] J. Montfort. "Photo-electron spectroscopy. General theoretical aspects and the calculation of peak positions and intensities in some simple systems." English. PhD thesis. 1980.

[41] A. Morrison, Z.-Q. You, and J. Herbert. "Ab Initio Implementation of the Frenkel-Davydov Exciton Model: A Naturally Parallelizable Approach to Computing Collective Excitations in Crystals and Aggregates". In: *Journal of Chemical Theory and Computation* 10 (2014), pp. 5366–5376.

[42] J. Olsen. "Novel methods for configuration interaction and orbital optimization for wave functions containing non-orthogonal orbitals with applications to the chromium dimer and trimer". In: *The Journal of Chemical Physics* 143.11 (2015), p. 114102.

[43] J. Olsen et al. "Transition probability calculations for atoms using nonorthogonal orbitals". In: *Phys. Rev. E* 52 (4 1995), pp. 4499–4508.

[44] W. Pauli. "Über den Zusammenhang des Abschlusses der Elektronengruppen im Atom mit der Komplexstruktur der Spektren". In: *Zeitschrift fur Physik* 31.1 (1925), pp. 765–783.

[45] J. P. Perdew and A. Zunger. "Self-interaction correction to density-functional approximations for many-electron systems". In: *Phys. Rev. B* 23 (10 1981), pp. 5048–5079.

[46] M. Petersilka, U. J. Gossmann, and E. K. U. Gross. "Excitation Energies from Time-Dependent Density-Functional Theory". In: *Phys. Rev. Lett.* 76 (8 1996), pp. 1212–1215.

[47] P. Pulay and T. P. Hamilton. "UHF natural orbitals for defining and starting MC-SCF calculations". In: *The Journal of Chemical Physics* 88.8 (1988), pp. 4926–4933.

[48] J. W. S. Rayleigh. *The theory of sound*. London: Macmillian, 1894.

[49] E. Runge and E. Gross. "Density-Functional Theory for Time Dependent Systems". In: *PRL* 52.12 (1984), pp. 997–1000.

[50] A. Sánchez-Mansilla et al. "On the role of dynamic electron correlation in non-orthogonal configuration interaction with fragments". In: *Phys. Chem. Chem. Phys.* 24 (19 2022), pp. 11931–11944.

[51] E. Schrödinger. "An Undulatory Theory of the Mechanics of Atoms and Molecules". In: *Physical Review* 28.6 (1926), pp. 1049–1070.

[52] E. Schrödinger. “Quantisierung als Eigenwertproblem”. In: *Annalen der Physik* 385.13 (1926), pp. 437–490.

[53] J. C. Slater. “The Theory of Complex Spectra”. In: *Phys. Rev.* 34 (10 1929), pp. 1293–1322.

[54] E. Teller. “On the stability of molecules in the Thomas-Fermi theory”. In: *Reviews of Modern Physics* 34.4 (1962), p. 627.

[55] L. H. Thomas. “The calculation of atomic fields”. In: *Mathematical proceedings of the Cambridge philosophical society*. Vol. 23. 5. Cambridge University Press. 1927, pp. 542–548.

[56] S. R. Yost and M. Head-Gordon. “Efficient Implementation of NOCI-MP2 Using the Resolution of the Identity Approximation with Application to Charged Dimers and Long C-C Bonds in Ethane Derivatives”. In: *Journal of Chemical Theory and Computation* 14.9 (2018), pp. 4791–4805.

[57] S. R. Yost and M. Head-Gordon. “Size consistent formulations of the perturb-then-diagonalize Møller-Plesset perturbation theory correction to non-orthogonal configuration interaction”. In: *The Journal of Chemical Physics* 145.5 (2016), p. 054105.

Chapter 3

GronOR

This chapter summarizes the features currently included in GronOR, a software that provides scalable and accelerated Non-Orthogonal Configuration Interaction for Molecular Fragment Wave Functions. The entire software is written in Fortran with some interfaces in C for the CUDA libraries. It is massively parallelized and accelerated through GPU offloading
The calculation procedure in GronOR from the point of view of the user is shown in Figure 3.1. In the initial setup phase (1) all preparatory calculations needed before a GronOR run are carried out. This includes the generation of the fragment states with SCF, CASSCF or any other wave function method, the generation of one- and two-electron integrals and the transformation of these integrals to the common MO basis. Transformation to a NTO basis for AIFDEM calculation is optional. Step (2) is the GronOR run where MEBFs are generated and the calculation of matrix elements is carried out. An optional step (3) involves the calculation of the effect of spin-orbit coupling and dynamic electron correlation

3.1 Generation of fragment states

As described in the previous chapter, the NOCI wave function Ψ that represents the whole ensemble is expanded in terms of MEBFs Θ_i. In the NOCI-Fragments method the MEBFs are spin-adapted linear combinations of an-

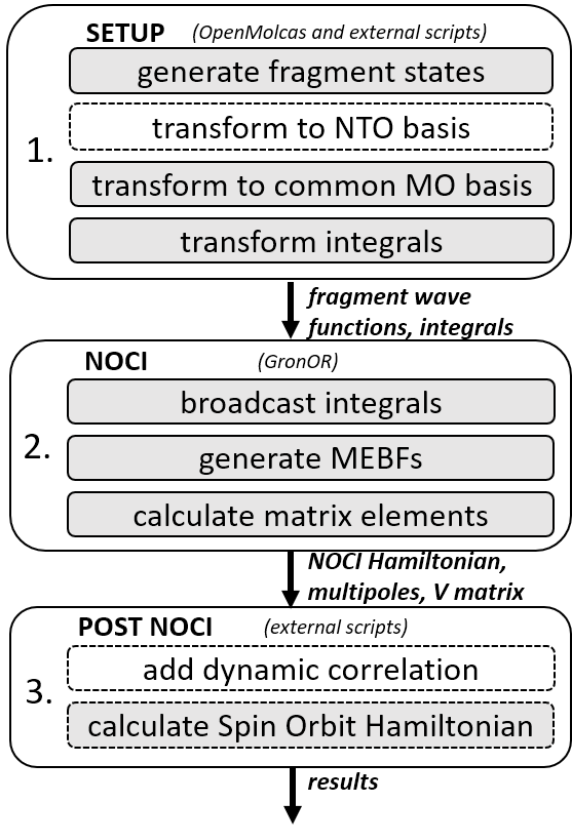

Figure 3.1: Schematic of the user interface of GronOR. 1: Preparatory setup stage involving generation of fragment input states, common MO basis construction and generation of one- and two-electron integrals in OpenMolcas and external scripts. 2: GronOR run involving generation of MEBFs and calculation of NOCI matrices. 3: Calculation of dynamic correlation correction and SO Hamiltonian. Dashed blocks are optional.

tisymmetric products of individual fragment states that can be denoted as

$$|\Theta^{Q}_{I_Q}\rangle_\sigma = \sum_i C_i^{\,I_Q} \Phi_i \tag{3.1}$$

where Q is the fragment in the ensemble, I_Q is the electronic state of the fragment and σ is its secondary spin number. The pre-script ^{I_Q} indicates that Φ_i is expressed in the set of optimized orbitals of state I_Q. These functions cannot act as MEBFs for the CI as they do not describe the whole ensemble but sole fragments or molecules. Computationally, each fragment wave function state is represented by a file containing the orbitals of the state expressed in a basis common to all MEBFs (the .vec file) and another file containing list of coefficients along with alpha-beta strings (the .det file).

```
1   -0.96190303E+00      222000
2    0.99051638E-01      220200
3    0.71654830E-01      220020
4    0.24515004E-01      220002
5    0.41696602E-03      20bbaa
6   -0.72981699E-03      20baba
7    0.31285097E-03      20baab
```

These alpha-beta strings introduced by Handy[4] in 1980 represent Slater determinants and each character is the occupation of each orbital in the active space. The example shown above represents a small portion of the list of determinants of a CAS(6,6)SCF calculation on a spin-singlet fragment state. The strings are the Slater determinants of the active space orbitals $\{\phi_1, \phi_2, \phi_3, \phi_4, \phi_5, \phi_6\}$. For example the determination number 7 is the Slater determinant $|\phi_1\bar{\phi}_1\bar{\phi}_3\phi_4\phi_5\bar{\phi}_6|$ with the coefficient $C_7 = 0.3128 \cdot 10^{-3}$. The determinants written on to the det file correspond to the state with $M = S$, the maximum M number.

After the construction of the common MO basis, the one- and two-electron integrals are generated for the whole ensemble. The one electron integrals contain the kinetic energy, the potential energy, the three dipole and six quadrupole moment components and the Average Mean Field Spin-Orbit integrals. The two-electron integrals only include the electron repulsion integrals. Typically the two-electron integral file is the biggest among these files, occupying more than 10 Gb in production cases.

For the generation of the fragment wave function states and the integral files GronOR is interfaced to OpenMolcas[7].

3.2 Reduced common molecular orbital basis

Because each state is expressed in its own set of optimal orbitals, the transformation of the one- and two-electron integrals to a molecular orbital basis is not straightforward. Therefore, all fragment states have to be expressed in a common molecular orbital basis. The initial basis is the formed by all occupied (inactive and active) orbitals optimized for each fragment state I_Q up to the total number of states K_Q of the fragment Q.

$$\mathcal{B}_Q = \{\phi_1^1, \phi_2^1, \dots, \phi_{n_1}^1, \dots, \phi_1^{I_Q}, \phi_2^{I_Q}, \dots, \phi_{n_I}^{I_Q}, \dots, \phi_1^{K_Q}, \phi_2^{K_Q}, \dots, \phi_{n_I}^{K_Q}\},\ \forall Q$$

of size $M = \sum_k n_k$. The reduced common orbital basis is built upon performing the diagonalization of the overlap matrix between the optimized orbitals of the K_Q states

$$\Lambda = U^\dagger S U \tag{3.2}$$

where S has dimension $M \times M$ and Λ is the diagonal matrix containing the eigenvalues λ_i. The matrix U defines a new set of MOs to describe the electronic states that diagonalize S. Linear dependences between MOs are removed by only consider those $L < M$ orbitals corresponding to eigenvalues larger than a given threshold $\lambda \geq \tau_{\text{MO}}$ specified by the user.

$$U \xrightarrow{\tau_{\text{MO}}} V \tag{3.3}$$

The new reduced common molecular orbital basis V of dimension $L \times M$ is now expressed in the AO basis by the transformation

$$B = C(\Lambda')^{-\frac{1}{2}} V \tag{3.4}$$

where the diagonal matrix Λ' contains only the L largest eigenvalues of Λ and the matrix B contains the $L \times N$ orbitals expressed in the AO basis that can be denoted as $\{b_1, \dots, b_L\}$. Finally, the MOs of every I_Q state are expressed in this new basis $\mathcal{B}$

$$D^{I_Q} = B^\dagger s C^{I_Q} \tag{3.5}$$

In a strictly orthogonal approach using one set of MOs to express all the fragment electronic states, the D^{I_Q} matrices are the identity, which is not the case here. The MOs are now written in terms of the new basis as

$$\phi_p^{I_Q} = \sum_i^L b_i^{I_Q} D_{pi}^{I_Q}, \quad \forall b \in \mathcal{B} \tag{3.6}$$

After repeating this procedure for all the K_Q fragment states for all G fragments, the one- and two-electron integrals are transformed to the common MO basis of the whole ensemble

$$I_1 = \sum_i^L \sum_j^L \underset{\mu,Q,V_{\mathrm{SO}}}{\langle b_i | \hat{h}_1 | \tilde{b}_j \rangle} \sum_p^N D_{ip}^{I_Q\dagger} D_{pj}^{I_Q} \tag{3.7}$$

$$I_2 = \sum_{ik}^L \sum_{jl}^L \langle b_i b_k | \hat{g}_{12}(1 - \hat{p}_{jl}) | b_j b_l \rangle \sum_{r>p}^N D_{ip}^{I_Q\dagger} D_{kr}^{I_Q\dagger} D_{pj}^{I_Q} D_{rl}^{I_Q} \tag{3.8}$$

where one-electron integrals include beside the transformed overlap, kinetic energy and electron-nuclear attraction integrals, also the transformed integrals for calculating additional properties. An increase of the value of the threshold τ_{MO} reduces the size of the integral files, but also leads to a loss of information about the nonorthogonality between the states in the common MO basis. The transformation to the common MO basis is carried out by an external script which takes the output states and MO integrals of the whole ensemble from the OpenMolcas calculation and expresses them in the new basis.

3.3 Frozen orbitals

Expressing the integrals in the common MO basis reduces the memory usage and the complexity of the calculation. An additional step to further reduce the problem can be taken freezing the core orbitals. These orbitals can safely be assumed to remain unchanged among the states K_Q of the same fragment Q. The contribution to the energy of these orbitals can be calculated beforehand and absorbed in the nuclear potential energy as a fixed

Figure 3.2: Overlap between MOs with frozen orthogonalized set.

term. The frozen orbitals can now be subtracted from the common MO basis (figure 3.2). The construction of this orthogonalized frozen orbital set consist in averaging the frozen orbitals of the different states in the fragment configuration. This is done by a sum of density matrices spanned by the individual fragment frozen orbital sets and the diagonalization of the resultant matrix. The result is a set of orbitals that is very similar to the previous sets. Consider the subsets of the basis $\mathcal{B}$ corresponding to the states of fragments $1, \dots, G$

$$\begin{aligned} \mathcal{B}_1 &= \{\phi_1^1, \phi_2^1, \dots, \phi_{n_{K_1}}^{K_1}\} \\ \mathcal{B}_2 &= \{\phi_1^1, \phi_2^1, \dots, \phi_{n_{K_2}}^{K_2}\} \\ &\dots \\ \mathcal{B}_G &= \{\phi_1^1, \phi_2^1, \dots, \phi_{n_{K_G}}^{K_G}\} \end{aligned} \tag{3.9}$$

The average frozen density matrices are

$$\rho^{F_1}(r,s) = \frac{1}{K_1}\sum_{I_1}^{K_1}\sum_{i,j} C_{r,i}^{I_1} C_{s,j}^{I_1\dagger}$$
$$\rho^{F_2}(r,s) = \frac{1}{K_2}\sum_{I_2}^{K_2}\sum_{i,j} C_{r,i}^{I_2} C_{s,j}^{I_2\dagger}$$
$$\cdots$$
$$\rho^{F_G}(r,s) = \frac{1}{K_G}\sum_{I_G}^{K_G}\sum_{i,j} C_{r,i}^{I_G} C_{s,j}^{I_G\dagger} \tag{3.10}$$

where r and s run over the frozen orbitals of each fragment. Diagonalization of these densities defines G frozen orbital sets $U^{F_1}, \ldots, U^{F_G}$ of size $F_i < n_i$.

$$\Lambda_A^{F_1} = U^{F_1\dagger}\rho^{F_1}U^{F_1}$$
$$\Lambda^{F_2} = U^{F_2\dagger}\rho^{F_2}U^{F_2}$$
$$\cdots$$
$$\Lambda^{F_G} = U^{F_G\dagger}\rho^{F_G}U^{F_G} \tag{3.11}$$

The G frozen orbital sets are Löwdin orthogonalized among each other

$$U'^{F} = S^{-\frac{1}{2}}U^{F} \tag{3.12}$$

In this way this set of orbitals can be left out in the construction of the common molecular orbital basis and the subsequent transformation of the integrals. As said before, the contribution of the frozen core orbitals to the energy is averaged and added to the nuclear energy. This operation implies a significant reduction in the number of two electron integrals, which grows with the fourth power in the number of orbitals. This reduction is not only noticeable in the amount of memory required, but also in the time-to-solution as will be illustrated in Section 4.1.

3.4 Transformation to the NTO basis

In the case of Ab Initio Frenkel Davydov Exciton Model (AIFDEM) calculations, the fragment states are expressed in terms of Natural Transition

Orbitals (NTO) as an additional step before the common MO basis transformation. In addition to the original implementation as described in the previous chapter, GronOR counts with some additional option to perform AIFDEM calculations. The original description of AIFDEM considers the ground-state as a SCF single determinant wave function and generate the excited states by means of a CIS calculation so no optimization of separate orbital sets is carried out

$$|\Theta_{\text{gs}}\rangle = |\Phi_0\rangle = \frac{1}{\sqrt{n}}|\phi_1\phi_2 \dots \phi_n| \tag{3.13}$$

$$|\Theta_{\text{exc}}\rangle = C_0\,|\Phi_0\rangle + \sum_{ia} C_i^a\,|\Phi_i^a\rangle \tag{3.14}$$

The 1-particle Transition Density Matrix (1-TDM) element p, q is calculated by taking $\hat{a}_p^\dagger \hat{a}_q$ excitations on the ground state determinant and computing the overlap with the excited configuration. However, as both states are expressed in the same orthonormal orbital set, the element p, q is simply the coefficient C_q^p of the determinant Φ_q^p as there is no overlap with other configurations.

$$T_{pq} = \sum_{ia} C_i^a \,\langle \Phi_i^a | \hat{a}_{p\alpha}^\dagger \hat{a}_{q\alpha} + \hat{a}_{p\beta}^\dagger \hat{a}_{q\beta} | \Phi \rangle = \sum_{ia} \delta_{qi}\delta_{p\alpha} C_q^p \tag{3.15}$$

so in this particular case, it is limited to

$$T_{ai} = \langle \Phi_i^a | \hat{a}_{a\alpha}^\dagger \hat{a}_{i\alpha} + \hat{a}_{a\beta}^\dagger \hat{a}_{i\beta} | \Phi \rangle = C_i^a \tag{3.16}$$

From the Singular Value decomposition of this matrix arises a pair of transformation matrices U and V which transform the orbitals to the NTO basis, hole and particle orbitals, respectively.

$$T = U\Lambda V^\dagger \quad \rightarrow \quad \begin{array}{l} h_i = U\phi_i \\ p_a = V\phi_a \end{array} \tag{3.17}$$

The expansion of the excited state is controlled by means of the singular values λ_σ

$$|\Theta_{\text{exc}}\rangle = \sum_{ia} \lambda_i^a\,|\Phi_i^a\rangle \tag{3.18}$$

$$\Phi_i^a = |\phi_1 \cdots h_i \cdots p_a \cdots \phi_n| \tag{3.19}$$

where as said in the previous chapter, the expansion can be truncated by imposing a threshold on the singular values. As a very simple example consider a He atom with three *s*-type basis functions. The ground state wave function and the excited state CIS wave function are

$$|\Theta_{\text{gs}}\rangle = |\phi_1\bar{\phi}_1| \tag{3.20}$$

$$|\Theta_{\text{exc}}\rangle = c_1\frac{1}{\sqrt{2}}\left[|\phi_1\bar{\phi}_2| - |\bar{\phi}_1\phi_2|\right] + c_2\frac{1}{\sqrt{2}}\left[|\phi_1\bar{\phi}_3| - |\bar{\phi}_1\phi_3|\right] \tag{3.21}$$

where $\{\phi_i\}$ is a set of orthonormal cannonical MOs. Since both wave functions are normalized then $c_1^2 + c_2^2 = 1$. Given the expression 3.15, the terms contributing to the 1-TDM are

$$\frac{1}{\sqrt{2}}c_1\langle\phi_1\bar{\phi}_2|\hat{a}^\dagger_{2\beta}\hat{a}_{1\beta}|\phi_1\bar{\phi}_1\rangle = \frac{1}{\sqrt{2}}c_1\langle\phi_1\bar{\phi}_1|\phi_1\bar{\phi}_1\rangle = \frac{1}{\sqrt{2}}c_1 \tag{3.22}$$

$$-\frac{1}{\sqrt{2}}c_1\langle\bar{\phi}_1\phi_2|\hat{a}^\dagger_{2\alpha}\hat{a}_{1\alpha}|\phi_1\bar{\phi}_1\rangle = \frac{1}{\sqrt{2}}c_1\langle\phi_1\bar{\phi}_1|\phi_1\bar{\phi}_1\rangle = \frac{1}{\sqrt{2}}c_1 \tag{3.23}$$

$$\frac{1}{\sqrt{2}}c_1\langle\phi_1\bar{\phi}_3|\hat{a}^\dagger_{3\beta}\hat{a}_{1\beta}|\phi_1\bar{\phi}_1\rangle = \frac{1}{\sqrt{2}}c_2\langle\phi_1\bar{\phi}_1|\phi_1\bar{\phi}_1\rangle = \frac{1}{\sqrt{2}}c_2 \tag{3.24}$$

$$-\frac{1}{\sqrt{2}}c_1\langle\bar{\phi}_1\phi_3|\hat{a}^\dagger_{3\alpha}\hat{a}_{1\alpha}|\phi_1\bar{\phi}_1\rangle = \frac{1}{\sqrt{2}}c_2\langle\phi_1\bar{\phi}_1|\phi_1\bar{\phi}_1\rangle = \frac{1}{\sqrt{2}}c_2 \tag{3.25}$$

and summing up the terms the 1-TDM of the active space dimension is

$$T = \begin{pmatrix} 0 & 0 & 0 \\ \sqrt{2}c_1 & 0 & 0 \\ \sqrt{2}c_2 & 0 & 0 \end{pmatrix} \tag{3.26}$$

that indicates two one electron transitions from ϕ_1 to ϕ_2 and ϕ_3 respectively. The SVD of this matrix yields

$$\Lambda = \begin{pmatrix} \sqrt{2} & 0 & 0 \\ 0 & 0 & 0 \\ 0 & 0 & 0 \end{pmatrix} \quad U = \begin{pmatrix} 0 & 0 & 1 \\ c_1 & -c_2 & 0 \\ c_2 & c_1 & 0 \end{pmatrix} \quad V = \begin{pmatrix} 1 & 0 & 0 \\ 0 & 0 & 1 \\ 0 & 1 & 0 \end{pmatrix} \tag{3.27}$$

with one non-zero singular value $\lambda = \sqrt{2}$ also called transition amplitude. The pair of hole-particle NTOs corresponding to this singular value are

$$h_1 = \phi_1 \tag{3.28}$$

$$p_1 = c_1\phi_2 + c_2\phi_3 \tag{3.29}$$

In this case, a threshold is not necessary to discard the other NTOs. The expression of the excited wave function in NTOs is

$$|\Theta_{\text{exc}}\rangle = \sqrt{2}\left[|h_1\bar{p}_1| - |\bar{h}_1 p_1|\right] \tag{3.30}$$

reducing the expression of the excited state to only two configuration that keeps all the information about the transition. Several extensions of this basic model have been implemented in GronOR. The first one still expresses the excited states in the ground state orbitals, but includes higher order excitations. Although these higher excitations do not show up in the 1-TDM, and hence, do not contribute directly to the generation of the hole-particle orbital sets, they can change the relative importance of the different single excitations.

$$|\Theta_{\text{exc}}\rangle = C_0\,|\Phi_0\rangle + \sum_{ia} C_i^a\,|\Phi_i^a\rangle + \sum_{ijab} C_{ij}^{ab}\,|\Phi_{ij}^{ab}\rangle \tag{3.31}$$

This reduces the importance of the ground state configuration and single excitations in the CI expansion as

$$\left(C_0\right)^2 + \sum_{ia}\left(C_i^a\right)^2 = 1 - \sum_{ijab}\left(C_{ij}^{ab}\right)^2 \tag{3.32}$$

The procedure is the same as in the CIS case, but the double and higher order excitations are ignored by the formula 3.15 to compute the 1-TDM. Another variant of this method introduces orbital optimization for the excited state, making that the two states are defined in different orbital sets x, w respectively. The calculation now involves the overlap between the two sets, which has to be computed in the same way as in the NOCI method, that is, by performing a corresponding orbital transformation. This procedure yields the final expression

$$T_{pq}^{\text{opt}} = \sum_{ia} C_i^a \left\langle {}^w\Phi_i^a | \hat{a}_{p\alpha}^\dagger \hat{a}_{q\alpha} + \hat{a}_{p\beta}^\dagger \hat{a}_{q\beta} | {}^x\Phi \right\rangle$$
$$= \left\langle {}^w\Phi_i^a | {}^x\Phi_q^p \right\rangle = \sum_{ia} C_i^a \prod_p^n {}^{wx}(\lambda_i^a)_p \quad (3.33)$$

where the λ_p are the singular values of the overlap between the two configurations. Finally, the most general implementation of AIFDEM is in which both orbital optimization and a multiconfigurational description of the ground and excited states are considered

$$|\Theta_{\text{gs}}\rangle = C_0 \, |{}^x\Phi_0\rangle + \sum_{ia} C_i^a \, |{}^x\Phi_i^a\rangle + \sum_{ijab} C_{ij}^{ab} \, |{}^x\Phi_{ij}^{ab}\rangle + \cdots \quad (3.34)$$

$$|\Theta_{\text{exc}}\rangle = D_0 \, |{}^w\Phi_0\rangle + \sum_{ia} D_i^a \, |{}^w\Phi_i^a\rangle + \sum_{ijab} D_{ij}^{ab} \, |{}^w\Phi_{ij}^{ab}\rangle + \cdots \quad (3.35)$$

The matrix element T_{pq} is

$$T_{pq} = \langle \Theta_{\text{exc}} | \hat{a}_{p\alpha}^\dagger \hat{a}_{q\alpha} + \hat{a}_{p\beta}^\dagger \hat{a}_{q\beta} | \Theta_{\text{gs}} \rangle$$
$$= \sum_{ia} D_i^a \prod_p^n {}^{wx}(\lambda_i^a)_p + \sum_{ijab} C_j^b D_{ij}^{ab} \prod_p^n {}^{wx}(\lambda_{ij}^{ab})_p$$
$$+ \sum_{ijkabc} C_{jk}^{bc} D_{ijk}^{abc} \prod_p^n {}^{wx}(\lambda_{ijk}^{abc})_p + \cdots \quad (3.36)$$

Considering the example of a boron atom and the following CAS(4,3) wave functions for the ground-state and first excited state

Ground State		First Excited	
0.98825618E+00	220	0.70710290E+00	2ab
-0.15278102E+00	202	-0.70710290E+00	2ba
0.19379666E-02	ab2	-0.23426576E-02	a2b
-0.19379666E-02	ba2	0.23426576E-02	b2a
-0.41367114E-03	022		

The 1-TDM computed for these states is

$$T = \begin{pmatrix} 0 & 0 & -0.003 \\ 0 & 0 & -0.216 \\ -0.005 & 1.398 & 0 \end{pmatrix} \tag{3.37}$$

The diagonalization of this matrix gives

$$\Lambda = \begin{pmatrix} 1.398 & 0 & 0 \\ 0 & 0.216 & 0 \\ 0 & 0 & 0 \end{pmatrix} \quad \rightarrow \quad \lambda_1 = 1.398 \quad \lambda_2 = 0.216 \tag{3.38}$$

$$U = \begin{pmatrix} 0 & 0.013 & -1 \\ 0 & 1 & 0.013 \\ -1 & 0 & 0 \end{pmatrix} \quad V = \begin{pmatrix} 0.003 & 0 & -1 \\ -1 & 0 & -0.003 \\ 0 & -1 & 0 \end{pmatrix} \tag{3.39}$$

that yields two pairs of NTOs

$$h_1 = 0.003\phi_1 - \phi_2 \tag{3.40}$$

$$h_2 = -\phi_3 \tag{3.41}$$

$$p_1 = -\phi_3 \tag{3.42}$$

$$p_2 = 0.013\phi_1 + \phi_2 \tag{3.43}$$

The $h_3 - p_3$ pair does not contribute to the excitation because the corresponding singular value (λ_3) is zero.

3.5 Generation of the MEBFs

The MEBFs of the ensemble are built as Spin Adapted Antisymmetrized Combinations (SAACs) of the fragment wave functions 3.1 that remain as eigenstates of the S_z and S^2 operators, so they are spin conserving. The general expression of MEBFs for an ensemble of G molecules in terms of fragment states is

$$|\Theta_i\rangle = \sum_{m_Q} \hat{A} \left(\prod_{Q}^{G} |\Theta_Q^{I_Q}\rangle_{m_Q} \right) \Bigg|_{\sum_Q m_Q = S} \tag{3.44}$$

where the summation over m_Q indicates that several antisymmetrized products of molecular functions with different S^2 and S_z eigenvalues, denoted as s and m respectively, are combined via spin coupling to generate MEBFs which are spin eigenstates with spin S and maximum S_z projection $M = S$, therefore $\sum_Q m_Q = S$ for the ensemble of G molecules and κ_{m_Q} is the corresponding Clebsch-Gordan coefficient for the spin coupling

$$\kappa = \langle s_1\ m_1\ s_2\ m_2 | S\ M \rangle \tag{3.45}$$

They appear when coupling angular momenta eigenstates

$$|s_1\ s_2\ S\ M\rangle = \sum_{m_1 m_2} |s_1\ s_2\ m_1\ m_2\rangle\ \langle s_1\ m_1\ s_2\ m_2 | S\ M\rangle \tag{3.46}$$

where

$$|s_1\ s_2\ m_1\ m_2\rangle = |s_1\ m_1\rangle \otimes |s_2\ m_2\rangle \tag{3.47}$$

is called uncoupled basis and in this case represent the product of two fragment states with $m_1 + m_2 = M$ which is also equal to S in this case. The Clebsch-Gordan coefficients are obtained iteratively by applying the angular momentum ladder operators and are usually grouped in a table 3.3. In GronOR they are generated by the recursive algorithm proposed by Zuo, Humbert and Esling[9]. The $m < s$ fragment states are generated from the $m = s$ state by applying the S^- operator

$$S^- = \sum_{pq} \hat{a}^\dagger_{p\beta} \hat{a}_{q\alpha} \tag{3.48}$$

that lowers by 1 the m value of a wave function without changing its s.
In the case that the number of fragments is greater than two, the fragment states are coupled composedly, i.e state of fragment 1 with state of fragment 2, then the coupled 1-2 state with state of fragment 3, etc. In this case the user has to choose the intermediate spin couplings S allowed for each coupling in the MEBF composition. It is up to the user to include all the possible combinations in the NOCI calculation or to select the relevant ones for the study. To illustrate this scheme consider a coupling between three monomer state wave functions, the first is a triplet state and the second and

third are doublet states.

$$\left|\Theta_1\right\rangle = \left|s_1, m_1\right\rangle = \left|1,1\right\rangle = \left|\alpha\alpha\right\rangle \tag{3.49}$$

$$\left|\Theta_2\right\rangle = \left|s_2, m_2\right\rangle = \left|\frac{1}{2}, \frac{1}{2}\right\rangle = \left|\alpha\right\rangle \tag{3.50}$$

$$\left|\Theta_3\right\rangle = \left|s_3, m_3\right\rangle = \left|\frac{1}{2}, \frac{1}{2}\right\rangle = \left|\alpha\right\rangle \tag{3.51}$$

Suppose the goal is to couple these functions to build a global triplet state $S = 1$. There are two possibilities for $m_1 + m_2 + m_3 = 1$, the first choice is to couple $|\Theta_1\rangle$ with $|\Theta_2\rangle$ to form a doublet and to couple the doublet $|\Theta_1\rangle \otimes |\Theta_2\rangle$ with Θ_3 to raise the spin to a triplet. The intermediate doublet requires $m_1 + m_2 = \frac{1}{2}$, which can be achieved by combining $|\Theta_1\rangle = |1,1\rangle$ with $|\Theta_2\rangle = |\frac{1}{2}, -\frac{1}{2}\rangle$ and $|\Theta_1\rangle = |1,0\rangle$ with $|\Theta_2\rangle = |\frac{1}{2}, \frac{1}{2}\rangle$. According to the table 3.3 the combination to generate a doublet from Θ_1 and Θ_2 is

$$|\Theta_{12}\rangle = |\frac{1}{2}, \frac{1}{2}\rangle = \sqrt{\frac{2}{3}}\,|1,1\rangle \otimes |\frac{1}{2}, -\frac{1}{2}\rangle - \sqrt{\frac{1}{3}}\,|1,0\rangle \otimes |\frac{1}{2}, \frac{1}{2}\rangle \tag{3.52}$$

The different m states of Θ_1 and Θ_2 are generated by applying repeatedly the S^- operator

$$|\Theta_1\ 1\ 0\rangle = S^-\,|\Theta\ 1\ 1\rangle = \sqrt{\frac{1}{2}}\,|\alpha\beta\rangle + \sqrt{\frac{1}{2}}\,|\beta\alpha\rangle \tag{3.53}$$

$$|\Theta_1\ 1\ -1\rangle = S^-\,|\Theta\ 1\ 0\rangle = |\beta\beta\rangle \tag{3.54}$$

$$|\Theta_2\ \frac{1}{2}\ -\frac{1}{2}\rangle = S^-\,|\Theta_2\ \frac{1}{2}\ \frac{1}{2}\rangle = |\beta\rangle \tag{3.55}$$

The composition 3.52 yields

$$\begin{aligned}|\Theta_{12}\ \frac{1}{2}\ \frac{1}{2}\rangle &= \sqrt{\frac{2}{3}}\,|\alpha\alpha\rangle\ |\beta\rangle - \sqrt{\frac{1}{3}}\left[\sqrt{\frac{1}{2}}\,|\alpha\beta\rangle + \sqrt{\frac{1}{2}}\,|\beta\alpha\rangle\right]\ |\alpha\rangle \\ &= \sqrt{\frac{2}{3}}\,|\alpha\alpha\beta\rangle - \sqrt{\frac{1}{6}}\,|\alpha\beta\alpha\rangle + \sqrt{\frac{1}{6}}\,|\beta\alpha\alpha\rangle\end{aligned} \tag{3.56}$$

The next step is to build the final triplet state combining $\left|\Theta_{12}\right\rangle$ and $\left|\Theta_3\right\rangle$ under the restriction that $m_{12} + m_3 = 1$. Since both m_{12} and m_3 are both

equal to $\frac{1}{2}$, there is no need to generate any of the other m substates. The final triplet is given by

$$|\Theta_{123}\rangle = |1,1\rangle = |\Theta_{12}\rangle \otimes |\Theta_3\rangle = |\frac{1}{2},\frac{1}{2}\rangle \otimes |\frac{1}{2},\frac{1}{2}\rangle \tag{3.57}$$

The composition of states 3.57 gives

$$|\Theta_{123}\rangle = |1,1\rangle = \sqrt{\frac{2}{3}}\,|\alpha\alpha\beta\alpha\rangle - \sqrt{\frac{1}{6}}\,|\alpha\beta\alpha\alpha\rangle + \sqrt{\frac{1}{6}}\,|\beta\alpha\alpha\alpha\rangle \tag{3.58}$$

which is used as a MEBF of the three fragment system. The second possibility to construct a triplet spin function, in which fragment 1 and 2 are coupled to a quartet and the coupling with fragment 3 lowers the spin to triplet, leads to

$$|\Theta'_{123}\rangle = \frac{1}{2}\sqrt{3}\,|\alpha\alpha\alpha\beta\rangle - \frac{1}{6}\sqrt{3}\,(\,|\alpha\alpha\beta\alpha\rangle + |\alpha\beta\alpha\alpha\rangle + |\beta\alpha\alpha\alpha\rangle) \tag{3.59}$$

3.6 Evaluation of matrix elements

The final NOCI wave function is written as a linear combination of the MEBFs, $\Psi_{\text{NOCI}} = \sum_i C_i\,|\Theta_i\rangle$ and the coefficients C_i are determined in the usual way with variational theory by solving the secular equation 2.100 for which the computation of the overlap and Hamiltonian matrix elements between the MEBFs are required.

The use of optimized orbitals for each individual molecular electronic state has a consequence that the orbitals used in the different MEBFs are non-orthogonal. Furthermore, the orbitals of one molecule are not orthogonalized to those of another, thus the orbitals in $|\Theta_Q^{I_Q}\rangle_\sigma$ are not orthogonal to those of $|\Theta^{I_{Q'}}\rangle_{Q'\sigma'}$ which implies that even the orbitals used inside one MEBF are not necessarily orthogonal to each other in the NOCI-F approach. The fragment wave functions have the following expansion in determinants.

$$|\Theta_Q^{I_Q}\rangle_{m_Q} = \sum_\mu c_{\mu\, m_Q}^{I_Q}\Phi_\mu^{I_Q} \tag{3.60}$$

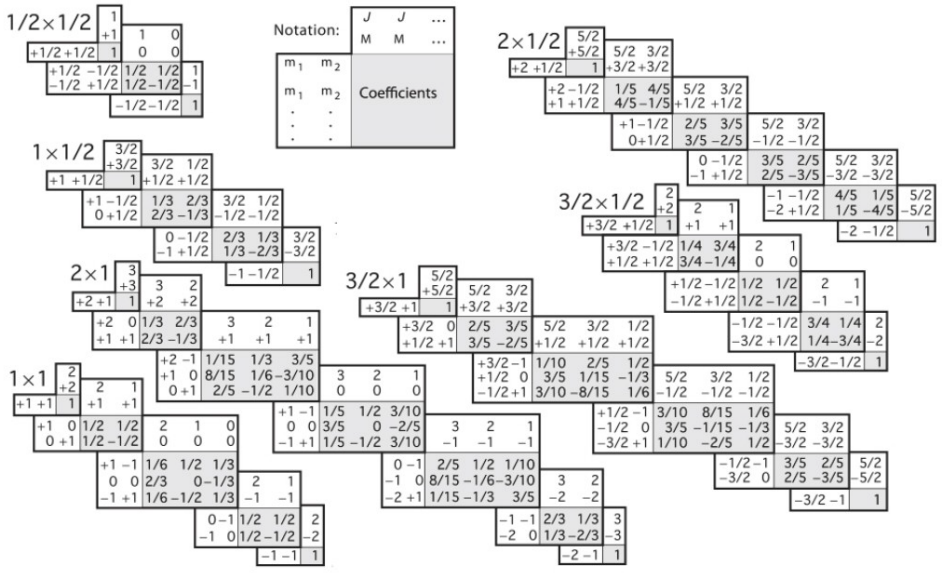

Figure 3.3: First section of the Clebsh-Gordan coefficient table.

where Φ as stated before represents a Slater determinant. The general expression of the MEBFs in terms of determinants is given by substituting equation 3.60 in expression 3.44:

$$|\Theta_i\rangle = \sum_{m_Q} \hat{A} \left[\prod_{Q}^{G} \left(\sum_{\mu} c_{\mu m_Q}^{I_Q} \Phi_{\mu}^{I_Q} \right) \right] \Bigg|_{\sum_Q^G m_Q = S} \equiv \sum_k c_k \Phi_k^{I_1 \ldots I_Q \ldots I_G} \quad (3.61)$$

where in the final step the equivalence $\equiv$ can be made knowing that the result of an antisymmetrized product of an arbitrary number of linear combinations of Slater determinants is another linear combination of Slater determinants as it must be also antisymmetric.

The orbitals used to construct the molecular Slater determinants $\Phi_{\mu}^{I_Q}$ are, within each respective optimal MO set, mutually orthogonal, but the combined orbital sets in the antisymmetrized product Slater determinants $\Phi_k^{I_1 \ldots I_G}$ are not mutually orthogonal. The Hamiltonian matrix elements in the MEBF basis

$$H_{ij} = \langle \Theta_i | \hat{H} | \Theta_j \rangle \quad (3.62)$$

can be written as a sum of matrix elements over antisymmetrized products, which in turn can be written as a sum of matrix elements over Slater determinants expressed in non-orthogonal orbitals,

$$H_{\mu\nu} = \langle \Phi_{\mu}^{I_1 \cdots I_G} | \hat{H} | \Phi_{\nu}^{J_1 \cdots J_G} \rangle \tag{3.63}$$

In principle, we must take into account all determinant pairs and follow the procedure described in the previous chapter. Fortunately, this number can be significantly reduced by removing those determinants pairs for which the CI coefficient product (c_k in expression 3.3) falls below a certain threshold τ_{CI}. Determinants expressed in corresponding orbitals (see previous Chapter) whose overlap has more than two singularities are discarded according to the Generalized Slater-Condon Rules.

The contribution of any determinant pair contribution is completely independent from the others and for that reason, GronOR is built on top of a Master-Worker design pattern. In this pattern, a master rank (or process) sends independent tasks to the worker ranks collects the results and sends new tasks ensuring that every worker is occupied at any time. For all communication operations the Message Passing Interface (MPI), a standard and portable message-passing system designed to function on a wide variety of parallel architectures.

Before starting the actual matrix element calculation, the determinant pair list is built on all ranks, so it is available for all ranks. Then, the master rank divides the list into tasks of m pairs and starts assigning tasks to each worker by broadcasting a 32-byte buffer to the workers containing four integers, two that define the matrix element the task belongs to and two more marking the beginning and ending position of in the determinant pair list. When a worker finishes a task, it sends the results back to the master (the sum of the m contributions to the H and S matrix elements) and awaits for a new task. Once all the tasks have been sent, the master starts sending duplicates of all outstanding tasks to the idle ranks ensuring that it only considers the first time a result is received. This master/worker model with duplicate tasks ensures an optimal load-balancing on heterogeneous architectures; slow nodes process a smaller amount of tasks than the faster nodes. Furthermore, it ensures that the contributions of all tasks are always received even when serious problems (node failure) occur with some specific ranks in the network. After

all results are received, the master sends an empty task buffer to all ranks indicating a terminate signal.
The worker routine scheme is shown in Figure 3.5. Inside the task loop, the worker evaluates the factorized cofactor matrices, overlap and one-electron contributions and batches the contributions from the two-electron integrals. Then it sums up all the results and returns them in a buffer to the master.
All the matrix element calculation procedure is designed to take full advantage of accelerators. For that purpose, when the worker rank has access to a GPU device, all the necessary data to perform the calculation is transferred to it beforehand. To ensure maximum portability to different architectures GronOR uses OpenACC or OpenMP target offloading libraries. The choice of one or the other can be specified at compile time. For CPU-only nodes that cannot benefice from acceleration, OpenMP multi-threading is used. These libraries are called through directives embedded in the source code with preprocessor macros in such way that both the combination of OpenACC for GPU and OpenMP multi-threading and the combination of OpenMP target for GPU and OpenMP multi-threading can be used. This approach ensures portability across a wide range of computer architectures and allows execution on hybrid computers, that is, simultaneously on accelerated and CPU-only partitions.
For the execution of the Singular Value Decomposition and eigenvalue solvers in the factorization of the second order cofactors matrices, GronOR can use (1) CUSOLVER library for NVIDIA GPU (2) either ROCSOLVER and HIPSOLVER libraries for AMD GPU (3) Math Kernel Library (MKL) for Intel CPUs or EISPACK library for all CPUs. The GPU solvers are significantly faster for molecular systems with more than 100 electrons than the alternative CPU routines. It is a remarkable fact that the singular values are not necessarily between 0 and 1 due to the non orthogonality within the set of orbitals of a MEBF.

3.7 Properties

Apart from energy calculations, other properties have been implemented in GronOR. This includes the calculation of (transition) dipole and quadrupole

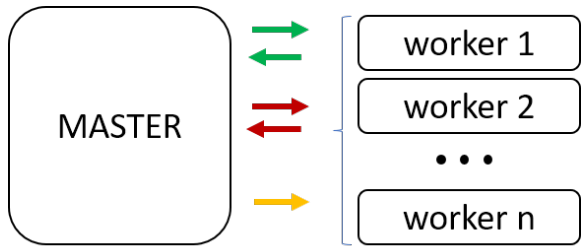

Figure 3.4: Task-based execution workflow; green: master rank receiving and processing results buffers and sending new tasks; red: master rank receiving not previously received results and sending duplicates of outstanding tasks; yellow: master rank sending terminate signals to all other ranks once the results have been received and processed.

moments and the construction of a Spin-Orbit Hamiltonian between MEBFs with different spin moment. Furthermore, a post NOCI analysis module was coded in which the effect of dynamic electron effects can be studied. The latter is especially relevant for effective electronic couplings among MEBFs.

3.7.1 Addition of dynamic correlation

Dynamic electron correlation can have a large impact on the relative energies of electronic states and is not accounted for in the standard NOCI-F procedure discussed so far. Two approaches were described to include dynamic electron correlation in the PhD thesis of R. K. Kathir and the article published in 2022[8]. The first approach consists in shifting the diagonal elements of the NOCI matrix by a previously calculated correlation energy correction for the particular fragment states that are used to construct the MEBFs of the NOCI. Consider the NOCI Hamiltonian expressed in the non-orthogonal MEBF basis, result of a NOCI calculation

$$H_{ij} = \langle \Theta_i | \hat{H} | \Theta_j \rangle \tag{3.64}$$

$$S_{ij} = \langle \Theta_i | \Theta_j \rangle \tag{3.65}$$

Under the assumption that the dynamic correlation among electrons belonging to different fragments is small, the shift applied for a particular MEBF

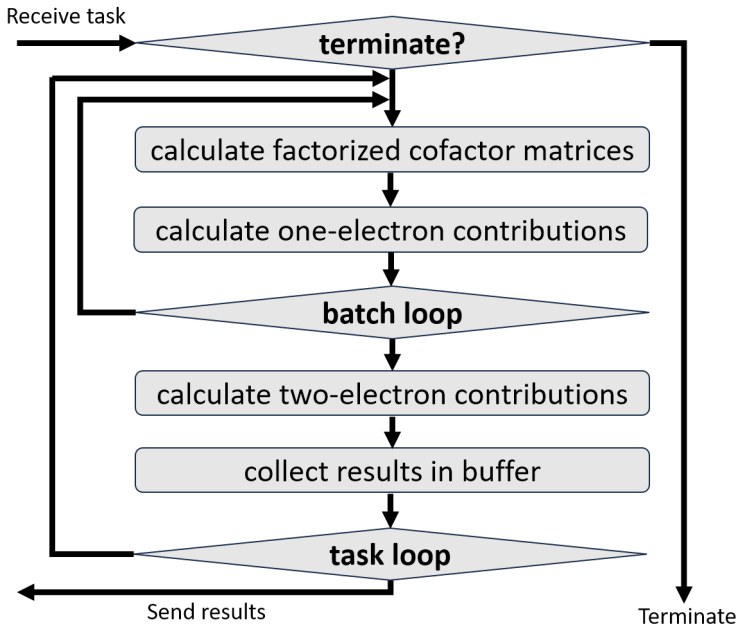

Figure 3.5: Schematic of the task-based execution workflow on the worker ranks; 1: Task received from master; 2: Evaluation of factorized cofactor matrices, optionally in batches, and accumulation of the one-electron contributions; 3: Evaluation and accumulation of the two-electron contributions; 4: Return the accumulated results back to the master rank; 5: termination after receiving the empty task buffer from the master rank.

Θ_i is roughly the sum of the correlation energies that are obtained for the fragment states that form it

$$\Delta E_i = \sum_Q \epsilon_Q^{I_Q} \tag{3.66}$$

The effect of shifting the diagonal matrix elements is illustrated in a 2×2 example. The secular equations read

$$\begin{pmatrix} H_{11} - ES_{11} & H_{21} - ES_{21} \\ H_{12} - ES_{12} & H_{22} - ES_{22} \end{pmatrix} \begin{pmatrix} c_1 \\ c_2 \end{pmatrix} = \begin{pmatrix} 0 \\ 0 \end{pmatrix} \tag{3.67}$$

and with $S_{12} = S_{21} = S$, $S_{11} = S_{22} = 1$, and $H_{12} = H_{21} = V$, the solutions are

$$E_\pm = \frac{-(2VS - H_{11} - H_{22})}{2(1 - S^2)} \pm \frac{\sqrt{(2VS - H_{11} - H_{22})^2 - 4(1 - S^2)(H_{11}H_{22} - V^2)}}{2(1 - S^2)} \tag{3.68}$$

By shifting H_{11} to $H_{11} + \alpha$, the energy difference becomes

$$E_+ - E_- = \frac{\sqrt{(2VS - H_{11} - \alpha - H_{22})^2 - 4(1 - S^2)((H_{11} + \alpha)H_{22} - V^2)}}{1 - S^2} \tag{3.69}$$

which reduces to

$$E_+ - E_- = \sqrt{\alpha^2 + 2\alpha(H_{11} - H_{22}) + (H_{11} - H_{22})^2 + 4V^2} \tag{3.70}$$

when H is expressed in an orthogonal basis, that is $S = 0$. This shows that $\Delta E = E_+ - E_-$ depends on the values of the diagonal matrix elements when the shift is applied in the non-orthogonal basis, that is, on the choice of the zero of energy, while it only depends on the difference of these elements when an orthogonal basis is used. As numerical example, substituting $H_{11} = 1$, $H_{22} = 2$, $\alpha = 0.2$, and $V = 0.1$ leads to $\Delta E = 0.8246$ for $S = 0$ and $\Delta E = 0.8131$ for $S = 0.1$. This energy difference remains the same in the non-overlapping case when H_{11} and H_{22} are changed to 2

and 3, but becomes 0.8666 for the non-orthogonal basis. Hence, in order to apply a shift to the diagonal, the basis must be orthogonalized to exclude unphysical energy differences of the NOCI states. That is done by Löwdin or symmetric orthogonalization

$$H'_{ij} = (S^{-\frac{1}{2}}) \langle \Theta_i | \hat{H} | \Theta_j \rangle (S^{\frac{1}{2}}) \tag{3.71}$$

The Hamiltonian is now written in the basis of the orthogonalized MEBFs with each being a linear combination of the original non-orthogonal MEBFs

$$S^{-\frac{1}{2}}\Theta_\mu = c_{\mu 1}\Theta_1 + c_{\mu 2}\Theta_2 + \cdots + c_{\mu n}\Theta_n \tag{3.72}$$

where the coefficients $c_{\mu i}$ are elements of the orthogonalization matrix $S^{-\frac{1}{2}}$ in the non-orthogonal MEBF basis. Due to the non-orthogonality, the sum of the squares of the coefficients does not equal one so the weight of each MEBF in the combination 3.72 has to be calculated using the Gallup-Norbeck scheme which takes into account the overlap between the MEBFs. The Gallup-Norbeck weight $\omega_{\mu i}^{GN}$ for the i-th original non-orthogonal MEBF in the new μ orthogonalized MEBF is given by

$$\omega_{\mu i}^{\mathrm{GN}} = \frac{N_\mu^{\mathrm{GN}} \cdot c_{\mu i}^2}{(S^{-1})_{ii}} \tag{3.73}$$

with the normalization constant being

$$N_\mu^{\mathrm{GN}} = \frac{1}{\sum_i c_{\mu i}^2 / (s^{-1})_{ii}} \tag{3.74}$$

The shift can now be applied considering the GN weight of each MEBF

$$H''_{\mu\mu} = H'_{\mu\mu} + \sum_i (\omega_{\mu i}^{\mathrm{GN}} \cdot \Delta E_i) \tag{3.75}$$

Then the Hamiltonian is transformed back to the non-orthogonal basis

$$H_{\mathrm{corr}} = (S^{-\frac{1}{2}}) H'' (S^{-\frac{1}{2}})^\dagger \tag{3.76}$$

The second method for including electron correlation modifies the fragment wave functions to include the effect of dynamic electron correlation by means of effective Hamiltonian theory. However, the changes in the wave function were shown to be rather small and the effect on the NOCI-F results were not essential for the systems studied in the 2022 paper[8].

3.7.2 Transition dipole and quadrupole moments

Energy is a central property in Quantum Chemical calculations, but the wave function contains much more information. For example, transition multipole moments (especially dipole), are relevant for the NOCI scheme as they allow to identify dark and bright states in a fragment localized basis. The dipole and quadrupole moment components are defined classically as

$$\mu(k) = \int \rho(\boldsymbol{r})(r_k - r'_k)d^3r \quad k = 1,2,3 \tag{3.77}$$

$$Q(k,l) = \int \rho(\boldsymbol{r})(3r_k r_l - \|\boldsymbol{r}\|^2\delta_{kl})d^3r \quad k,l = 1,2,3 \tag{3.78}$$

The dipole moment is a vector with three components $(\mu(x), \mu(y), \mu(z))$ whereas the quadrupole is a symmetric tensor with six non-redundant components $(Q(x,x), Q(x,y), Q(x,z), Q(y,y), Q(y,z), Q(z,z))$. These moments depend in general on the choice of the origin. In line with the definition in other Quantum Chemical packages, GronOR uses the Cartesian origin $(0,0,0)$ for the dipole and the center of mass

$$\boldsymbol{r}_{\mathrm{CoM}} = \frac{\sum_i^{\mathrm{n}} m_i \boldsymbol{r}_i}{M} \tag{3.79}$$

for the quadrupole, where i runs over all n atoms of the system. The quantum mechanical definition of the moments is based on the expectation value of the operators corresponding to the respective observables. In the fragment MO basis these expectation values are given by the sum over the following one-electron integrals

$$\langle\hat{\mu}(k)\rangle = \sum_p^n \sum_q^n \langle\phi_p|\hat{\mu}(k)|\phi_q\rangle \tag{3.80}$$

$$\langle\hat{Q}(k,l)\rangle = \sum_p^n \sum_q^n \langle\phi_p|\hat{Q}(k,l)|\phi_q\rangle \tag{3.81}$$

where p and q run over the n occupied orbitals. These integrals are calculated in OpenMolcas and transformed to the common MO basis in which

the NOCI-F calculations in GronOR are done

$$\langle \hat{\mu}(k) \rangle = \sum_{i}^{L} \sum_{j}^{L} \langle b_i | \hat{\mu}(k) | b_j \rangle \sum_{p}^{N} D_{ip}^{I_Q \dagger} D_{pj}^{I_Q} \tag{3.82}$$

$$\langle \hat{Q}(k,l) \rangle = \sum_{i}^{L} \sum_{j}^{L} \langle b_j | \hat{Q}(k,l) | b_j \rangle \sum_{p}^{N} D_{ip}^{I_Q \dagger} D_{pj}^{I_Q} \tag{3.83}$$

After the calculation of the electronic part in the basis of the MEBFs the nuclear contribution given by the classic definition is added. The dipole is

$$\mu_{ij}(k) = \langle \Theta_i | \hat{\mu}(k) | \Theta_j \rangle + \sum_{i}^{\mathrm{n}} Z(r_k - r_{0k}) \quad k = 1,2,3 \tag{3.84}$$

and the quadrupole

$$Q_{ij}(k,l) = \langle \Theta_i | \hat{Q}(k,l) | \Theta_j \rangle + \sum_{i}^{\mathrm{n}} Z(r_k - r_{0k})(r_l - r_{0l}) \quad k,l = 1,2,3 \tag{3.85}$$

where Z is the nuclear charge and i runs over all n atoms. Usually, for $i = j$ the total contribution of the dipole is given

$$|\boldsymbol{\mu}_{ii}| = \sqrt{\sum_{k}^{3} \mu_{ii}^2(k)} \tag{3.86}$$

that is the dipole moment associated to an MEBF, whereas for $i \neq j$ the value μ_{ij} is known as transition dipole moment, and is often converted into an oscillator strength that expresses the probability of absorption or emission of electromagnetic radiation in transitions between energy levels

$$f_{ij} = \frac{2}{3} \left(H_{jj} - H_{ii} \right) |\boldsymbol{\mu}_{ij}|^2 \tag{3.87}$$

The $i = j$ components of the quadrupole moments are presented in traceless form with the transformation

$$\begin{pmatrix} Q'_{xx} \\ Q'_{xy} \\ Q'_{xz} \\ Q'_{yy} \\ Q'_{yz} \\ Q'_{zz} \end{pmatrix} = \begin{pmatrix} 1 & 0 & 0 & -0.5 & 0 & -0.5 \\ 0 & 1.5 & 0 & 0 & 0 & 0 \\ 0 & 0 & 1.5 & 0 & 0 & 0 \\ -0.5 & 0 & 0 & 1 & 0 & -0.5 \\ 0 & 0 & 0 & 0 & 1.5 & 0 \\ -0.5 & 0 & 0 & -0.5 & 0 & 1 \end{pmatrix} \begin{pmatrix} Q_{xx} \\ Q_{xy} \\ Q_{xz} \\ Q_{yy} \\ Q_{yz} \\ Q_{zz} \end{pmatrix} \tag{3.88}$$

This form is common in the literature partly because many experiments cannot detect the spherically-symmetric part of the quadrupole tensor.
The dipole and quadrupole moments are then obtained for the NOCI wavefunctions as linear combination of those of the MEBFs

$$\langle \Psi_A | \hat{\mu}(k) | \Psi_B \rangle = \sum_{ij} C_i^A C_j^B \langle \Theta_i | \hat{\mu}(k,l) | \Theta_j \rangle \tag{3.89}$$

$$\langle \Psi_A | \hat{Q}(k,l) | \Psi_B \rangle = \sum_{ij} C_i^A C_j^B \langle \Theta_i | \hat{Q}(k,l) | \Psi_j \rangle \tag{3.90}$$

where C_i^A and C_i^B are the NOCI coefficients of the two NOCI wave functions.

3.7.3 Spin Orbit Hamiltonian

To calculate the effect of spin-orbit coupling, GronOR follows the so-called Spin Orbit Mean Field (SOMF) approximation. This approach eliminates the need for explicit treatment of two-electron spin-orbit interactions by using effective one-electron spin-orbit coupling operators. To better understand this approach, it is necessary to first examine the one-particle Dirac equation and its extension to many-body systems. The upcoming text also explains the steps involved in transforming the original 4-component form of the equation to a decoupled 2-component expression through the Douglas-Kroll transformation, as well as the specifics of the subsequent mean field approximation.
The goal of formulating a relativistic Schrödinger equation is to quantize the relationship between energy and momentum, as expressed by the equation

$E^2 = p^2c^2 + m^2c^4$. This leads to the Klein-Gordon equation for a free particle in a four-dimensional coordinate space (x, y, z, t):

$$-\hbar^2 \frac{\partial^2}{\partial t^2}\Psi = -\hbar^2 c^2 \nabla^2 \Psi + m^2 c^2 \Psi \tag{3.91}$$

or in momentum form:

$$(-p_0^2 + \boldsymbol{p}^2 + m^2c^2)\Psi = 0 \tag{3.92}$$

where $p_0 = i\frac{\hbar}{c}\frac{\partial^2}{\partial t^2}$ and $\boldsymbol{p} = \hbar c \boldsymbol{\nabla}$. However, this equation has a drawback in that it is not a first-order equation in time. This means that one must make the choice of two initial conditions, one for Ψ and the other for its time first derivative Ψ', at some time $t = t_0$ that can result in a negative probability density ρ as discussed in the work of Dirac[3]. To overcome this issue, the Dirac equation is introduced as a way to factorize the above equation and transform it into a first-order equation in time. This ensures that only the initial condition for Ψ must be chosen so the wave function at any time determines the wave function at any other time. After factorization, the equation 3.91 becomes:

$$(-i\hbar\frac{\partial}{\partial t} + c\boldsymbol{\alpha}\cdot\boldsymbol{p} + \beta mc^2)(i\hbar\frac{\partial}{\partial t} + c\boldsymbol{\alpha}\cdot\boldsymbol{p} + \beta mc^2)\Psi = 0 \tag{3.93}$$

By applying the necessary restrictions for all $i, j \in 1, 2, 3$, $i \neq j$, to reproduce equation 3.92:

$$\alpha_j^2 = \beta^2 = 1, \quad \alpha_i\alpha_j + \alpha_j\alpha_i = 0 \quad \text{and} \quad \alpha_j\beta + \beta\alpha_j = 0 \tag{3.94}$$

Note that these relations are non-commutative, so they cannot be fulfilled with plain numbers. The minimum dimension required to solve equation 3.94 with Hermitian matrices is four. A possible choice for α and β is:

$$\alpha_j = \begin{pmatrix} 0 & \sigma_j \\ \sigma_j & 0 \end{pmatrix} \quad \text{and} \quad \beta = \begin{pmatrix} I_2 & 0 \\ 0 & -I_2 \end{pmatrix} \tag{3.95}$$

with I_2 representing a unit matrix of dimension 2 and the Pauli matrices σ:

$$\sigma_1 = \begin{pmatrix} 0 & 1 \\ 1 & 0 \end{pmatrix} \quad \sigma_2 = \begin{pmatrix} 0 & -i \\ i & 0 \end{pmatrix} \quad \sigma_3 = \begin{pmatrix} 1 & 0 \\ 0 & -1 \end{pmatrix} \tag{3.96}$$

The Dirac equation in Hamiltonian form is obtained as:

$$i\hbar\frac{\partial}{\partial t}\Psi = \hat{H}\Psi \quad \text{with} \quad \hat{H} = c\boldsymbol{\alpha}\cdot\boldsymbol{p} + \beta mc^2 \tag{3.97}$$

By introducing the gamma matrices,

$$\gamma^0 = \beta = \begin{pmatrix} I_2 & 0 \\ 0 & -I_2 \end{pmatrix} \tag{3.98}$$

$$\gamma^j = \beta\alpha_j = \begin{pmatrix} 0 & \sigma_j \\ -\sigma_j & 0 \end{pmatrix} \tag{3.99}$$

the equation can be simplified to:

$$(i\hbar\sum_{\mu=0}^{3}\gamma^\mu\frac{\partial}{\partial\mu} - mc)\Psi = 0 \tag{3.100}$$

and is often expressed in the literature using Einstein's summation convention for repeated indexes such that $\sum_\mu \gamma^\mu\frac{\partial}{\partial\mu} = \gamma^\mu\partial_\mu$

$$(i\hbar\gamma^\mu\partial_\mu - mc)\Psi = 0 \tag{3.101}$$

where

$$\Psi = \begin{pmatrix} \Psi_1 \\ \Psi_2 \\ \Psi_3 \\ \Psi_4 \end{pmatrix} \tag{3.102}$$

is the solution, called the Dirac spinor. Initially, the meaning of the four components of the wave function was unclear. However, it was found that the first two components Ψ_1 and Ψ_2 are dominant in the positive energy solutions and can be grouped into a 2-spinor, denoted as Ψ_+, which encodes the two possibilities for the spin of the particle. The third and fourth components Ψ_3 and Ψ_4, on the other hand, encode information about a negative energy solution with a positive probability density, known as an antiparticle and denoted as the Ψ_- 2-spinor. The information about both particles is coupled in the Dirac equation. The Dirac spinor can also be expressed as:

$$\Psi = \begin{pmatrix} \Psi_+ \\ \Psi_- \end{pmatrix} \qquad \Psi_+ = \begin{pmatrix} \Psi_1 \\ \Psi_2 \end{pmatrix} \quad \Psi_- = \begin{pmatrix} \Psi_3 \\ \Psi_4 \end{pmatrix} \tag{3.103}$$

However, Ψ_- becomes smaller in the positive energy solutions due to the term βmc^2 in the equation, which subtracts the mass and adds it in the first component:

$$\beta mc^2 = \begin{pmatrix} mc^2 I_2 & 0 \\ 0 & -mc^2 I_2 \end{pmatrix} \tag{3.104}$$

As a result, the Dirac wave function can be divided into large and small components, $\Psi_+ = \Psi_l$ and $\Psi_- = \Psi_s$, which are completely decoupled in the non-relativistic limit and differ by a ratio v/c in a relativistic treatment. The relativistic version of the many-body quantum mechanical problem is described by the Dirac-Coulomb-Breit Hamiltonian, which takes into account the magnetic Gaunt term and the retardation (finite speed of interaction) in addition to the Dirac and Coulomb interactions. It is represented as:

$$H^{\mathrm{DCB}} = \sum_i \hat{H}_i^{\mathrm{Dirac}} + \sum_{iK} \frac{1}{r_{iK}} + \frac{1}{2} \sum_{ij} \frac{1}{r_{ij}} + \frac{1}{2} \sum_{ij} \hat{H}_{ij}^{\mathrm{Breit}} \tag{3.105}$$

where $\hat{H}_i^{\mathrm{Dirac}}$ is the single-particle Dirac Hamiltonian, the second RHS terms represents the electron-nucleus interactions, and $\hat{H}_{ij}^{\mathrm{Breit}}$ is the Breit operator which accounts for the magnetic Gaunt term and retardation:

$$H_{ij}^{\mathrm{Breit}} = -\frac{1}{r_{ij}} \left[\alpha_i \cdot \alpha_j - \frac{(\alpha_i \cdot \boldsymbol{r}_{ij})(\alpha_j \cdot \boldsymbol{r}_{ij})}{2r_{ij}^2} \right] \tag{3.106}$$

To simplify this expression, the positive energy solutions of the Dirac equation are isolated by decoupling the two components of the Dirac spinor. This can be achieved through the Foldy-Wouthuysen (FW) or Douglas-Kroll (DK) transformation, resulting in the Breit-Pauli or Douglas-Kroll-Hess Hamiltonian, respectively. The FW transformation is applied to the Hamiltonian of the system by using a unitary transformation operator U, which is defined as follows:

$$\hat{U} = \begin{pmatrix} \frac{1}{\sqrt{1+\hat{\chi}^\dagger \hat{\chi}}} & \frac{1}{\sqrt{1+\hat{\chi}^\dagger \hat{\chi}}} \hat{\chi}^\dagger \\ -\frac{1}{\sqrt{1+\hat{\chi}^\dagger \hat{\chi}}} \hat{\chi} & \frac{1}{\sqrt{1+\hat{\chi}^\dagger \hat{\chi}}} \end{pmatrix} \tag{3.107}$$

where the operator $\hat{\chi}$ connects Ψ_+ and Ψ_-

$$\Psi_- = \hat{\chi}\Psi_+ \tag{3.108}$$

The transformed Hamiltonian $\hat{H}'$ is given by:

$$\hat{H}' = \hat{U}^\dagger \hat{H} \hat{U} = \begin{pmatrix} \hat{H}_+ & 0 \\ 0 & \hat{H}_- \end{pmatrix} \tag{3.109}$$

which is a diagonal matrix in the positive-energy and negative-energy basis, with the eigenvalues corresponding to the positive- and negative-energy states of the system. The exact form of the transformation can only be applied consistently for non-interacting particles, so approximations are often made.

The FW transformation has been used to simplify the Hamiltonian of a wide range of relativistic quantum mechanical systems, including atoms, molecules, and solids. It is particularly useful for systems with strong spin-orbit interactions, such as heavy atoms and transition metal compounds. It is also used in the study of the behavior of particles with relativistic speeds, such as in high energy physics and particle accelerators. The problem of the FW transformation is that it leads to an unbounded Hamiltonian which is variationally unstable. Applying the FW transformation to the DCB Hamiltonian in the absence of a magnetic field gives the Breit-Pauli Hamiltonian:

$$\hat{H}^{\mathrm{BP}} = H^{\mathrm{P}} + \sum_i \sum_{j>i} \left(g^{\mathrm{SOC}} + g_{ij}^{\mathrm{SOOC}} + g_{ij}^{\mathrm{SSC}} + g_{ij}^{\mathrm{Darwin}} + g_{ij}^{\mathrm{OOC}} \right) \tag{3.110}$$

where the terms are: Spin-Same-Orbit (SOC), Spin-Other-Orbit) (SOOC), Spin-Spin (SSC), Darwin Term (Darwin) and Orbit-Orbit (OCC). It can be shown that the spin orbit terms are the most energetically significant in the Breit-Pauli Hamiltonian, hence the Orbit-Orbit, Spin-Spin and Fermi contact terms can be neglected and the resulting spin-orbit part of the Hamiltonian is

$$\hat{H}_{\mathrm{SO}}^{\mathrm{BP}} = \frac{1}{2m^2c^2} \left(\sum_i \sum_I \frac{Z_I}{r_{iI}^3} \hat{\boldsymbol{l}}_{iI} \cdot \hat{\mathbf{s}}_i - \sum_i \sum_{j \neq i} \frac{1}{r_{ij}^3} \hat{\boldsymbol{l}}_{ij} \cdot (\hat{\mathbf{s}}_i + 2\hat{\mathbf{s}}_j) \right) \tag{3.111}$$

where $\boldsymbol{l}$ and $\boldsymbol{s}$ are the angular momentum and spin operators acting on a single electron i. This operator is unbounded from below due to the presence of coupling with the positronic states. This instability can be addressed through the use of the Douglas-Kroll (DK) transformation. The DK transformation differs from the Foldy-Wouthuysen (FW) transformation in the way it handles the spin-orbit coupling term. The FW transformation eliminates coupling between positive-energy and negative-energy states through a unitary transformation based on the spin operator, while the DK transformation eliminates coupling through a unitary transformation based on the angular momentum operator.
By implementing these modifications, the Hamiltonian is made bounded from below and a more accurate description of the electronic structure of a system can be obtained. The result of applying the Douglas-Kroll transformation is the Douglas-Kroll-Hess (DKH) Hamiltonian:

$$\hat{H}^{+}_{\mathrm{SO}} = 2c^2 \sum_i \sum_I \frac{A_i}{E_i + mc^2} \frac{Z_I}{r^3_{iI}} \hat{\boldsymbol{l}}_{iI} \cdot \hat{\boldsymbol{s}}_i \frac{A_i}{E_i + mc^2} \tag{3.112}$$

$$-2c^2 \sum_i \sum_{i \neq j} \frac{A_i A_j}{E_i + mc^2} \times \left[\frac{1}{r^3_{ij}} \hat{\boldsymbol{s}}_{ij} \cdot (\hat{\boldsymbol{s}}_i + 2\hat{\boldsymbol{s}}_j) \right] \frac{A_i A_j}{E_i + mc^2} \tag{3.113}$$

where E_i is the relativistic kinetic energy operator $E_i = \sqrt{p_i^2 c^2 + m^2 c^4}$ and A_i is the kinematic factor

$$A_i = \sqrt{\frac{E_i + mc^2}{2E_i}} \tag{3.114}$$

It only differs from $\hat{H}^{\mathrm{SO}}_{\mathrm{BP}}$ by the kinematical factors which effectively cut off the r^{-3} singularity of the Hamiltonian. The Hamiltonian described above is separated in a one electron 3.112 and a two electron part 3.113. The one electron part 3.112 can be expressed, as a effective operator consisting of the product of the radial part and the spin part

$$\hat{H}^{+}_{\mathrm{SO}}(i) \equiv \sum_i \xi(\boldsymbol{r}_i)\, \hat{\boldsymbol{l}}_i \cdot \hat{\boldsymbol{s}}_i \tag{3.115}$$

where

$$\xi(\boldsymbol{r}_i) = 2c^2 \sum_i \frac{A_i}{E_i + mc^2} \frac{Z}{r_i^3} \frac{A_i}{E_i + mc^2} \tag{3.116}$$

is the radial part and for simplicity the summation index I over the nuclei is omitted. The operator 3.115 is mixed, that is, it affects both spatial and spin parts of an electronic wave function. In the literature, the expectation value of such operator comes expressed using the second-quantization formalism, that is, in terms of the creation and annihilation operator. A general evaluation of a mixed operator in second quantization is[5] given by the integral

$$f_{pq} = \sum_{pq\sigma\tau} \int \phi_p(\boldsymbol{r})^* \sigma(m_s)^* \hat{f}(\boldsymbol{r}, m_s) \phi_q(\boldsymbol{r}) \tau(m_s) d^3 r dm_s \hat{a}^\dagger_{p\sigma} \hat{a}_{q\tau} \tag{3.117}$$

substituting $\hat{f}$ by the expression of the effective one-electron spin orbit operator 3.115 results in the integral

$$H^+_{\mathrm{SO}} = \sum_{pq\sigma\tau} \int \phi_p(\boldsymbol{r})^* \sigma(m_s)^* \xi(\boldsymbol{r})\, \hat{\boldsymbol{l}} \cdot \hat{\mathbf{s}}\, \phi_q(\boldsymbol{r}) \tau(m_s) d^3 r dm_s \hat{a}^\dagger_{p\sigma} \hat{a}_{q\tau} \tag{3.118}$$

The spatial part is covered by the introduction of the integral V_{pq}

$$V_{pq}(\mu) = \frac{1}{2} \int \phi_p(\boldsymbol{r})^* \xi(r) \hat{l}(\mu) \phi_q(\boldsymbol{r}) d^3 r \tag{3.119}$$

The spin part of the integral corresponds to the expectation value of the spin operator $\hat{\mathbf{s}}$ whose components act on a single electron as

$$\hat{s}_+ \beta = \alpha, \qquad \hat{s}_+ \alpha = 0 \tag{3.120}$$

$$\hat{s}_- \beta = 0, \qquad \hat{s}_- \alpha = \beta \tag{3.121}$$

$$\hat{s}_z \beta = -\frac{1}{2}\beta, \qquad \hat{s}_z \alpha = \frac{1}{2}\alpha \tag{3.122}$$

and the x and y components given by

$$\hat{s}_x = \frac{1}{2}(\hat{s}_+ + \hat{s}_-) \tag{3.123}$$

$$\hat{s}_y = \frac{1}{2i}(\hat{s}_+ - \hat{s}_-) \tag{3.124}$$

whose integrals evaluated on the spin part are

$$\sum_{pq\sigma\tau}\int \sigma(m_s)^* s_x \tau(m_s) dm_s \hat{a}^\dagger_{p\sigma}\hat{a}_{q\tau} = \frac{1}{2}\sum_{\sigma\tau}(\delta_{\sigma\alpha}\delta_{\tau\beta}+\delta_{\sigma\alpha}\delta_{\tau\beta})\sum_{pq}\hat{a}^\dagger_{p\sigma}\hat{a}_{q\tau} = \frac{1}{2}\sum_{pq}(\hat{a}^\dagger_{p\alpha}\hat{a}_{q\beta}+\hat{a}^\dagger_{p\beta}\hat{a}_{q\alpha}) \quad (3.125)$$

$$\sum_{pq\sigma\tau}\int \sigma(m_s)^* s_y \tau(m_s) dm_s \hat{a}^\dagger_{p\sigma}\hat{a}_{q\tau} = \frac{1}{2i}\sum_{\sigma\tau}(\delta_{\sigma\alpha}\delta_{\tau\beta}-\delta_{\sigma\alpha}\delta_{\tau\beta})\sum_{pq}\hat{a}^\dagger_{p\sigma}\hat{a}_{q\tau} = \frac{1}{2i}\sum_{pq}(\hat{a}^\dagger_{p\alpha}\hat{a}_{q\beta}-\hat{a}^\dagger_{p\beta}\hat{a}_{q\alpha}) \quad (3.126)$$

$$\sum_{pq\sigma\tau}\int \sigma(m_s)^* s_z \tau(m_s) dm_s \hat{a}^\dagger_{p\sigma}\hat{a}_{q\tau} = \frac{1}{2}\sum_{\sigma\tau}\delta_{\sigma\tau}(\delta_{\sigma\alpha}-\delta_{\sigma\beta})\sum_{pq}\hat{a}^\dagger_{p\sigma}\hat{a}_{q\tau} = \frac{1}{2}\sum_{pq}(\hat{a}^\dagger_{p\alpha}\hat{a}_{q\beta}-\hat{a}^\dagger_{p\beta}\hat{a}_{q\alpha}) \quad (3.127)$$

these expressions lead to the following expression of the Hamiltonian for spin-orbit coupling in terms of V integrals and second-quantization operators:

$$\hat{H}^+_{\mathrm{SO}} = \frac{1}{2}V_{pq}(x)\sum_{pq}(\hat{a}^\dagger_{p\alpha}\hat{a}_{q\beta}+\hat{a}^\dagger_{p\beta}\hat{a}_{q\alpha}) + \frac{1}{2i}V_{pq}(y)\sum_{pq}(\hat{a}^\dagger_{p\alpha}\hat{a}_{q\beta}-\hat{a}^\dagger_{p\beta}\hat{a}_{q\alpha}) + \frac{1}{2}V_{pq}(z)\sum_{pq}(\hat{a}^\dagger_{p\alpha}\hat{a}_{q\beta}-\hat{a}^\dagger_{p\beta}\hat{a}_{q\alpha}) \quad (3.128)$$

All of these excitation terms can be grouped using a basis set of irreducible spin tensor operators $\hat{T}^{[k]}(\mu)$. These operators do transform under rotations of spin space as spin eigenfunctions with spin k and spin projection μ

$$\left[\hat{S}_\pm, \hat{T}^{[k]}(\mu)\right] = \sqrt{k(k+1)-\mu(\mu\pm 1)}\hat{T}^{[k]}(\mu) \quad (3.129)$$

$$\left[\hat{S}_z, \hat{T}^{[k]}(\mu)\right] = M\hat{T}^{[k]}(\mu) \quad (3.130)$$

thus ensuring that the resulting wave function under the action of the spin orbit operator remains as a spin eigenfunction. Expression 3.128 contains only single excitations, and therefore, the description only requires the $k = 1$ triplet spin tensor operators acting over spin orbitals by means of excitations $\hat{a}^{\dagger}_{p\sigma}\hat{a}_{q\tau}$. These operators are usually defined as

$$\hat{E}_{pq} = \hat{a}^{\dagger}_{p\alpha}\hat{a}_{q\alpha} + \hat{a}^{\dagger}_{p\beta}\hat{a}_{q\beta} \tag{3.131}$$

$$\hat{T}^{[1]}_{pq}(1) = -\hat{a}^{\dagger}_{p\alpha}\hat{a}_{q\beta} \tag{3.132}$$

$$\hat{T}^{[1]}_{pq}(0) = \frac{1}{\sqrt{2}}\left(\hat{a}^{\dagger}_{p\alpha}\hat{a}_{q\alpha} - \hat{a}^{\dagger}_{p\beta}\hat{a}_{q\beta}\right) \tag{3.133}$$

$$\hat{T}^{[1]}_{pq}(-1) = \hat{a}^{\dagger}_{p\beta}\hat{a}_{q\alpha} \tag{3.134}$$

but as the AMFI integrals are in the Cartesian basis, the Cartesian projections $(T(x), T(y), T(z))$ of these operators are used instead

$$\left(\hat{T}^{[1]}_{pq}(x), \hat{T}^{[1]}_{pq}(y), \hat{T}^{[1]}_{pq}(z)\right) = \left(\hat{T}^{[1]}_{pq}(1), \hat{T}^{[1]}_{pq}(-1), \hat{T}^{[1]}_{pq}(0)\right)\begin{pmatrix} -\frac{1}{2} & -\frac{1}{2i} & 0 \\ \frac{1}{2} & -\frac{1}{2i} & 0 \\ 0 & 0 & \frac{1}{\sqrt{2}} \end{pmatrix}$$

$$\hat{T}^{[1]}_{pq}(x) = \frac{1}{2}\left(\hat{a}^{\dagger}_{p\alpha}\hat{a}_{q\beta} + \hat{a}^{\dagger}_{p\beta}\hat{a}_{q\alpha}\right) \tag{3.135}$$

$$\hat{T}^{[1]}_{pq}(y) = \frac{1}{2i}\left(\hat{a}^{\dagger}_{p\alpha}\hat{a}_{q\beta} - \hat{a}^{\dagger}_{p\beta}\hat{a}_{q\alpha}\right) \tag{3.136}$$

$$\hat{T}^{[1]}_{pq}(z) = \frac{1}{2}\left(\hat{a}^{\dagger}_{p\alpha}\hat{a}_{q\alpha} - \hat{a}^{\dagger}_{p\beta}\hat{a}_{q\beta}\right) \tag{3.137}$$

leading to the irreducible tensor representation of the one particle spin-orbit operator

$$\hat{H}^{1\,\mathrm{el}}_{\mathrm{SO}} = \sum_{pq}\left(V_{pq}(x)\hat{T}_{pq}(x) + V_{pq}(y)\hat{T}_{pq}(y) + V_{pq}(z)\hat{T}_{pq}(z)\right) \tag{3.138}$$

The same procedure can be repeated with the two electron part 3.113

$$\hat{H}^{2\,\mathrm{el}}_{\mathrm{SO}} = \sum_{pqrs}\left(W_{pqrs}(x)\hat{T}_{pqrs}(x) + W_{pqrs}(y)\hat{T}_{pqrs}(y) + W_{pqrs}(z)\hat{T}_{pqrs}(z)\right) \tag{3.139}$$

where the two electron excitation operators are defined as

$$\hat{T}_{pqrs}(\mu) = \hat{T}_{pq}(\mu)\hat{E}_{rs} - \delta_{rq}\hat{T}_{ps}(\mu) \tag{3.140}$$

However, the two electron part can be fairly well approximated by an effective one electron Hamiltonian, e.g. as done by Hess, Marian, et al.[6]. This involves the contraction of the two electron integrals W_{pqrs} over a one-particle reference density matrix to avoid the explicit calculation of the two electron part. In this so-called Spin-Orbit Mean Field approximation for the two-electron spin orbit interaction the variable occupations of the partially filled orbitals k is replaced with average occupation numbers n_k, defined as p/m (p particles in m partially occupied orbitals). A matrix element of this effective one-electron Hamiltonian is

$$\begin{aligned}\langle i(1)|\hat{H}^{\mathrm{mf}}_{\mathrm{SO}}|j(1)\rangle &= \langle i(1)|\hat{h}_{\mathrm{SO}}(1)|j(1)\rangle \\ +\frac{1}{2}\sum_k n_k \Big[2\langle i(1)k(2)|\hat{H}_{\mathrm{SO}}(1,2)|j(1)k(2)\rangle &- 3\langle k(1)i(2)|\hat{H}_{\mathrm{SO}}(1,2)|j(1)k(2)\rangle \\ &- 3\langle i(1)k(2)|\hat{H}_{\mathrm{SO}}(1,2)|k(1)j(2)\rangle \Big]\end{aligned} \tag{3.141}$$

where $\hat{h}_{\mathrm{so}}(1)$ and $\hat{H}_{\mathrm{SO}}(1,2)$ represent the one- and two-electron terms, respectively. There is a second approximation based on the r^{-3}-dependence of the spin-orbit operators and only regions closer to the atomic nucleus are expected to contribute. Thus, the elimination of the integrals of more than one atomic center should not lead to serious errors, an idea which have been confirmed in the studies such as the named above. Restricting the integrals to one-center only makes that the one-particle reference density matrix (the k-orbitals in the equation) are in fact average atomic densities, which can be tabulated for each element of the periodic table. Therefore, all contributions can be included in the one-electron spin-orbit operator $\hat{H}^{1\,\mathrm{el}}_{\mathrm{SO}}$ 3.138 through the terms $V_{pq}(\mu)$ which are now called Atomic Mean Field Integrals (AMFI) calculated in the Seward module of OpenMolcas alongside the standard one- and two-electron integrals. These integrals are transformed to the common MO basis and used as input for GronOR

$$V_{ij}(\mu) = \sum_{pq} V_{pq}(\mu) D^{\dagger}_{ip} D_{qj} \tag{3.142}$$

where V_{ij} are the integrals in the common basis. The following procedure is used to calculate the matrix elements involving the products $V_{ij}(\mu)\hat{T}^{[1]}_{ij}(\mu)$ evaluated on the determinant pairs. The code takes advantage of the Wigner-Eckart theorem that asserts that the $(2S'+1)(2S''+1)(2\kappa+1)$ spin-orbit matrix elements between two states A and B with total spin S', S'' and spin projection M', M'' respectively can be obtained from a single reduced matrix element, non-dependent of M' and M'', in terms of the Wigner 3-j symbols:

$$\begin{aligned}&\langle A\ S'\ M'|\hat{T}^{[\kappa]}(\mu)|B\ S''\ M''\rangle \\ &\qquad = (-1)^{S''+M'-\kappa}\begin{pmatrix} S'' & \kappa & S' \\ M'' & \mu & M' \end{pmatrix}\langle A\ S'\|\hat{\boldsymbol{T}}^{[\kappa]}\|B\ S''\rangle \end{aligned} \quad (3.143)$$

which, expressing the 3-j in terms of Clebsch-Gordan coefficients is

$$\begin{aligned}&\langle A\ S'\ M'|\hat{T}^{[\kappa]}(\mu)|B\ S''\ M''\rangle \\ &\qquad = \frac{(-1)^{S''+M'-\kappa}}{\sqrt{2S''+1}}\langle S''\ M''\ \kappa\ \mu|S'\ M'\rangle\langle A\ S'\|\hat{\boldsymbol{T}}^{[\kappa]}\|B\ S''\rangle \end{aligned} \quad (3.144)$$

The last term is called the Wigner-Eckart reduced one-particle transition density matrix, denoted as Γ^{AB}, which does not depend on M' nor M''. It is expressed in terms of any spin tensor matrix element as

$$\begin{aligned}\Gamma^{AB}_{ij} &= \langle A\ S'\|\hat{\boldsymbol{T}}^{[\kappa]}_{ij}\|B\ S''\rangle \\ &= (-1)^{S''+M'-\kappa}\frac{\sqrt{2S''+1}\,\langle A\ S'\ M'|\hat{T}^{[\kappa]}(\mu)|B\ S''\ M''\rangle}{\langle S''\ M''\ \kappa\ \mu|S'\ M'\rangle} \end{aligned} \quad (3.145)$$

Consider a pair of Slater determinants Φ_a and Φ_b belonging to different MEBFs Θ_A and Θ_B respectively. The value of Γ^{ab} for the pair of determinants is derived in GronOR by computing exclusively the $\hat{T}^{[1]}(0)$ matrix element. Its value is only non-zero if $M' = M''$ and $|S' - S''| \leq 1$ from

the C-G coefficients. There are three options that fulfill both conditions

$$\Gamma^{ab} = \sum_{ij} \frac{\sqrt{2S+3}\,\langle \Phi_a\ S+1\ S|\hat{T}^{[1]}_{ij}(0)|\Phi_b\ S\ S\rangle}{\langle S\ S\ 1\ 0|S+1\ S\rangle} \tag{3.146}$$

$$\Gamma^{ab} = \sum_{ij} \frac{\sqrt{2S+1}\,\langle \Phi_a\ S\ S|\hat{T}^{[1]}_{ij}(0)|\Phi_b\ S\ S\rangle}{\langle S\ S\ 1\ 0|S\ S\rangle} \tag{3.147}$$

$$\Gamma^{ab} = \sum_{ij} \frac{-\sqrt{2S-1}\,\langle \Phi_a\ S-1\ S-1|\hat{T}^{[1]}_{ij}(0)|\Phi_b\ S\ S-1\rangle}{\langle S\ S-1\ 1\ 0|S-1\ S-1\rangle} \tag{3.148}$$

As GronOR only stores the MEBFs with the highest spin projection $M = S$, the lower $M < S$ components must be obtained on-the-fly by applying the S_- operator to Φ_a or Φ_b depending which one has the greatest M. The spin tensor matrix element present in the expressions is computed according to 3.133

$$\begin{aligned}
&\langle \Phi_a\ S'\ M'|\hat{T}^{[1]}_{ij}(0)|\Phi_b\ S''\ M''\rangle \\
&\qquad = -\frac{1}{2}\langle \Phi_a\ S'\ M'|\hat{a}^\dagger_{i\alpha}\hat{a}_{j\alpha} - \hat{a}^\dagger_{i\beta}\hat{a}_{j\beta}|\Phi_b\ S''\ M''\rangle \\
&= \frac{1}{2}\left[\langle \Phi_a\ S'\ M'|(\Phi_b)^{i\beta}_{j\beta}\ S''\ M''\rangle - \langle \Phi_a\ S'\ M'|(\Phi_b)^{i\alpha}_{j\alpha}\ S''\ M''\rangle\right] \\
&\qquad = \frac{1}{2}\left[\left(\prod_m \lambda_m\right)^{i\beta}_{j\beta} - \left(\prod_m \lambda_m\right)^{i\alpha}_{j\alpha}\right]
\end{aligned} \tag{3.149}$$

which means; 1: for each i, j in the active space generate the new excited determinants $(\Phi_b)^{i\alpha}_{j\alpha}$, $(\Phi_b)^{i\beta}_{j\beta}$ as a result of applying the $T^{[1]}(0)$ operator; 2: calculate the overlap between Φ_a and the new determinants and 3: compute the difference between β and α contributions. This calculation is the most expensive of the process as it carries a SVD performed on the GPU for each i, j because the transformations U and V that decompose the overlap matrix are in general different for each excitation. Having computed this term the obtainment of Γ^{ab} is trivial. The reduced density Γ^{ab}_{ij} is contracted with the AMFI integrals V_{ij} in the calculation of the one-electron properties (step 2

in figure 3.5)

$$V_{ab}(x) = \sum_{ij} \Gamma_{ij}^{ab} V_{ij}(x) \tag{3.150}$$

$$V_{ab}(y) = \sum_{ij} \Gamma_{ij}^{ab} V_{ij}(y) \tag{3.151}$$

$$V_{ab}(z) = \sum_{ij} \Gamma_{ij}^{ab} V_{ij}(z) \tag{3.152}$$

The contributions from all determinant pairs are accumulated in the same way as the other one-electron properties to get the total contribution of the MEBF pair Θ_A, Θ_B.

$$V_{AB}(x, y, z) = \sum_{ab} V_{ab}(x, y, z) \tag{3.153}$$

grouped in the matrices $\{V(x), V(y), V(z)\}$ in the MEBF basis. These scalar quantities are sufficient to form all the $(2S'+1)(2S''+1)$ Spin Orbit Hamiltonian matrix elements over the $(2S'+1)(2S''+1)$ pairs of spin components of the MEBFs by applying the result of the WE theorem 3.143 to the Cartesian form of the triplet spin tensors. Then, the expression of the Hamiltonian 3.138 matrix element for two MEBFs Θ_A and Θ_B becomes

$$\begin{aligned}\langle \Theta_A\ S'\ M'|\hat{H}_{SO}|\Theta_B\ S''\ M''\rangle = \frac{(-1)^{S''+M'-\kappa}}{\sqrt{2S''+1}} \\ \times\Bigg(\frac{1}{2}\left[\langle S''\ M''\ 1\ -1|S'\ M'\rangle - \langle S''\ M''\ 1\ 1|S'\ M'\rangle\right] V_{AB}(x) \\ -\frac{1}{2i}\left[\langle S''\ M''\ 1\ 1|S'\ M'\rangle + \langle S''\ M''\ -1\ 1|S'\ M'\rangle\right] V_{AB}(y) \\ +\frac{1}{\sqrt{2}}\langle S''\ M''\ 1\ 0|S'\ M'\rangle\, V_{AB}(z)\Bigg)\end{aligned} \tag{3.154}$$

that gives the following non-zero H^{SO} terms

$$\begin{aligned}\langle \Theta_A\ S\ M|\hat{H}_{\mathrm{SO}}|\Theta_B\ S+1\ M\pm 1\rangle \\ = -\frac{\sqrt{(S\pm M+1)(S\pm M+2)}}{2}\left(\pm V_{AB}(x) + iV_{AB}(y)\right)\end{aligned}$$

$$\langle \Theta_A\ S\ M|\hat{H}_{\mathrm{SO}}|\Theta_B\ S+1\ M\rangle = \sqrt{(S+1)^2 - M^2}\ V_{AB}(z)$$

$$\langle \Theta_A\ S\ M|\hat{H}_{\mathrm{SO}}|\Theta_B\ S\ M\pm 1\rangle = -\frac{\sqrt{(S\mp M)(S\pm M+1)}}{2}\left(\pm V_{AB}(x) + iV_{AB}(y)\right)$$

$$\langle \Theta_A\ S\ M|\hat{H}_{\mathrm{SO}}|\Theta_B\ S\ M\rangle = MV_{AB}(z)$$

$$\langle \Theta_A\ S\ M|\hat{H}_{\mathrm{SO}}|\Theta_B\ S-1\ M\pm 1\rangle = -\frac{\sqrt{(S\mp M)(S\mp M-1)}}{2}\left(\pm V_{AB}(x) + iV_{AB}(y)\right)$$

$$\langle \Theta_A\ S\ M|\hat{H}_{\mathrm{SO}}|\Theta_B\ S-1\ M\rangle = \sqrt{S^2 - M^2}\ V_{AB}(z)$$

This part of the code does not carry a significant computational cost and is carried out serially. The complete Hamiltonian with all SO contributions can be visualized in blocks of multiplicity. The diagonal $(2S+1)\times(2S+1)$ blocks contain the interaction terms between the states of the same spin S number and different M and the spin orbit coupling terms between $|SM\rangle$ and $|SM\pm 1\rangle$ states. The sub-diagonal blocks are pure Spin Orbit contributions between different spin $S \neq S'$ states.

3.7.4 Next steps

A next step in GronOR involve the implementation of an efficient second quantization algorithm for the calculation of transition density matrices. A possible choice is to implement the Generalized non-orthogonal Wick's theorem

Taking advantage of Generalized Wick's theorem

The implementation of Generalized Wick's theorem can improve greatly the current state of GronOR in several stages of the calculation,
The 1-TDM matrix elements $\langle|\hat{a}_p^\dagger \hat{a}_q|\rangle$ where the $\hat{a}$'s are MO creation and annihilation operators can be used as a general starting point for computing

all kind of one-body operators in the second quantization formalism. In GronOR the code only uses it for computing the NTOs in the setup stage and in the calculation of the Wigner-Eckart reduced density matrix.
At the moment, 1-TDM matrix elements between non-orthogonal configurations is computed by exciting the left determinant and computing the overlap with the right determinant by a corresponding orbital transformation carried out on the GPUs. Instead two different orbital sets x and w as in the references[2] and[1], GronOR works in the non-orthogonal common MO basis in the whole calculation so it is safe to denote as $\hat{a}_p^\dagger \hat{a}_q$ the creation and annihilation operators in this basis and there is no need to use the pre-script notation ^{x,w}. The 1-TDM matrix elements between two different configurations Φ_1 and Φ_2 that can belong to different CASSCF expansion type MEBFs Θ_1 and Θ_2

$$T_{pq} = \langle \Phi_1 | \overbrace{\hat{a}_p^\dagger \hat{a}_q} | \Phi_2 \rangle = \tilde{S}_{12} X_{qp} \tag{3.155}$$

and for example, an excited term

$$\begin{aligned} T_{pq} = \left\langle (\Phi_1)_i^a \middle| \hat{a}_p^\dagger \hat{a}_q \middle| \Phi_2 \right\rangle &= \langle \Phi_2 | \hat{a}_i^\dagger \hat{a}_a \hat{a}_p^\dagger \hat{a}_q | \Phi_2 \rangle \\ &= \langle \Phi_1 | \overbrace{\hat{a}_i^\dagger \hat{a}_a} \overbrace{\hat{a}_p^\dagger \hat{a}_q} | \Phi_2 \rangle + \langle \Phi | \overbrace{\hat{a}_i^\dagger \hat{a}_a \hat{a}_p^\dagger \hat{a}_q} | \Phi_2 \rangle \\ &= \tilde{S}_{12} \sum_{\substack{\omega_1 \omega_2 \\ \omega_1 + \omega_2 = \omega}} \left(X_{ai}^{(\omega_1)} X_{qp}^{(\omega_2)} - X_{iq}^{(\omega_1)} X_{ap}^{(\omega_2)} \right) \end{aligned} \tag{3.156}$$

A strategy could be to, from Θ_1 and Θ_2, choose the configurations Φ_1 and Φ_2 as references and write the rest as strings $\hat{A}$ and $\hat{B}$ of excitation pairs of operators $\hat{a}^\dagger \hat{a}$ of arbitrary length $\hat{A}, \hat{B} \sim \hat{a}^\dagger \ldots \hat{a}$ that act on these references

$$|\Theta_1\rangle = \left(\sum_i c_i \hat{A}_i \right) |\Phi_1\rangle \tag{3.157}$$

$$|\Theta_2\rangle = \left(\sum_i d_i \hat{B}_i \right) |\Phi_2\rangle \tag{3.158}$$

with $A_0 = B_0 = \hat{I}$. Therefore, one can deduct the expressions of all kind of matrix elements of two MEBFs as products of contractions as states the Generalized Wick's theorem.

References

[1] H. G. A. Burton. “Generalized nonorthogonal matrix elements for arbitrary excitations”. In: *arXiv e-prints*, arXiv:2208.10208 (2022), arXiv:2208.10208.

[2] H. G. A. Burton. “Generalized nonorthogonal matrix elements: Unifying Wick’s theorem and the Slater-Condon rules”. In: *The Journal of Chemical Physics* 154.14 (2021), p. 144109.

[3] P. A. M. Dirac and R. H. Fowler. “The quantum theory of the electron”. In: *Proceedings of the Royal Society of London. Series A, Containing Papers of a Mathematical and Physical Character* 117.778 (1928), pp. 610–624.

[4] N. C. Handy. “Multi-root configuration interaction calculations”. In: *Chemical Physics Letters* 74.2 (1980), pp. 280–283.

[5] T. Helgaker and J. O. P. Jørgensen. *Molecular Electronic Structure Theory*. Chichester: John Wiley & Sons, LTD, 2000.

[6] B. A. Hess et al. “A mean-field spin-orbit method applicable to correlated wavefunctions”. In: *Chemical Physics Letters* 251.5 (1996), pp. 365–371.

[7] G. Li Manni et al. “The OpenMolcas Web: A Community-Driven Approach to Advancing Computational Chemistry”. In: *Journal of Chemical Theory and Computation* (2023).

[8] A. Sánchez-Mansilla et al. “On the role of dynamic electron correlation in non-orthogonal configuration interaction with fragments”. In: *Phys. Chem. Chem. Phys.* 24 (19 2022), pp. 11931–11944.

[9] Zuo, L. and Humbert, M. and Esling, C. “An effective algorithm for calculation of the Clebsch–Gordan coefficients”. In: *Journal of Applied Crystallography* 26.2 (1993), pp. 302–304.

Chapter 4

Applications

4.1 Frozen orbitals

This section is about a practical case in where freezing the core orbitals can reduce significantly the size of the two-electron integrals file and the amount of required computational time. The case of study is a Diketopyrrolopyrrole (DPP) dimer (Figure 4.2), a known singlet fission candidate. Separate CAS(6,6)SCF calculations with ano-s basis set (Table 4.1) of the ground-state S_0 and the first excited S_1 have been carried out for each fragment to be used as input for GronOR. The total number of orbitals in each fragment MO basis set is 32 inactive + 6 of the active space. For this comparison, the 1s orbitals of each atom have been frozen, being 10 in total for each fragment.
Table 4.3 shows a speedup of a factor $2 \sim 3$ and a memory saving of a factor ~ 2, while Table 4.2 shows that relative energies are almost the same. While these factors of speedup depend on the size of the system (number of atoms, active space, basis set...) it has been proven that freezing the core orbitals entails big savings in memory usage and computation time.

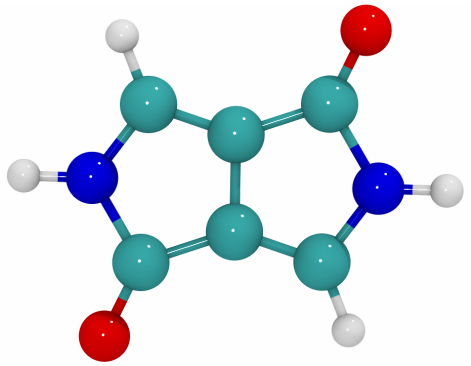

Figure 4.1: Diketopyrrolopyrrole (DPP) molecule

Table 4.1: CAS(6,6)SCF relative energies of the DPP molecule.

State	ΔE (eV)
S_0	0.00
S_1	10.57

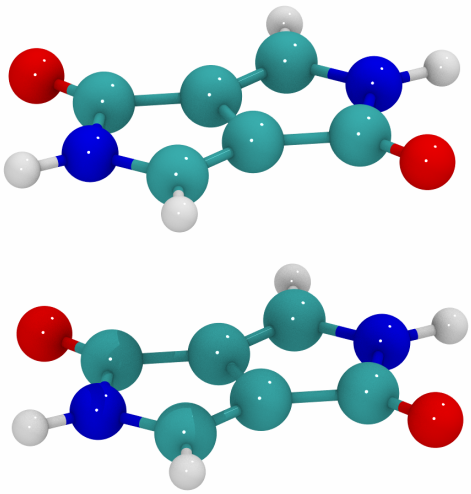

Figure 4.2: Diketopyrrolopyrrole (DPP) dimer.

Table 4.2: Energies of diabatic states with and without freezing the 1s orbitals for the NVidia V100 and A30 GPUs.

# frozen orbitals	$\Delta E(S_0S_1)$(eV)	$\Delta E(S_1S_0)$ (eV)	$\Delta E(S_1S_1)$ (eV)
0	4.91	4.91	9.89
10+10	4.89	4.89	9.84

Table 4.3: Timings with and without freezing the 1s orbitals for the NVidia V100 and A30 GPUs.

# frozen MO	Size 2-el. (Mb)	V100 Δt (s)	A30 Δt (s)
0	211	60.30	55.36
10+10	110	22.74	25.69

4.2 Model calculations of delocalized orbitals

This section contains an analysis of the electronic coupling in various ensembles of singlet fission chromophores. Some examples of such chromophores are the larger acenes like tetracene and pentacene, indolonaphtherydine derivatives, perylenediimides, among others. The primary goal is to establish to what extent exciton delocalization over the chromophores affects the electronic coupling between the excited singlet state and the singlet-coupled double triplet state. For that purpose, a simple Many Electron Tight Binding (METB) model that parametrizes the coupling γ is built. Using a localized or delocalized basis for the model Hamiltonian, the transition probability is proportional to the average of the squared couplings between the initial state and the various accessible final states of the SF ensemble, considering two different scenarios for the SF decay pathways. After the estimation of the transition probabilities in both a localized and delocalized description for different geometries, the results are verified with NOCI calculations in order see if the conclusions derived using the simple model are meaningful.
The METB model is based on the following assumptions: the many electron wave functions are orthogonal and only nearest neighbors interact with each other,

$$\langle i|j\rangle = \delta_{ij} \tag{4.1}$$

$$\langle S(i)|\hat{H}|^1TT(jk)\rangle = \gamma\delta_{ij} \tag{4.2}$$

that is, the coupling is γ between a S_1 and a ^1TT state if molecule i is one of the triplets of the combination, which means that i must be j or k.
The following scenarios are evaluated: (i) from the lowest singlet to the lowest biexcitonic state, (ii) from the lowest singlet to all ^1TT states, (iii) from all excited singlets to all biexcitonic singlets ^1TT.

4.2.1 A stack of molecules on a line

The first topology to deal with is an ensemble of an increasing number of chromophores in a stack as shown in Figure 4.3 where dots represent molecules of any singlet fission candidate. We start with two interacting molecules. In the singlet fission setup, a singlet excited state S_1 is produced on one molecule and is combined with a neighbor in the ground state S_0. This state is denoted as S_1S_0. Subsequently, energy transfer from the excited molecule to its neighbor leads to two resultant triplet states T_1, which are initially coupled into a singlet biexciton ${}^1TT$. Therefore, in the localized description of the ensembles, the set of many-electron basis functions (MEBF) consists on excited singlets for each molecule and a singlet coupled triplet for all pairs of neighboring molecules.
Starting with two molecules, the states to consider in the localized description are

$$|S_1^A S_0^B\rangle$$
$$|S_0^A S_1^B\rangle$$
$${}^1|T_1^A T_1^B\rangle$$

Where as mentioned above, the triplets T_1^A, T_1^B are coupled into a biexcitonic singlet state. The superscript "^{1}" will be omitted in the notation for clarity. In this initial localized description, the coupling matrix elements of interest are

$$\langle S_1^A S_0^B|\hat{H}|{}^1T_1^A T_1^B\rangle = \langle S_0^A S_1^B|\hat{H}|T_1^A T_1^B\rangle = \gamma \tag{4.3}$$

Next, the coupling is determined but now considering delocalization of the states over the entire system. Obviously, there is no delocalization of the ${}^1TT$ state when only two molecules are considered. Taking the interactions

Figure 4.3: Line scheme for the model.

between neighboring S_1 excitations to be negative, the delocalized excited singlet states are, in order of energy

$$S^{(1)} = \frac{1}{\sqrt{2}}(\,|S_1^A S_0^B\rangle + |S_0^A S_1^B\rangle) \tag{4.4}$$

$$S^{(2)} = \frac{1}{\sqrt{2}}(\,|S_1^A S_0^B\rangle - |S_0^A S_1^B\rangle) \tag{4.5}$$

which means that the only non-zero interaction arises from the singlet $S^{(1)}$ as follows

$$\langle S^{(1)}|\hat{H}|TT\rangle = \frac{1}{\sqrt{2}}(\,\langle S_1^A S_0^B|\hat{H}|T_1^A T_1^B\rangle + \left\langle S_0^A S_1^B\middle|\hat{H}\middle|T_1^A T_1^B\right\rangle) = \frac{2}{\sqrt{2}}\gamma$$

$$\langle S^{(2)}|\hat{H}|^1TT\rangle = \frac{1}{\sqrt{2}}(\,\langle S_1^A S_0^B|\hat{H}|T_1^A T_1^B\rangle - \langle S_0^A S_1^B|\hat{H}|T_1^A T_1^B\rangle) = 0$$

The mean transition probability or mean transition strength, according to the Fermi's Golden Rule is given by the mean of the square of the interactions over the number of singlets, that gives us $1/2(\gamma^2+\gamma^2) = \gamma^2$ for the localized basis and $1/2((2/\sqrt{2}\gamma)^2 + 0^2) = \gamma^2$ in the delocalized picture, being the same as expected. This is because the delocalization involves only a unitary transformation that preserves the inner product of the space. One can show that unitary transformations do not change the norm of matrices including the Frobenius norm that is defined as

$$|A|_F^2 = \sum_{ij} A_{ij}^2 \tag{4.6}$$

so the sum of the squared elements of the inner product, known as the square of the Frobenius norm, does not change. Hence, the average transition strength

$$\tau = \frac{\sum_i \langle S^{(i)}|\hat{H}|TT\rangle^2}{\#\text{ singlets}} \tag{4.7}$$

is equal in both descriptions. Consider now three molecules in a stack. Let introduce the more compact notation $[A, B, \ldots]$ for excited singlet states in molecules $A, B, \ldots$ and $[AB, BC, \ldots]$ for triplet pairs in the localized

description. Now there are three excited singlet states $[A, B, C]$ and two coupled triplets $[AB, BC]$. The interactions are

$$\langle A|\hat{H}|AB\rangle = \gamma \tag{4.8}$$

$$\langle B|\hat{H}|AB\rangle = \langle B|\hat{H}|BC\rangle = \gamma \tag{4.9}$$

$$\langle C|\hat{H}|BC\rangle = \gamma \tag{4.10}$$

$$\langle A|\hat{H}|BC\rangle = \langle C|\hat{H}|AB\rangle = 0 \tag{4.11}$$

where it has been taken into account that the excited singlet can only transfer energy to a neighboring molecule. So, an interaction matrix takes the form

$$\Gamma = \begin{pmatrix} \gamma & 0 \\ \gamma & \gamma \\ 0 & \gamma \end{pmatrix} \tag{4.12}$$

where $\Gamma_{ij} = \langle S^{(i)}|\hat{H}|TT^{(j)}\rangle$. To transform the localized basis to the delocalized basis, the adjacency matrices A_S and A_{TT} are introduced

$$A_S = \begin{pmatrix} 0 & 1 & 0 \\ 1 & 0 & 1 \\ 0 & 1 & 0 \end{pmatrix} \quad A_{TT} = \begin{pmatrix} 0 & 1 \\ 1 & 0 \end{pmatrix} \tag{4.13}$$

The eigenvectors of these matrices give the delocalized orbitals for singlets, with corresponding eigenvalues λ

$$S^{(1)} = \frac{1}{2}|A + \sqrt{2}B + C\rangle \qquad \lambda(1) = \sqrt{2} \tag{4.14}$$

$$S^{(2)} = \frac{1}{\sqrt{2}}|A - C\rangle \qquad \lambda(2) = 0 \tag{4.15}$$

$$S^{(3)} = \frac{1}{2}|A - \sqrt{2}B + C\rangle \qquad \lambda(3) = -\sqrt{2} \tag{4.16}$$

and for coupled triplets

$$TT^{(1)} = \frac{1}{\sqrt{2}}|AB + BC\rangle \qquad \lambda'(1) = 1 \tag{4.17}$$

$$TT^{(2)} = \frac{1}{\sqrt{2}}|AB - BC\rangle \qquad \lambda'(2) = -1 \tag{4.18}$$

The interactions for all possible combinations in the ensemble in the delocalized scheme are given by

$$\begin{aligned}\Gamma_{\text{deloc}} &= S^{\dagger}\Gamma_{\text{loc}}T \\ &= \begin{pmatrix} \frac{1}{2} & \sqrt{2} & 1 \\ \frac{1}{\sqrt{2}} & 0 & -1 \\ \frac{1}{2} & -\sqrt{2} & 1 \end{pmatrix}\begin{pmatrix} \gamma & 0 \\ \gamma & \gamma \\ 0 & \gamma \end{pmatrix}\begin{pmatrix} \frac{1}{\sqrt{2}} & \frac{1}{\sqrt{2}} \\ \frac{1}{\sqrt{2}} & -\frac{1}{\sqrt{2}} \end{pmatrix} = \begin{pmatrix} \frac{1}{\sqrt{2}}\gamma + \gamma & 0 \\ 0 & \gamma \\ \frac{1}{\sqrt{2}}\gamma - \gamma & 0 \end{pmatrix}\end{aligned} \tag{4.19}$$

There are three possible transitions corresponding to the three non-zero matrix elements. The strongest coupling comes from the lowest energy singlet with the lowest energy pair of triplets, with a coupling $\frac{1}{\sqrt{2}}\gamma + \gamma$. The other two transitions are the highest to lowest and middle to highest.

$$\langle S^{(1)}|\hat{H}|TT^{(1)}\rangle = \frac{1}{2\sqrt{2}}\langle A + \sqrt{2}B + C|\hat{H}|AB + BC\rangle = \frac{1}{\sqrt{2}}\gamma + \gamma \tag{4.20}$$

$$\langle S^{(3)}|\hat{H}|TT^{(1)}\rangle = \frac{1}{2\sqrt{2}}\langle A - \sqrt{2}B + C|\hat{H}|AB + BC\rangle = \frac{1}{\sqrt{2}}\gamma - \gamma \tag{4.21}$$

$$\langle S^{(1)}|\hat{H}|TT^{(2)}\rangle = \frac{1}{2\sqrt{2}}\langle A + \sqrt{2}B + C|\hat{H}|AB - BC\rangle = 0 \tag{4.22}$$

$$\langle S^{(3)}|\hat{H}|TT^{(2)}\rangle = \frac{1}{2\sqrt{2}}\langle A - \sqrt{2}B + C|\hat{H}|AB - BC\rangle = 0 \tag{4.23}$$

$$\langle S^{(2)}|\hat{H}|TT^{(1)}\rangle = \frac{1}{2}\langle A - C|\hat{H}|AB + BC\rangle = 0 \tag{4.24}$$

$$\langle S^{(2)}|\hat{H}|TT^{(2)}\rangle = \frac{1}{2}\langle A - C|\hat{H}|AB - BC\rangle = \gamma \tag{4.25}$$

The model predicts an average transition strength $\frac{4\gamma^2}{3}$ for both localized and delocalized pictures, as expected.
The model can be generalized knowing that every molecule is linked only with its immediate neighbors. Hence, the adjacency matrices only have 1's

in their sub and super diagonal, and the TT adjacency matrix A_{TT} for N is equivalent to A_S for $N-1$ because there is one TT state less than localized excited singlets S. The interaction matrix Γ_{TS} contains the couplings between S states (rows) and TT states (columns). The dimensions are $[N-1]$, $[N-2]$ and $[N-1, N-2]$ for A_S, A_{TT} and Γ_{TS} respectively.

$$A_S = \begin{pmatrix} 0 & 1 & 0 & \cdots & 0 & 0 \\ 1 & 0 & 1 & \cdots & 0 & 0 \\ 0 & 1 & 0 & \cdots & 0 & 0 \\ & & & \ddots & & \\ 0 & 0 & 0 & \cdots & 0 & 1 \\ 0 & 0 & 0 & \cdots & 1 & 0 \end{pmatrix} \tag{4.26}$$

$$A_{TT} = \begin{pmatrix} 0 & 1 & 0 & \cdots & 0 & 0 \\ 1 & 0 & 1 & \cdots & 0 & 0 \\ 0 & 1 & 0 & \cdots & 0 & 0 \\ & & & \ddots & & \\ 0 & 0 & 0 & \cdots & 0 & 1 \\ 0 & 0 & 0 & \cdots & 1 & 0 \end{pmatrix} \tag{4.27}$$

$$\Gamma = \begin{pmatrix} \gamma & 0 & 0 & \cdots & 0 & 0 \\ \gamma & \gamma & 0 & \cdots & 0 & 0 \\ 0 & \gamma & \gamma & \cdots & 0 & 0 \\ & & & \ddots & & \\ 0 & 0 & 0 & \cdots & \gamma & \gamma \\ 0 & 0 & 0 & \cdots & 0 & \gamma \end{pmatrix} \tag{4.28}$$

The average transition strength is obtained by summing all squared matrix elements of $S^{\dagger}\Gamma TT$ and dividing by the number of singlet states. For N molecules, it follows the trend given by the expression,

$$\bar{P}(N) = 2\frac{N-1}{N}\gamma^2 \tag{4.29}$$

This average reaches $2\gamma^2$ for an infinite number of molecules as shown in figure 4.4. As changing from a localized to a delocalized basis involves a unitary transformation, the outcomes of the model will not change as long as one sticks to the full space, i.e., considering the transitions from all singlets to all TT states. However, internal conversion is presumably much

faster than the singlet fission process, and the assumption that all singlets are equally populated is not very realistic. More interesting are therefore the transition probabilities from the lowest singlet to either the lowest singlet coupled triplet ($\tau_{(1)\to(1)}$) and to all TT states ($\tau_{(1)\to(:)}$). For a fast internal conversion, the lowest singlet is the only populated one. These magnitudes are defined as

$$\tau_{(1)\to(1)} = \left(\Gamma_{11}\right)^2 \tag{4.30}$$

$$\tau_{(1)\to(:)} = \sum_{i=1,n_T} \left(\Gamma_{1i}\right)^2 \tag{4.31}$$

In the localized framework, all states are degenerate and the transition probability is $2\gamma^2$ except for the two molecules case, in which it is γ^2. For the delocalized scheme, figure 4.5 compares the model predictions for transition from the lowest singlet either to all triplet pairs or only to the lowest. The difference between these two assumptions is illustrated in 4.6, which has a peak at $N = 6$. For $N = 2$, the difference is trivially zero as there is only one triplet pair. Increasing the number of molecules in the ensemble opens the possibility of more triplet pairs, increasing the transition probability in the one to all scenario. However, the lowest-to-lowest transition gradually increases its importance relative to the other transitions and hence the difference between the two scenarios becomes smaller. This means that the lowest-to-lowest transition ($\tau_{(1)\to(1)}$) becomes more important as the number of molecules increases and it describes the whole interaction for $N \to \infty$ although the difference is small.

Figure 4.7 compares the different scenarios described above. The dashed lines indicate the limits for an infinite number of chromophores on a line. The blue lines (solid and dashed) show that the average transition strength in an all-to-all scenario converges to $2\gamma^2$. The green and red lines represent the lowest to lowest and lowest to all scenarios, which both converge to $4\gamma^2$. Although the average transition for the dimers (leftmost part of the graph) is smaller than for larger ensembles, the order of magnitude is correct, indicating that even a simple dimer calculation of the coupling provides useful information about the singlet fission coupling even when the singlet exciton is delocalized over several entities as predicted from the TD-DFT calcualtions reported in[2]. We are currently investigating the delocalization of the

S_1 exciton with the NOCI-F approach.

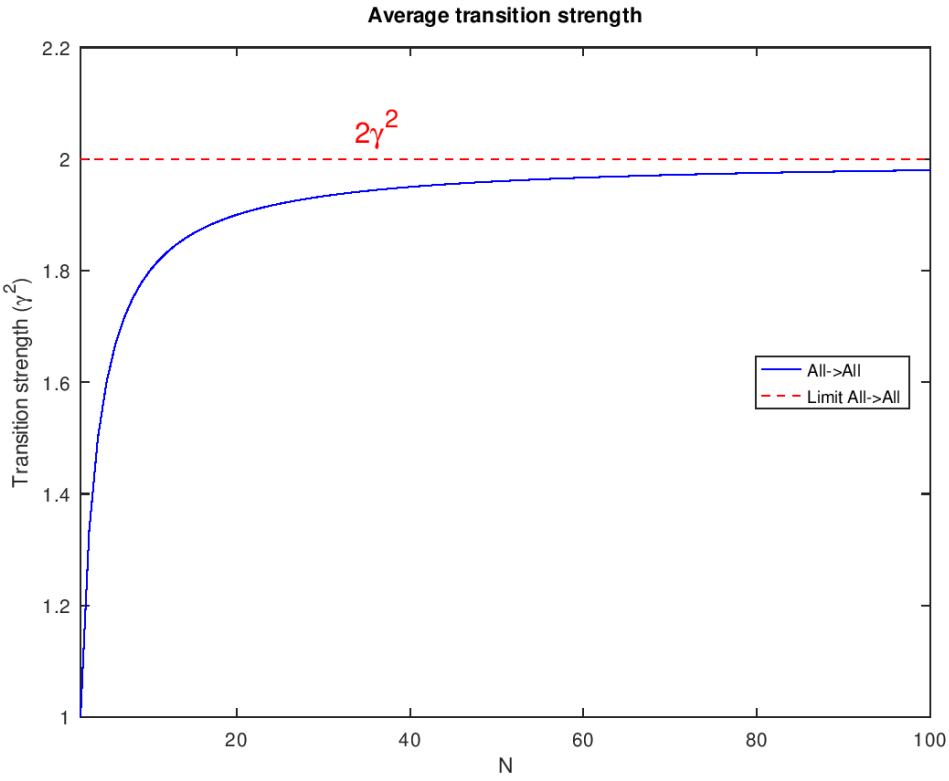

Figure 4.4: Transition probability for a given number of molecules in a stack in the all-to all scenario, using delocalized singlet and triplet functions.

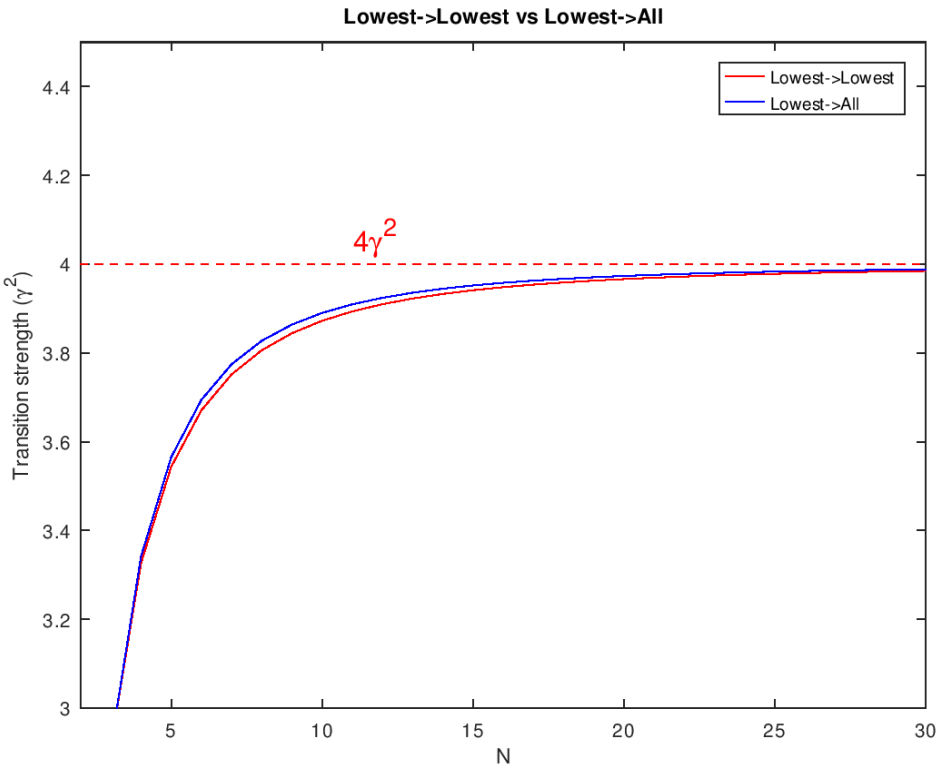

Figure 4.5: Transition probability in the lowest-to-all scenario and in the lowest-to-lowest scenario, using delocalized singlet and triplet functions.

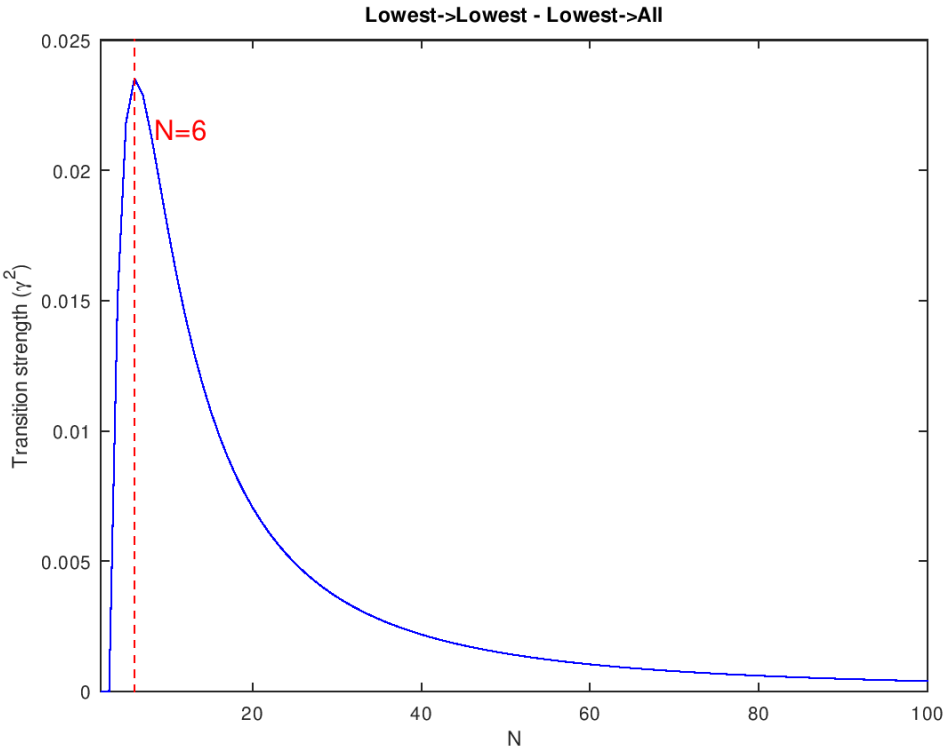

Figure 4.6: Difference between transition probability curves in the lowest-to-lowest and lowest-to-all scenarios

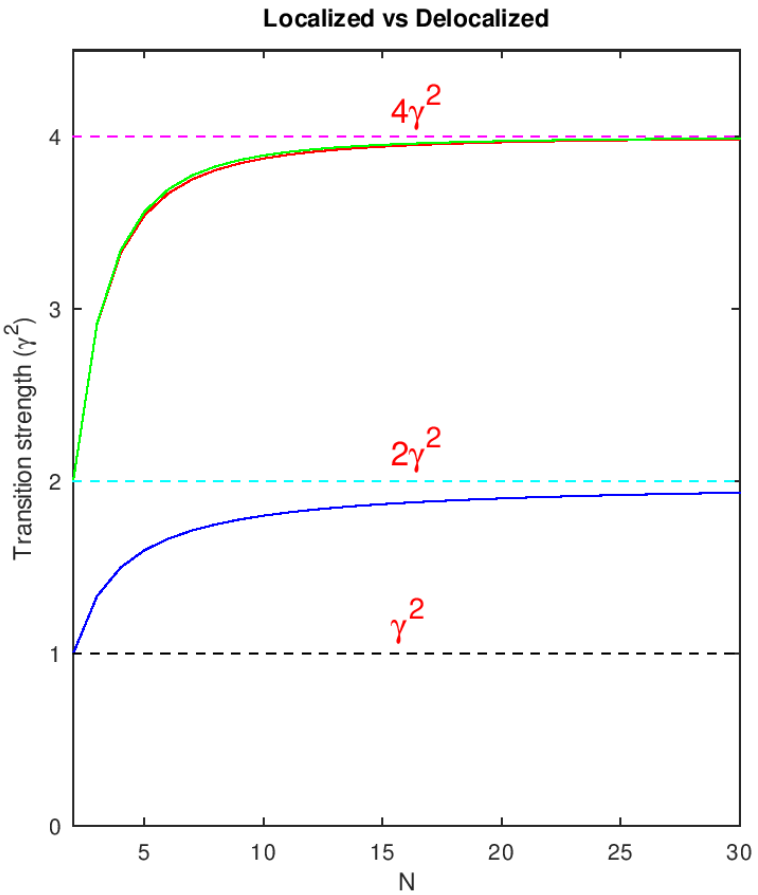

Figure 4.7: Comparison between transition probability curves in the localized and delocalized scenarios

4.2.2 Other geometries

In this part some different geometries are considered, shown in figure 4.8 (a). The equilateral triangle case, in which the adjacency matrices are slightly different from the previous case as now all molecules are adjacent to each other, giving rise to an extra TT state (AC) and additional interactions.

$$A_S = \begin{pmatrix} 0 & 1 & 1 \\ 1 & 0 & 1 \\ 1 & 1 & 0 \end{pmatrix} \quad A_{TT} = \begin{pmatrix} 0 & 1 & 1 \\ 1 & 0 & 1 \\ 1 & 1 & 0 \end{pmatrix} \quad \Gamma_{\text{loc}} = \begin{pmatrix} \gamma & 0 & \gamma \\ \gamma & \gamma & 0 \\ 0 & \gamma & \gamma \end{pmatrix} \tag{4.32}$$

The eigenvectors that arise from these matrices are

$$S^{(1)} = \frac{1}{\sqrt{3}} |A + B + C\rangle \tag{4.33}$$

$$S^{(2)} = \frac{1}{\sqrt{2}} |-A + B\rangle \tag{4.34}$$

$$S^{(3)} = \frac{1}{\sqrt{6}} |-A - B + 2C\rangle \tag{4.35}$$

for singlets and

$$TT^{(1)} = \frac{1}{\sqrt{3}} |AB + BC + AC\rangle \tag{4.36}$$

$$TT^{(2)} = \frac{1}{\sqrt{2}} |-AB + BC\rangle \tag{4.37}$$

$$TT^{(3)} = \frac{1}{\sqrt{6}} |-AB - BC + 2AC\rangle \tag{4.38}$$

for triplets, with eigenvalues $\lambda = 2, -1, -1$ respectively. Considering the "all-to-all" scenario, the average transition probability for the triangle coincides with the value of the line case with $N \to \infty$, giving $(\gamma^2 + \gamma^2 + \gamma^2 + \gamma^2 + \gamma^2 + \gamma^2)/3 = 2\gamma^2$. It is of course the same in the delocalized case, and is calculated by means of the interaction matrix

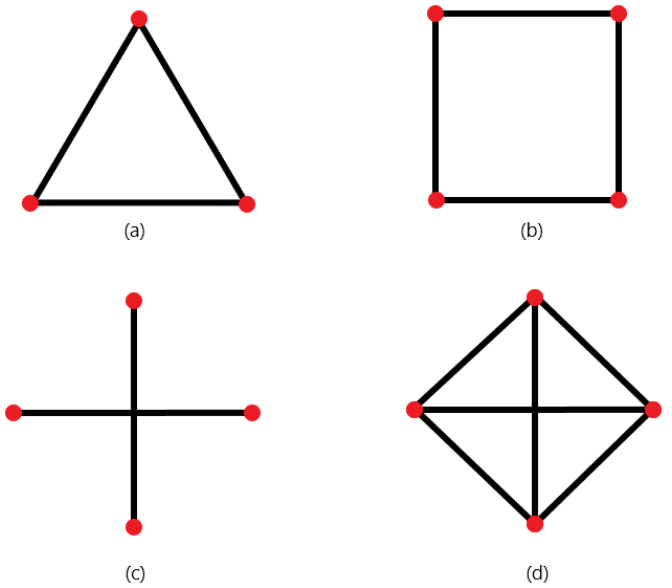

Figure 4.8: Geometries used in the "Other geometries" subsection: (a) Triangle (b) Square (c) Cross (d) Cross connected.

$$\Gamma_{\text{deloc}} = \begin{pmatrix} \frac{1}{\sqrt{3}} & \frac{1}{\sqrt{3}} & \frac{1}{\sqrt{3}} \\ -\frac{1}{\sqrt{2}} & \frac{1}{\sqrt{2}} & 0 \\ -\frac{1}{\sqrt{6}} & -\frac{1}{\sqrt{6}} & \frac{2}{\sqrt{6}} \end{pmatrix} \begin{pmatrix} \gamma & 0 & \gamma \\ \gamma & \gamma & 0 \\ 0 & \gamma & \gamma \end{pmatrix} \begin{pmatrix} \frac{1}{\sqrt{3}} & -\frac{1}{\sqrt{2}} & -\frac{1}{\sqrt{6}} \\ \frac{1}{\sqrt{3}} & \frac{1}{\sqrt{2}} & -\frac{1}{\sqrt{6}} \\ \frac{1}{\sqrt{3}} & 0 & \frac{2}{\sqrt{6}} \end{pmatrix}$$
$$= \begin{pmatrix} 2\gamma & 0 & 0 \\ 0 & 0.5\gamma & -0.866\gamma \\ 0 & 0.866\gamma & 0.5\gamma \end{pmatrix} \quad (4.39)$$

which also leads to $\bar{P} = \sum_{ij} |\Gamma_{\text{deloc},ij}|^2 = 2\gamma^2$ as proven before. The lowest to lowest transition probability is

$$\frac{1}{9} \langle A + B + C | \hat{H} | AB + BC + AC \rangle^2 = 4\gamma^2 \quad (4.40)$$

and for the lowest to all transition we have

$$\frac{1}{3} \langle A + B + C | \hat{H} | AB + BC + AC \rangle^2 + \frac{1}{\sqrt{6}} \langle A + B + C | \hat{H} | -AB + BC \rangle^2 + \frac{1}{3\sqrt{2}} \langle A + B + C | \hat{H} | -AB - BC + 2AC \rangle^2 = 4\gamma^2 \quad (4.41)$$

Another interesting case is the square geometry shown in figure 4.8 (b). This geometry has four molecules placed at the vertices of the square, considering every vertex has interaction only with its two immediate neighbors. The characteristic matrices of the system are constructed in the same way as in the triangular case

$$A_S = \begin{pmatrix} 0 & 1 & 0 & 1 \\ 1 & 0 & 1 & 0 \\ 0 & 1 & 0 & 1 \\ 1 & 0 & 1 & 0 \end{pmatrix} \quad A_{TT} = \begin{pmatrix} 0 & 1 & 0 & 1 \\ 1 & 0 & 1 & 0 \\ 0 & 1 & 0 & 1 \\ 1 & 0 & 1 & 0 \end{pmatrix} \quad \Gamma = \begin{pmatrix} \gamma & 0 & 0 & \gamma \\ \gamma & \gamma & 0 & 0 \\ 0 & \gamma & \gamma & 0 \\ 0 & 0 & \gamma & \gamma \end{pmatrix} \quad (4.42)$$

giving the all-to-all transition probability $2\gamma^2$. Applying the transformation to a delocalized basis, the states obtained are

$$S^{(1)} = \frac{1}{2}\,|A + B + C + D\rangle \tag{4.43}$$

$$S^{(2)} = \frac{1}{\sqrt{2}}\,|A - C\rangle \tag{4.44}$$

$$S^{(3)} = \frac{1}{\sqrt{2}}\,|-B + D\rangle \tag{4.45}$$

$$S^{(4)} = \frac{1}{2}\,|A - B + C - D\rangle \tag{4.46}$$

$$\tag{4.47}$$

and

$$TT^{(1)} = \frac{1}{2}\,|AB + BC + CD + AD\rangle \tag{4.48}$$

$$TT^{(2)} = \frac{1}{\sqrt{2}}\,|AB - CD\rangle \tag{4.49}$$

$$TT^{(3)} = \frac{1}{\sqrt{2}}\,|-BC + AD\rangle \tag{4.50}$$

$$TT^{(4)} = \frac{1}{2}\,|AB - BC + CD - AD\rangle \tag{4.51}$$

with eigenvalues $\lambda = 2, 0, 0, -2$ respectively. These interactions give a transition probability $2\gamma^2$ for all-to-all and $4\gamma^2$ for lowest-to-all and lowest-to-lowest transitions.

The closed topologies are generalized by considering ring structures of increasing size where every molecule has two neighbors and the first is adjacent to the last. For simplicity, all molecules in the chain perfectly interact with each other so the coupling γ is constant and equal for every pair. The adjacency and interaction matrices have the same form as in the line scheme

except for the first and the last elements which are now coupled.

$$A_S = \begin{pmatrix} 0 & 1 & 0 & \cdots & 0 & 1 \\ 1 & 0 & 1 & \cdots & 0 & 0 \\ 0 & 1 & 0 & \cdots & 0 & 0 \\ & & & \ddots & & \\ 0 & 0 & 0 & \cdots & 0 & 1 \\ 1 & 0 & 0 & \cdots & 1 & 0 \end{pmatrix} \tag{4.52}$$

$$A_{TT} = \begin{pmatrix} 0 & 1 & 0 & \cdots & 0 & 1 \\ 1 & 0 & 1 & \cdots & 0 & 0 \\ 0 & 1 & 0 & \cdots & 0 & 0 \\ & & & \ddots & & \\ 0 & 0 & 0 & \cdots & 0 & 1 \\ 1 & 0 & 0 & \cdots & 1 & 0 \end{pmatrix} \tag{4.53}$$

$$\Gamma_{\text{loc}} = \begin{pmatrix} \gamma & 0 & 0 & \cdots & 0 & \gamma \\ \gamma & \gamma & 0 & \cdots & 0 & 0 \\ 0 & \gamma & \gamma & \cdots & 0 & 0 \\ & & & \ddots & & \\ 0 & 0 & 0 & \cdots & \gamma & 0 \\ 0 & 0 & 0 & \cdots & \gamma & \gamma \end{pmatrix} \tag{4.54}$$

where the last column corresponds to the coupled triplets formed by $(1, N-1)$. Now there is no smooth transition for the finite and the infinite length case as in the line, because there are no boundaries and all nodes are equal, being always coupled to two neighbors. The minimum closed ring (triangle) and beyond are analogous to the infinite line case where the boundary effect is fully diluted. The only transition that contributes is the lowest-to-lowest one, as in the infinite line model estimation, so can be concluded that any closed ring picture is equivalent to the infinite line case. The average transition strength is constant at $2\gamma^2$ and the lowest-to-all and lowest-to-lowest transition probabilities are equal to $4\gamma^2$ for any number of molecules N.

For the last case, the cross alike geometry is considered shown in figure 4.8 (c). The intention of this is to illustrate how the number of connections increases the transition probability.

Consider first that the molecules in the outside ring do not interact with each other. Molecule A is in the center and molecules B, C, D, E are placed on

the outside, being the only possible coupled triplet states AB, AC, AD and AE. The total number of interactions or edges in the graph is four. The matrices of the system are

$$A_S = \begin{pmatrix} 0 & 1 & 1 & 1 & 1 \\ 1 & 0 & 0 & 0 & 0 \\ 1 & 0 & 0 & 0 & 0 \\ 1 & 0 & 0 & 0 & 0 \\ 1 & 0 & 0 & 0 & 0 \end{pmatrix} \quad A_{TT} = \begin{pmatrix} 0 & 1 & 1 & 1 \\ 1 & 0 & 1 & 1 \\ 1 & 1 & 0 & 1 \\ 1 & 1 & 1 & 0 \end{pmatrix} \quad \Gamma_{\text{loc}} = \begin{pmatrix} \gamma & \gamma & \gamma & \gamma \\ \gamma & 0 & 0 & 0 \\ 0 & \gamma & 0 & 0 \\ 0 & 0 & \gamma & 0 \\ 0 & 0 & 0 & \gamma \end{pmatrix} \tag{4.55}$$

having a mean transition probability $8\gamma^2/5 = 1.6\gamma^2$, which is equal to the obtained for five molecules on a stack. The delocalized states are

$$S^{(1)} = \frac{1}{2}\,|\sqrt{2}A + B + C + D + E\rangle \tag{4.56}$$

$$S^{(2)} = |-0.689B + 0.725C - 0.020D - 0.016E\rangle \tag{4.57}$$

$$S^{(3)} = |-0.311B - 0.284C - 0.270D + 0.866E\rangle \tag{4.58}$$

$$S^{(4)} = |-0.423B - 0.380C + 0.823D - 0.026E\rangle \tag{4.59}$$

$$S^{(5)} = \frac{1}{2}\,|-\sqrt{2}A + B + C + D + E\rangle \tag{4.60}$$

and

$$TT^{(1)} = \frac{1}{2}\,|AB + AC + AD + AE\rangle \tag{4.61}$$

$$TT^{(2)} = TT^{(1)} = \frac{1}{\sqrt{2}}\,|AB + AC\rangle \tag{4.62}$$

$$TT^{(3)} = \frac{1}{\sqrt{6}}\,|-AB - AC + AD\rangle \tag{4.63}$$

$$TT^{(4)} = \frac{1}{2\sqrt{3}}\,|AB - AC - AD + AE\rangle \tag{4.64}$$

The lowest-to-lowest transition probability is $4.5\gamma^2$ and the lowest-to-all is $7.75\gamma^2$. This increase is mostly due to the transition to the second triplet pair state, which has a significant probability of $2.25\gamma^2$. These probabilities are larger than in the five on a line case. Next, the interaction between the

molecules on the outside of the ensemble is also considered, see figure 4.8 (d). The number of possible TT combinations rises up to 8: AB, AC, AD, AE, BC, CD, DE and BE. The characteristic of the ensemble now read

$$\theta_S = \begin{pmatrix} 0 & 1 & 1 & 1 & 1 \\ 1 & 0 & 1 & 0 & 1 \\ 1 & 1 & 0 & 1 & 0 \\ 1 & 0 & 1 & 0 & 1 \\ 1 & 1 & 0 & 1 & 0 \end{pmatrix} \tag{4.65}$$

$$\theta_{TT} = \begin{pmatrix} 0 & 1 & 1 & 1 & 1 & 0 & 0 & 1 \\ 1 & 0 & 1 & 1 & 1 & 1 & 0 & 0 \\ 1 & 1 & 0 & 1 & 0 & 1 & 1 & 0 \\ 1 & 1 & 1 & 0 & 0 & 0 & 1 & 1 \\ 1 & 1 & 0 & 0 & 0 & 1 & 0 & 1 \\ 0 & 1 & 1 & 0 & 1 & 0 & 1 & 0 \\ 0 & 0 & 1 & 1 & 0 & 1 & 0 & 1 \\ 1 & 0 & 0 & 1 & 1 & 0 & 1 & 0 \end{pmatrix} \tag{4.66}$$

$$\Gamma_{\text{loc}} = \begin{pmatrix} \gamma & \gamma & \gamma & \gamma & 0 & 0 & 0 & 0 \\ \gamma & 0 & 0 & 0 & \gamma & 0 & 0 & \gamma \\ 0 & \gamma & 0 & 0 & \gamma & \gamma & 0 & 0 \\ 0 & 0 & \gamma & 0 & 0 & \gamma & \gamma & 0 \\ 0 & 0 & 0 & \gamma & 0 & 0 & \gamma & \gamma \end{pmatrix} \tag{4.67}$$

Here there are more transition possibilities from singlets and the average transition strength for the all-to-all scenario increases to $16\gamma^2/5 = 3.2\gamma^2$ which is exactly twice the value obtained without the lateral interactions. This is not unexpected as the number of edges in the graph duplicates, hence the number of non-zero elements in the interaction matrix Γ also duplicates, but the number of excited singlets does not. The relevant delocalized states

in this geometry are

$$S^{(1)} = |0.53A + 0.43B + 0.43C + 0.43D + 0.43E\rangle \tag{4.68}$$
$$S^{(2)} = |-0.03B - 0.03C + 0.03D + 0.71E\rangle \tag{4.69}$$
$$S^{(3)} = |-0.71B + 0.03C + 0.71D - 0.03E\rangle \tag{4.70}$$
$$S^{(4)} = |-0.85A + 0.26B + 0.26C + 0.26D + 0.26E\rangle \tag{4.71}$$
$$S^{(5)} = |-0.5B + 0.5C - 0.5D + 0.5E\rangle \tag{4.72}$$
$$TT^{(1)} = |-0.39AB - 0.39AC - 0.39AD - 0.39AE\rangle + |-0.31BC - 0.31CD - 0.31DE - 0.31BE\rangle \tag{4.73}$$
$$TT^{(2)} = \dots$$
$$\dots$$

where it can be observed that the lowest singlet is the only one that has contributions from all molecules in the ensemble, while the higher singlets have zero coefficients for the central molecule A. For the triplets, the lowest state can be written as

$$^1|TT\rangle_{\text{lowest}} = -0.79\,|\text{CROSS}\rangle - 0.62\,|\text{RING}\rangle \tag{4.74}$$

by grouping together the terms that contain center A (CROSS) and those with zero coefficient on A (RING). The lowest-to-lowest transition probability becomes $6.482\gamma^2$ while the lowest-to-all process has a total probability of $7.370\gamma^2$ to occur, meaning that the transition from the lowest singlet to the lowest coupled triplet represents 88% of the transitions that can occur from the lowest singlet.

4.2.3 Similarities with Tight-Binding Approximation

Tight-Binding Approximation (TBA) is a well known cheap method for calculating band structures of crystals. This method deals with mono electronic atomic orbitals, that are tightly bound to atoms

$$\phi_l(\mathbf{r} - \mathbf{t}_i) \tag{4.75}$$

with l the type of orbital (s, p, d, ...) and $\mathbf{t}_i$ the position of the atom in a unit cell. In order to construct a model Hamiltonian for these ensembles, the

most basic tight binding approximation considers that all atomic orbitals are orthogonal and only nearest neighbors do interact, in a similar fashion our METB model.
Consider the case of 1D linear chain with s or p orbitals along the x axis. First, the periodic basis must be constructed in order to obey the Bloch theorem, so the states

$$\chi_{kl}(x) = \sum_{n=-\infty}^{\infty} e^{ikx}\phi_l(x - na) \tag{4.76}$$

are solutions of the Schrödinger equation of a periodic 1D solid, with a the length of the unit cell. This means that in each point of the chain, a sum is taken over atomic wavefunctions of same type from all unit cells, such that the resulting state has the so called Bloch character

$$\chi_{kli}(x + d) = e^{ikd}\chi_{kli}(x) \tag{4.77}$$

The orthogonality and only nearest neighbor interaction assumptions lead to

$$\langle \phi_l(x) | \phi_l(x - na) \rangle = \delta_{n0} \tag{4.78}$$

$$\langle \phi_l(x) | \hat{H} | \phi_l(x - na) \rangle = \epsilon_l \delta_{n0} + t_l \delta_{n\pm1} \tag{4.79}$$

so the interaction between different atoms is t_l if they are neighbors, that is $n \pm 1$, and 0 otherwise. This resembles the METB model in which only neighboring states do interact with coupling t_l. In this model the band structure calculation is

$$\epsilon_k = \epsilon_l + 2t_l \cos(ka) \tag{4.80}$$

while in the model, as the phase is not taken into account, it is

$$\epsilon_k = \epsilon_l + 2\gamma \tag{4.81}$$

with $\epsilon_l = 0$ and $t_l = \gamma$ between different contiguous states S and TT. That results in the value $4\gamma^2$ for the S-TT transition strength in the lowest-to-lowest scenario.

4.2.4 Conclusions from the model

The results described in this section show that

1. Localized and delocalized description in the all-to-all scenario are strictly equivalent.

2. Lowest-to-all and lowest-to-lowest give constant transition probability in the localized basis (γ^2).

3. In the other two scenarios the transition probability in the delocalized basis is systematically larger than in the localized representation.

4. Lowest-to-all and lowest-to-lowest are very similar, converge to the same value for large N and the maximum difference is found for $N = 6$.

5. Ring systems (lines with periodic boundaries) give all the same result, coinciding with the molecules on a line ensemble for infinite N.

6. Increasing the number of connection keeping N constant increases the transition probability.

4.3 NOCI estimations

In this section, the same topologies as in the model studies above are reproduced with benzene molecules through NOCI-F calculations. The fragment wave functions are either obtained from a CASSCF(6,6) calculation including the π orbitals in the active space, or by the AIFDEM procedure, using a single determinant for the ground state, a two-determinant wave function for the charge-transfer doublets and CI-singles wave functions for excited singlets and triplets expressed in the NTO basis. The latter leads to very compact expansions of the many-electron wave functions in terms of determinants and can therefore be used for the larger ensembles. The goal is twofold. First, the CAS(6,6)SCF input results are used to check the consistency of the model discussed above. Secondly, the suitability of the AIFDEM approach is tested by comparing the outcomes with the CAS(6,6)SCF input calculations. This computationally less expensive method could be an interesting alternative for the CASSCF NOCI-F calculation, especially for the larger ensembles.

4.3.1 Two molecules on a stack

First, consider two parallel benzene molecules, slightly displaced in the x-y plane ($\Delta x = 2.25$ Å, $\Delta y = 1.25$ Å), as shown in figure 4.9. The intermolecular distance $d_{AB} = \Delta z = 3.25$ Å is rather small, but leads to stronger S_0S_1-^1TT interactions, facilitating the analysis. The relative CAS(6,6)SCF and AIFDEM energies of the benzene fragment are listed in Table 4.4. Both input wave functions are calculated using a atomic natural orbital double-ζ basis set (ano-s-vdzp). Rather large discrepancies are observed, 0.21 eV for S_1 and 1.29 eV for T_1 energies respect the ground state. Benzene does not fulfill the singlet fission criteria $E(S_1) \geq 2E(T_1)$ as the triplet lies much higher in energy, but it is a simple chromophore that can be used to illustrate delocalization check the consistency of the model.
Using the same nomenclature as for the model including also the charge transfer states $A^+B^- = D^+D^-$ and vice-versa, Table 4.5 shows the energies of the localized states showing degeneracy as expected and the first discrepancy between CASSCF and AIFDEM inputs. Energies of charge transfer

states D^+D^- and D^-D^+ lie below AB energy in the AIFDEM approach while being higher when using CASSCF inputs. This can be a great source of errors when including these states as their presence in the adiabatic NOCI wave functions could be overweighted depending on the chromophores chosen for the study.

Table 4.6 show that the electronic coupling between A, B and AB is symmetric, with an average coupling of 13 meV with CASSCF and 12 meV with AIFDEM input. Here, states are not orthogonal, so the expression of electronic coupling is given by expression 4.29 involving the overlap rather than only the off-diagonal Hamiltonian matrix element as in the model. According to the model, for two molecules on a stack the all-to-all average transition strength can be calculated as γ^2 that yields $\tau_{\text{CASSCF}} = 169$ and $\tau_{\text{AIFDEM}} = 144$.

The final NOCI wave functions are shown in Table 4.7 in which can be appreciated the one to one correspondence with the delocalized states in the model 4.5 except for the charge transfer states $CT^{(1)}$ and $CT^{(2)}$

$$S^{(0)} = \text{G-S} \tag{4.82}$$

$$S^{(1)} \approx |\frac{1}{\sqrt{2}}A + \frac{1}{\sqrt{2}}B\rangle \tag{4.83}$$

$$S^{(2)} \approx |\frac{1}{\sqrt{2}}A - \frac{1}{\sqrt{2}}B\rangle \tag{4.84}$$

$$TT^{(1)} \approx |AB\rangle \tag{4.85}$$

In the so-called delocalized or adiabatic description, both states $S^{(1)}$ and $S^{(2)}$ represent the resonance $A \pm B$ between Frenkel excitons (see Chapter 1 for the definition) in both molecules while $TT^{(1)}$ is practically the pure coupled triplet AB. The degeneracy of the two singlet states is a direct consequence of the small interaction between A and B which is $\sim$ 16 meV. The upper section of Table 4.8 reflects approximately that the simple model makes the right prediction for the coupling without taking into account the CT states, giving zero for $S^{(1)}$ and $\frac{2}{\sqrt{2}}\gamma \approx -17$ meV for $S^{(2)}$. As expected, CT states have only presence in the wave functions with an AIFDEM input as a consequence of being lower in energy than the coupled triplets AB, and it has a big impact in the magnitude of the electronic coupling as shown in the lower

part of table 4.8. This means that the charge transfer states are much better described by a two determinant wave function than the singlets and triplets by a CIS expansion. For that reason and because they have nearly zero representation in the CASSCF wave functions, these states will be omitted in the next examples, hence the Charge Transfer Mediated singlet fission mentioned in Chapter 1 will not be analyzed and only the direct mechanism will be discussed.

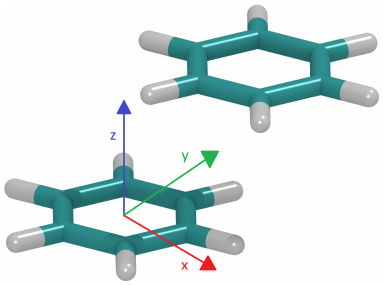

Figure 4.9: Benzene dimer. Distances: $\Delta z = 3.25$ Å, $\Delta x = 2.25$ Å and $\Delta y = 1.25$ Å.

Table 4.4: Relative energy levels for the benzene molecule (eV) for CAS(6,6)SCF and AIFDEM calculations.

	ΔE (eV)	
	CASSCF	AIFDEM
S_0	0.00	0.00
S_1	5.94	6.15
T_1	4.83	3.54
D^+	9.66	9.22
D^-	3.60	3.27

Table 4.5: NOCI-F energies of the benzene dimer (eV) in the localized representation.

	ΔE (eV)	
	CASSCF	AIFDEM
S_0S_0	0.00	0.00
A	5.92	6.19
B	5.92	6.19
AB	9.59	9.90
A^+B^-	10.54	9.20
A^-B^+	10.54	9.20

Table 4.6: Electronic couplings for two benzene molecules in the localized description (meV)

	CASSCF	AIFDEM
	AB	AB
A	-13.23	12.06
B	13.23	-11.95

Table 4.7: Delocalized NOCI wave functions in terms of localized states for two benzene molecules on a stack..

CASSCF						
ΔE (eV)	0.00	5.90	5.94	9.59	10.48	10.60
	$S^{(0)}$	$S^{(1)}$	$S^{(2)}$	$TT^{(1)}$	$CT^{(1)}$	$CT^{(2)}$
G-S	-1.00	0.00	0.00	0.00	-0.02	0.00
A	0.00	-0.71	-0.71	0.00	-0.01	-0.01
B	0.00	-0.71	0.71	0.00	0.01	-0.01
AB	0.00	0.00	0.00	-1.00	0.00	0.00
A^+B^-	0.00	0.00	0.00	0.00	-0.70	-0.71
A^-B^+	0.00	0.00	0.00	0.00	-0.70	0.71
AIFDEM						
ΔE (eV)	0.00	6.16	6.21	9.22	9.25	9.93
	$S^{(0)}$	$S^{(1)}$	$S^{(2)}$	$CT^{(1)}$	$CT^{(2)}$	$TT^{(1)}$
G-S	-1.00	-0.00	-0.00	-0.08	0.00	0.02
A	-0.00	0.70	0.71	-0.02	0.07	-0.00
B	0.00	0.70	-0.71	0.02	0.07	-0.00
AB	-0.00	0.00	-0.00	-0.18	-0.00	-0.98
A^+B^-	-0.00	-0.04	0.01	0.70	0.70	-0.14
A^-B^+	0.00	-0.04	-0.01	-0.70	0.71	0.14

Table 4.8: Electronic couplings for two benzene molecules in the delocalized description (meV)

without CT		
	CASSCF	AIFDEM
	$TT^{(1)}$	$TT^{(1)}$
$S^{(1)}$	0.00	-0.07
$S^{(2)}$	18.73	-17.07
with CT		
	CASSCF	AIFDEM
	$TT^{(1)}$	$TT^{(1)}$
$S^{(1)}$	0.00	-0.23
$S^{(2)}$	18.70	8.32

4.3.2 Three molecules on a stack

The case with three chromophores (Figure 4.10) on a stack is more interesting as it also allows to study the triplet separation phenomenon by including the state $AC = T_1S_0T_1$ consisting of two separated triplets in the ensemble. Energies in Table 4.9 show that localized states on molecule B have lower energy, which could be expected, as monomers that are inner in the ensemble are stabilized by surrounding molecules.
Table 4.10 shows the coupling interactions from which the parity with the interaction matrix of the model can be appreciated with a slightly deviations for the outer localized states. The average interaction strengths for these localized states are $\tau^{\text{CASSCF}} = 242.17$ meV^2 and $\tau^{\text{AIFDEM}} = 202.63$ meV^2. With the $\frac{4}{3}\gamma^2$ value given by the model, the values obtained for the coupling are $\gamma = 13.48$ meV and $\gamma = 12.32$ meV CASSCF and AIFDEM inputs, respectively. These values are very similar to those obtained from the two molecules case so the trend shown in plot 4.4 is obeyed. Table 4.11 shows the electronic coupling with the triplet separation state, small but existent for A, B and C and comparable to γ with the coupled triplets AB and CD that hints a mixing of these three states as appreciated in the delocalized states displayed in Table 4.12. This suggest that the triplet separation process does not happen separately from singlet fission but the two phenomena are simultaneous.
In what regards to the model predictions, the adiabatic states show the same delocalization pattern as in the model (Expressions 4.15 to 4.18). Electronic coupling values in the delocalized description (Table 4.13) can be easily identified as the values from the model 4.20 ignoring the phase factor

$$\frac{1}{\sqrt{2}}\gamma + \gamma \approx -20.85, \quad 19.45 \tag{4.86}$$

$$\gamma \approx 13.77, \quad -12.43 \tag{4.87}$$

$$\frac{1}{\sqrt{2}}\gamma - \gamma \approx -7.21, \quad 5.57 \tag{4.88}$$

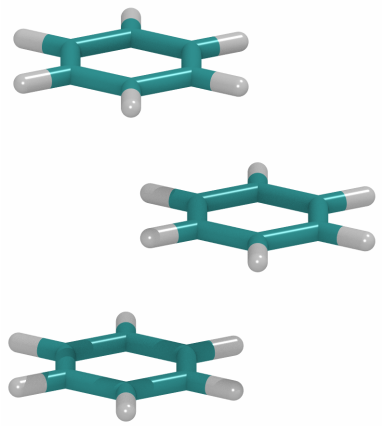

Figure 4.10: Benzene trimer.

Table 4.9: Relative NOCI energy levels for three benzene molecules on a stack in the localized description (eV).

	ΔE (eV)	
	CASSCF	AIFDEM
G-S	0.00	0.00
A	5.91	6.19
B	5.90	6.18
C	5.91	6.19
AB	9.55	9.87
BC	9.55	9.88
AC	9.59	9.91
A^+B^-	10.81	9.28
A^+B^-	10.44	9.11
B^+C^-	11.42	9.11
B^+C^-	11.42	9.28

Table 4.10: Electronic couplings of three benzene molecules in the localized description (meV).

	CASSCF		AIFDEM	
	AB	***BC***	***AB***	***BC***
A	-13.60	0.15	-12.44	0.06
B	13.35	13.35	12.22	12.32
C	0.15	-13.60	0.07	-12.33

Table 4.11: Electronic coupling with the triplet separation state AC in the localized description (meV).

	CASSCF	AIFDEM
	AC	***AC***
A	-0.08	-0.06
B	0.11	0.04
C	-0.08	-0.06
AB	11.53	9.51
BC	11.53	9.52

Table 4.12: Delocalized NOCI wave functions in terms of localized states.

CASSCF							
ΔE	0.00	5.88	5.91	5.93	9.55	9.55	9.60
	$S^{(0)}$	$S^{(1)}$	$S^{(2)}$	$S^{(3)}$	$TT^{(1)}$	$TT^{(2)}$	$TT^{(3)}$
G-S	1.00	0.00	0.00	0.00	0.00	0.00	0.00
A	0.00	-0.41	0.71	0.58	0.00	0.00	0.00
B	0.00	-0.82	0.00	-0.58	0.00	0.00	0.00
C	0.00	-0.41	-0.71	0.58	0.00	0.00	0.00
AB	0.00	0.00	0.00	0.00	0.67	-0.71	-0.22
BC	0.00	0.00	0.00	0.00	0.67	0.71	-0.22
AC	0.00	0.00	0.00	0.00	-0.31	0.00	-0.95
AIFDEM							
ΔE (eV)	0.00	6.16	6.19	6.21	9.87	9.88	9.92
	$S^{(0)}$	$S^{(1)}$	$S^{(2)}$	$S^{(3)}$	$TT^{(1)}$	$TT^{(2)}$	$TT^{(3)}$
G-S	1.00	0.00	0.00	0.00	0.00	0.00	0.00
A	0.00	0.44	-0.71	-0.55	0.00	0.00	0.00
B	0.00	0.78	0.00	0.62	0.00	0.00	0.00
C	0.00	0.44	0.71	-0.55	0.00	0.00	0.00
AB	0.00	0.00	0.00	0.00	0.70	-0.68	-0.22
BC	0.00	0.00	0.00	0.00	0.64	0.73	-0.22
AC	0.00	0.00	0.00	0.00	-0.31	-0.01	-0.95

Table 4.13: Electronic couplings for three benzene molecules on a stack in the delocalized description (meV)

	CASSCF			AIFDEM		
	$TT^{(1)}$	$TT^{(2)}$	$TT^{(3)}$	$TT^{(1)}$	$TT^{(2)}$	$TT^{(3)}$
$S^{(1)}$	-7.21	0.00	2.41	5.57	0.31	-1.83
$S^{(2)}$	0.00	13.77	0.00	0.55	-12.43	0.00
$S^{(3)}$	-20.85	0.00	7.03	19.45	0.78	-6.53

4.3.3 Four molecules on a stack

In a similar fashion as the trimer stack opens the possibility to study Triplet Separation, the stack of four molecules (Figure 4.11) adds up a new situation to the mix allowing to study the so-called Triplet Diffusion mechanism by adding the $AD = T_1S_0S_0T_1$ state to the simulation pretending to describe the propagation of both T_1 charge carries across the ensemble. Energies (Table 4.14) and electronic couplings (Tables 4.15) follow the same trend as in the trimer stack, slightly favoring the inner localized states in energy (+0.02 eV). Separation and diffusion electronic couplings (Table 4.16) show a general trend that will be followed in any bigger stack of these characteristics, that is, a strong coupling between coupled AB, BC, CD and separated AC, BD triplets and the same coupling of these with the triplet diffusion state AD.

In delocalized states (Tables 4.17 and 4.18) are noticeable the effects of boundaries causing that the more internally localized states in the chain are the lowest in energy, so delocalization is not as uniform as in the model. This effect makes diagonal elements of Hamiltonian non-uniform, but ideally these diagonal elements and the couplings are equal in an infinite line and the propagation of the charge carriers is uniform. Despite this, there is a mixing of coupled triplets with triplet separation and for the other side, a mixing of triplet separation with triplet diffusion, and so on.

In what concerns to METB theory, it can be observed the pattern observed in classic atomic TB theory of solids that predict the phase of the nodes in the ensemble. Paying attention to the signs of each MEBF the patterns arisen are illustrated in Figure 4.12 with $S^{(1)}$ being the state with all excited singlets in phase and also the lowest in energy and the alternate phase state $S^{(4)}$ being the highest.

Table 4.14: NOCI relative energy levels for four benzene molecules on a stack in the localized description (eV).

	ΔE (eV)	
	CASSCF	AIFDEM
G-S	0.00	0.00
A	5.82	6.19
B	5.80	6.17
C	5.80	6.17
D	5.82	6.19
AB	9.41	9.87
BC	9.38	9.85
CD	9.41	9.87
AC	9.43	9.89
BD	9.43	9.89
AD	9.43	9.91

Table 4.15: Electronic couplings for four benzene molecules on a stack in the localized description (meV)

	CASSCF			AIFDEM		
	AB	BC	CD	AB	BC	CD
A	-13.74	0.15	0.02	-12.47	0.06	0.01
B	13.48	13.86	-0.18	12.25	12.70	-0.08
C	0.18	-13.86	-13.48	0.08	-12.60	-12.34
D	-0.02	-0.15	13.74	-0.01	-0.07	12.36

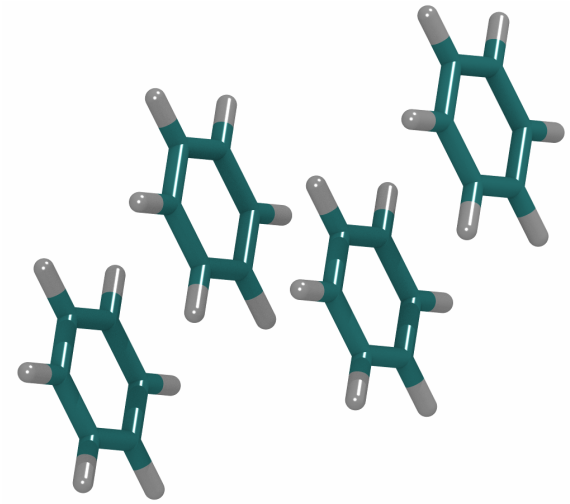

Figure 4.11: Benzene tetramer.

Table 4.16: Electronic coupling with the triplet separation AC, BC and triplet diffusion AD states in the localized description (meV).

	CASSCF			AIFDEM		
	AC	BD	AD	AC	BD	AD
A	-0.08	0.00	0.00	-0.06	0.00	0.00
B	0.12	0.08	0.00	0.04	0.06	0.00
C	-0.08	-0.12	0.00	-0.06	-0.04	0.00
D	0.00	0.08	0.00	0.00	0.06	0.00
AB	12.18	0.00	0.29	9.95	0.00	0.22
BC	11.58	11.58	-0.03	9.54	9.54	-0.01
CD	0.00	12.18	0.29	0.00	9.95	0.22
AC	-	-0.02	11.76	-	-0.01	9.61
BD	-0.02	-	11.76	-0.01	-	9.61

Table 4.17: Delocalized NOCI wave functions in terms of localized states with CASSCF input wave functions.

ΔE	0.00	5.78	5.80	5.83	5.84	9.38	9.40	9.40	9.43	9.44	9.47
	$S^{(0)}$	$S^{(1)}$	$S^{(2)}$	$S^{(3)}$	$S^{(4)}$	$TT^{(1)}$	$TT^{(2)}$	$TT^{(3)}$	$TT^{(4)}$	$TT^{(5)}$	$TT^{(6)}$
G-S	1.00	0.00	0.00	0.00	0.00	0.00	0.00	0.00	0.00	0.00	0.00
A	0.00	-0.25	0.48	0.66	0.52	0.00	0.00	0.00	0.00	0.00	0.00
B	0.00	-0.66	0.52	-0.25	-0.48	0.00	0.00	0.00	0.00	0.00	0.00
C	0.00	-0.66	-0.52	-0.25	0.48	0.00	0.00	0.00	0.00	0.00	0.00
D	0.00	-0.25	-0.48	0.66	-0.52	0.00	0.00	0.00	0.00	0.00	0.00
AB	0.00	0.00	0.00	0.00	0.00	-0.08	-0.65	0.64	-0.27	0.28	-0.08
BC	0.00	0.00	0.00	0.00	0.00	-0.94	0.00	-0.23	-0.25	0.00	-0.10
CD	0.00	0.00	0.00	0.00	0.00	-0.08	0.65	0.64	-0.27	-0.28	-0.08
AC	0.00	0.00	0.00	0.00	0.00	0.23	0.28	-0.24	-0.52	0.65	-0.35
BD	0.00	0.00	0.00	0.00	0.00	0.23	-0.28	-0.24	-0.52	-0.65	-0.35
AD	0.00	0.00	0.00	0.00	0.00	-0.07	0.00	0.10	0.49	0.00	-0.86

Table 4.18: Delocalized NOCI wave functions in terms of localized states with AIFDEM input wave functions.

ΔE	0.00	6.15	6.17	6.19	6.20	9.84	9.87	9.87	9.89	9.89	9.92
	$S^{(0)}$	$S^{(1)}$	$S^{(2)}$	$S^{(3)}$	$S^{(4)}$	$TT^{(1)}$	$TT^{(2)}$	$TT^{(3)}$	$TT^{(4)}$	$TT^{(5)}$	$TT^{(6)}$
G-S	1.00	0.00	0.00	0.00	0.00	0.00	0.00	0.00	0.00	0.00	0.00
A	0.00	-0.28	-0.53	0.65	0.47	0.00	0.00	0.00	0.00	0.00	0.00
B	0.00	-0.65	-0.47	-0.28	-0.53	0.00	0.00	0.00	0.00	0.00	0.00
C	0.00	-0.65	0.47	-0.28	0.53	0.00	0.00	0.00	0.00	0.00	0.00
D	0.00	-0.28	0.53	0.65	-0.47	0.00	0.00	0.00	0.00	0.00	0.00
AB	0.00	0.00	0.00	0.00	0.00	-0.08	0.76	-0.49	0.30	0.29	-0.08
BC	0.00	0.00	0.00	0.00	0.00	-0.93	-0.05	0.24	0.25	-0.01	-0.09
CD	0.00	0.00	0.00	0.00	0.00	-0.08	-0.50	-0.75	0.27	-0.31	-0.08
AC	0.00	0.00	0.00	0.00	0.00	0.24	-0.34	0.18	0.55	0.62	-0.34
BD	0.00	0.00	0.00	0.00	0.00	0.23	0.24	0.30	0.49	-0.66	-0.34
AD	0.00	0.00	0.00	0.00	0.00	-0.07	0.02	-0.10	-0.48	0.02	-0.87

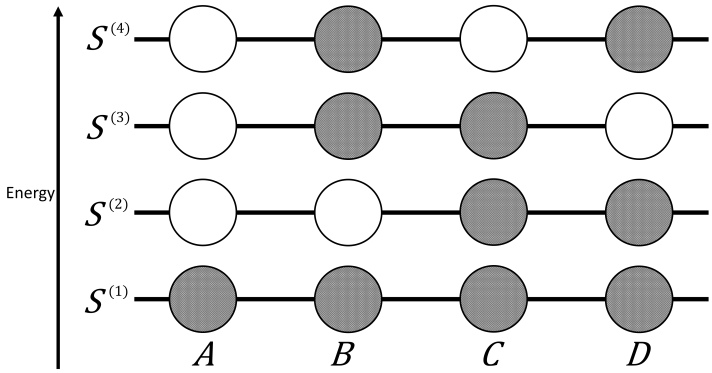

Figure 4.12: Representation of the phase of the localized states forming the singlet delocalized wave functions.

Table 4.19: Electronic couplings for four benzene molecules on a stack in the delocalized description (meV)

	CASSCF					
	$TT^{(1)}$	$TT^{(2)}$	$TT^{(3)}$	$TT^{(4)}$	$TT^{(5)}$	$TT^{(6)}$
$S^{(1)}$	0.00	7.26	0.00	0.00	-3.21	0.00
$S^{(2)}$	-13.66	0.00	-2.91	-3.84	0.00	-1.49
$S^{(3)}$	0.00	16.17	0.00	0.00	-7.22	0.00
$S^{(4)}$	14.48	0.00	-14.41	10.84	0.00	3.49
	AIFDEM					
	$TT^{(1)}$	$TT^{(2)}$	$TT^{(3)}$	$TT^{(4)}$	$TT^{(5)}$	$TT^{(6)}$
$S^{(1)}$	0.06	5.70	-1.27	-0.10	-2.68	-0.01
$S^{(2)}$	11.12	0.87	-3.73	-2.60	0.12	1.04
$S^{(3)}$	0.05	14.47	-3.01	-0.30	-6.94	-0.01
$S^{(4)}$	14.36	-2.54	12.22	-10.45	0.42	3.22

4.3.4 Six and eight benzene molecules on a stack

The calculation is extended to six (Figure 4.13) and eight benzenes (Figure 4.14) on a stack. These calculations are too expensive to be carried out with CAS(6,6)SCF input wave functions so will be restricted to the AIFDEM approximation. Localized energies of the hexamer are shown in Table 4.20 following the aforementioned trend with centered states having lesser energy and higher $S-{}^1TT$ coupling. In the delocalized states of the hexamer (Tables 4.22 and 4.23) can be appreciated the delocalization up to triplet separation states hinted by the previous case while direct triplet diffusion is harder, for that reason they are not included in the octamer case (Tables 4.27 and 4.28).

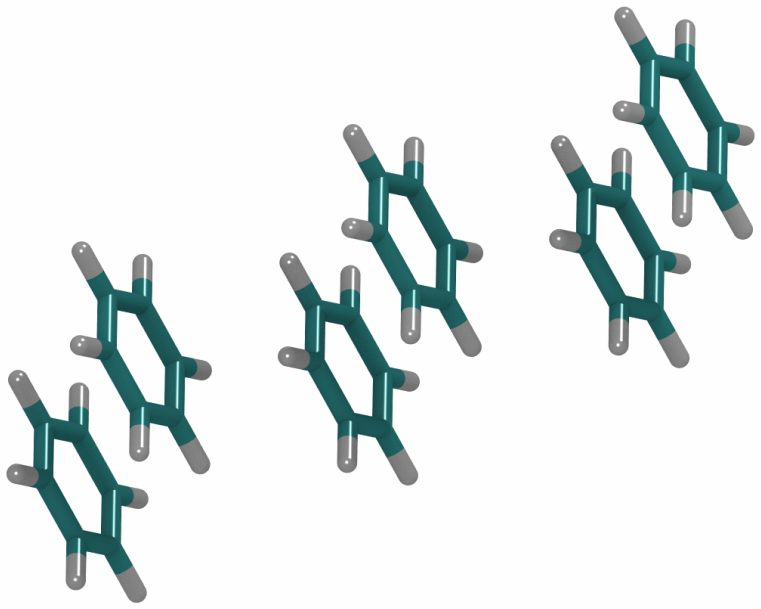

Figure 4.13: Six benzenes on a stack.

Table 4.20: NOCI relative energy levels for six benzene molecules on a stack in the localized description (eV).

ΔE (eV) AIFDEM			
G-S	0.00	AC	9.88
A	6.19	BD	9.86
B	6.17	CE	9.86
C	6.17	DF	9.88
D	6.17	AD	9.88
E	6.17	BE	9.86
F	6.19	CF	9.88
AB	9.87	AE	9.89
BC	9.85	BF	9.89
CD	9.84		
DE	9.85		
EF	9.87		

Table 4.21: Singlet fission electronic couplings for six benzene molecules on a stack in the localized description (meV)

	AB	BC	CD	DE	EF
A	12.47	-0.06	-0.01	-0.01	-0.01
B	-12.25	-12.74	0.08	0.03	0.02
C	-0.08	12.64	12.76	-0.08	-0.03
D	0.03	0.08	-12.66	-12.73	0.08
E	-0.02	-0.03	-0.08	12.64	12.35
F	0.01	0.01	0.02	0.07	-12.37

Table 4.22: Singlet delocalized NOCI wave functions in terms of localized states.

ΔE	0.00	6.14	6.15	6.17	6.18	6.20	6.20
	$S^{(0)}$	$S^{(1)}$	$S^{(2)}$	$S^{(3)}$	$S^{(4)}$	$S^{(5)}$	$S^{(6)}$
G-S	1.00	0.00	0.00	0.00	0.00	0.00	0.00
A	0.00	-0.13	0.29	0.43	-0.51	-0.54	0.39
B	0.00	-0.38	0.57	0.42	-0.01	0.43	-0.42
C	0.00	-0.58	0.31	-0.37	0.49	-0.15	0.41
D	0.00	-0.58	-0.31	-0.37	-0.49	-0.15	0.41
E	0.00	-0.38	-0.57	0.42	0.01	0.43	0.42
F	0.00	-0.13	-0.29	0.43	0.51	-0.54	-0.39

Table 4.23: Triplet delocalized NOCI wave functions in terms of localized states.

ΔE	9.83	9.84	9.84	9.87	9.87
	$TT^{(1)}$	$TT^{(2)}$	$TT^{(3)}$	$TT^{(4)}$	$TT^{(5)}$
AB	-0.02	-0.04	-0.05	0.83	-0.01
BC	-0.30	-0.61	-0.55	-0.15	0.03
CD	-0.64	0.00	0.58	0.03	-0.03
DE	-0.30	0.61	-0.56	-0.02	0.15
EF	-0.02	0.04	-0.05	-0.02	-0.83
AC	0.07	0.16	0.15	-0.46	0.01
BD	0.40	0.29	0.01	0.12	0.05
CE	0.40	-0.29	0.01	-0.06	-0.12
DF	0.07	-0.15	0.14	0.01	0.46
AD	-0.09	-0.10	-0.04	0.21	-0.03
BE	-0.26	0.00	-0.01	-0.04	0.04
CF	-0.09	0.10	-0.04	0.02	-0.22
AE	0.06	0.02	0.01	-0.07	-0.01
BF	0.06	-0.02	0.01	0.01	0.08

Table 4.24: Singlet fission electronic couplings for six benzene molecules on a stack in the delocalized description (meV)

	$TT^{(1)}$	$TT^{(2)}$	$TT^{(3)}$	$TT^{(4)}$	$TT^{(5)}$
$S^{(1)}$	-0.09	2.98	0.01	2.91	2.85
$S^{(2)}$	8.56	0.08	-3.02	-1.90	2.07
$S^{(3)}$	-0.06	12.31	0.03	1.56	1.45
$S^{(4)}$	0.86	0.05	-11.44	-5.87	6.08
$S^{(5)}$	-0.01	10.07	0.02	-9.24	-8.82
$S^{(6)}$	-6.61	-0.01	-13.06	6.62	-6.90

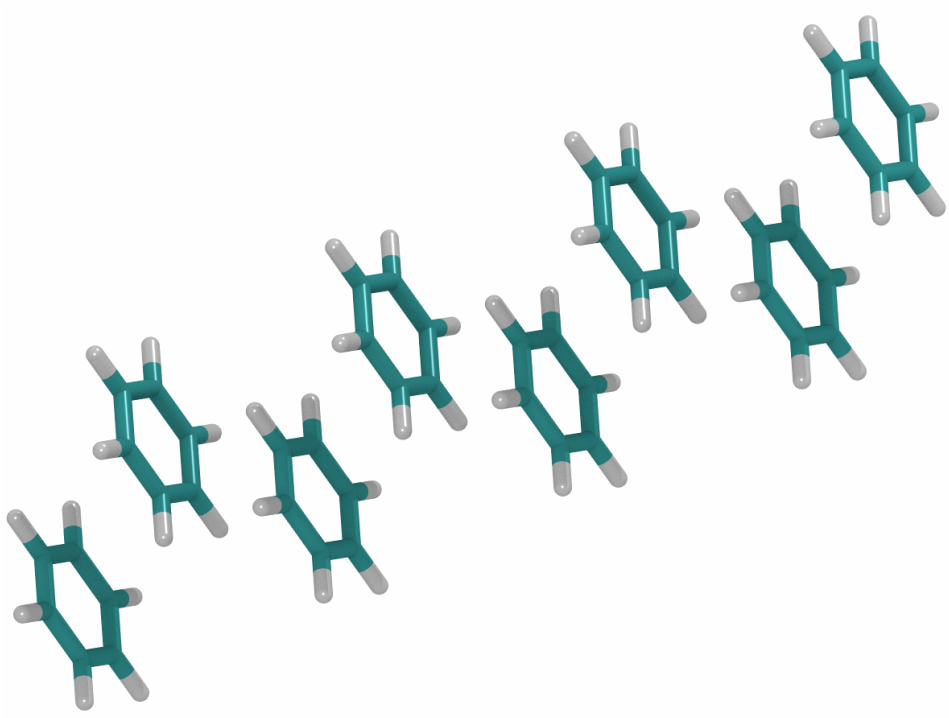

Figure 4.14: Eight benzenes on a stack.

Table 4.25: Relative energy levels for eight benzene molecules on a stack in the localized description (eV).

	ΔE (eV)		ΔE (eV)
S_0	0.00	AB	9.87
A	6.19	BC	9.85
B	6.17	CD	9.85
C	6.17	DE	9.85
D	6.17	EF	9.85
E	6.17	FG	9.85
F	6.17	GH	9.87
G	6.17		
H	6.19		

Table 4.26: Electronic couplings for eight benzene molecules on a stack in the localized description (meV).

	AB	BC	CD	DE	EF	FG	GH
A	12.48	-0.06	-0.01	-0.01	-0.01	-0.01	-0.01
B	-12.25	-12.74	0.08	0.03	0.03	0.03	0.02
C	-0.08	12.64	12.77	-0.08	-0.03	-0.03	-0.02
D	0.03	0.08	-12.67	-12.77	0.08	0.03	0.02
E	-0.02	-0.03	-0.08	12.67	12.77	-0.08	-0.03
F	0.02	0.03	0.03	0.08	-12.67	-12.74	0.08
G	-0.02	-0.03	-0.03	-0.03	-0.08	12.64	12.35
H	0.01	0.01	0.01	0.01	0.02	0.07	-12.37

Table 4.27: Singlet delocalized NOCI wave functions in terms of localized states.

ΔE	0.00	6.14	6.15	6.16	6.17	6.18	6.19	6.20	6.20
	$S^{(0)}$	$S^{(1)}$	$S^{(2)}$	$S^{(3)}$	$S^{(4)}$	$S^{(5)}$	$S^{(6)}$	$S^{(7)}$	$S^{(8)}$
G-S	1.00	0.00	0.00	0.00	0.00	0.00	0.00	0.00	-0.01
A	0.00	-0.08	0.17	0.28	-0.38	0.44	-0.45	0.48	0.36
B	0.00	-0.23	0.43	0.49	-0.38	0.11	0.18	-0.43	-0.38
C	0.00	-0.41	0.49	0.16	0.31	-0.48	0.21	0.28	0.35
D	0.00	-0.52	0.22	-0.39	0.35	0.26	-0.47	-0.10	-0.33
E	0.00	-0.52	-0.22	-0.39	-0.35	0.26	0.47	-0.10	0.33
F	0.00	-0.41	-0.49	0.16	-0.31	-0.48	-0.21	0.28	-0.35
G	0.00	-0.23	-0.43	0.49	0.38	0.11	-0.18	-0.43	0.38
H	0.00	-0.08	-0.17	0.28	0.38	0.44	0.45	0.48	-0.36

Table 4.28: Triplet delocalized NOCI wave functions in terms of localized states.

ΔE	9.83	9.83	9.84	9.84	9.84	9.87	9.87
	$TT^{(1)}$	$TT^{(2)}$	$TT^{(3)}$	$TT^{(4)}$	$TT^{(5)}$	$TT^{(6)}$	$TT^{(7)}$
AB	0.00	-0.01	-0.02	0.04	-0.04	0.60	-0.42
BC	-0.12	-0.26	-0.41	0.59	-0.49	-0.08	0.18
CD	-0.42	-0.55	-0.28	-0.30	0.41	0.12	-0.02
DE	-0.58	0.00	0.57	0.00	-0.38	0.05	-0.26
EF	-0.42	0.55	-0.28	0.29	0.41	-0.13	-0.05
FG	-0.12	0.26	-0.41	-0.59	-0.49	0.03	0.18
GH	0.00	0.01	-0.02	-0.04	-0.04	-0.58	-0.53
AC	0.02	0.05	0.09	-0.14	0.12	-0.28	0.14
BD	0.17	0.28	0.27	-0.14	0.04	0.08	0.26
CE	0.34	0.21	-0.13	0.16	-0.02	0.22	-0.32
DF	0.34	-0.21	-0.13	-0.16	-0.02	-0.10	-0.36
EG	0.17	-0.28	0.27	0.14	0.04	-0.21	0.22
FH	0.02	-0.05	0.08	0.13	0.12	0.29	0.20

Table 4.29: Singlet fission electronic couplings for eight benzene molecules on a stack in the delocalized description (meV)

	$TT^{(1)}$	$TT^{(2)}$	$TT^{(3)}$	$TT^{(4)}$	$TT^{(5)}$	$TT^{(6)}$	$TT^{(7)}$
$S^{(1)}$	0.03	-0.39	0.00	-3.35	-0.11	2.90	0.29
$S^{(2)}$	-5.66	-0.02	0.12	-0.10	4.47	-0.34	4.46
$S^{(3)}$	0.07	-5.45	-0.01	-9.45	-0.04	-0.86	-0.12
$S^{(4)}$	-11.82	-0.04	3.51	-0.01	-5.57	-0.94	5.54
$S^{(5)}$	-0.03	14.22	0.02	-2.89	-0.04	3.25	0.19
$S^{(6)}$	2.15	0.03	-14.08	-0.03	2.81	0.35	3.67
$S^{(7)}$	-0.01	-10.17	-0.01	8.71	0.04	13.32	1.39
$S^{(8)}$	-7.85	-0.01	-14.22	0.03	-5.76	0.04	-8.17

4.3.5 Naphthalene trimer

Performing now the same calculation for three naphthalene molecules on a stack (Figure 4.15), it can be seen in table 4.30 that the monomer does not either fulfill the singlet fission condition. On the other hand, there are not big discrepancies between the AIFDEM and CASSCF results.
Its behavior is similar to that seen in the benzene case but, although the difference of the singlet with the triplet rises making the species more near to the singlet fission condition, the values of the singlet fission and triplet separation electronic couplings (Tables 4.32 and 4.33) are lower in general and it is remarkable that the triplet separation phenomena will be less favored than in the benzene stack as its associated coupling is half of those of singlet fission. The consequence of this is that state AC is not mixed with AB and CD in the delocalized description, but still very near in energy (0.01 eV) to these and with a relevant electronic coupling (Table 4.35) with $TT^{(1)}$ and $TT^{(2)}$ (1.18 meV). Hence, here the triplet separation process is not mixed with singlet fission.

Table 4.30: Relative energy levels for the naphthalene molecule (eV).

	ΔE (eV)	
	CASSCF	AIFDEM
S_0	0.00	0.00
S_1	5.88	5.42
T_1	4.19	3.33
$D+$	7.92	7.97
$D-$	2.42	2.14

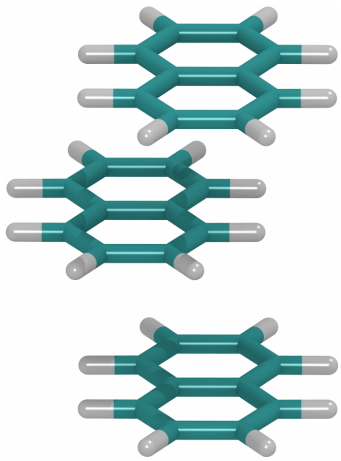

Figure 4.15: Naphthalene trimer.

Table 4.31: Relative energy levels for three naphthalene molecules on a stack in the localized description (eV).

	ΔE (eV)	
	CASSCF	AIFDEM
$G-S$	0.00	0.00
A	5.88	5.41
B	5.87	5.40
C	5.88	5.41
AB	8.46	6.65
BC	8.46	6.65
AC	8.47	6.66
A^+B-	7.53	7.17
A^-B^+	7.23	6.87
B^+C^-	7.23	6.87
B^-C^+	7.53	7.17

Table 4.32: Electronic couplings of three naphthalene molecules in the localized description (meV).

	CASSCF		AIFDEM	
	AB	***BC***	***AB***	***BC***
A	3.55	-0.04	-4.27	0.01
B	-3.46	-3.46	4.22	4.22
C	-0.04	3.55	0.01	-4.27

Table 4.33: Electronic coupling with the triplet separation state AC in the localized description (meV).

	CASSCF	AIFDEM
	AC	***AC***
A	0.02	-0.02
B	-0.02	0.01
C	0.02	-0.02
AB	-1.20	-2.35
BC	-1.20	-2.35

Table 4.34: Delocalized NOCI wave functions in terms of localized states of three naphthalene molecules on a stack.

AIFDEM							
ΔE (eV)	0.00	5.38	5.40	5.41	6.55	6.55	6.66
	$S^{(0)}$	$S^{(1)}$	$S^{(2)}$	$S^{(3)}$	$TT^{(1)}$	$TT^{(2)}$	$TT^{(3)}$
G-S	1.00	0.00	0.00	-0.01	0.00	0.00	0.00
A	0.00	0.38	0.70	-0.60	0.00	0.00	0.00
B	0.00	0.84	0.00	0.53	0.00	0.00	0.00
C	0.00	0.38	-0.70	-0.60	0.00	0.00	0.00
AB	0.00	0.00	0.00	0.00	0.62	0.62	-0.01
BC	0.00	0.00	0.00	0.00	0.62	-0.62	-0.01
AC	0.00	0.00	0.00	0.00	0.02	0.00	1.00
A^+B^-	0.01	0.06	0.01	0.03	-0.16	-0.13	0.00
A^-B^+	-0.01	0.04	0.06	-0.04	0.28	0.30	-0.01
B^+C^-	-0.01	0.04	-0.06	-0.04	0.28	-0.30	-0.01
B^-C^+	0.01	0.06	-0.01	0.03	-0.16	0.13	0.00
CASSCF							
ΔE (eV)	0.00	5.87	5.87	5.88	8.53	8.53	8.48
	$S^{(0)}$	$S^{(1)}$	$S^{(2)}$	$S^{(3)}$	$TT^{(1)}$	$TT^{(2)}$	$TT^{(3)}$
G-S	1.00	0.00	0.00	-0.01	0.00	0.00	0.00
A	0.00	0.37	-0.70	0.60	0.00	0.00	0.00
B	0.00	0.84	0.00	-0.52	0.00	0.00	0.00
C	0.00	0.37	0.70	0.60	0.00	0.00	0.00
AB	0.00	0.00	0.00	0.00	0.69	0.70	-0.02
BC	0.00	0.00	0.00	0.00	-0.69	0.70	-0.02
AC	0.00	0.00	0.00	0.00	0.00	-0.03	-1.00
A^+B^-	-0.01	0.06	-0.01	-0.02	-0.13	-0.12	0.00
A^-B^+	0.01	0.05	-0.06	0.04	0.10	0.10	0.00
B^+C^-	0.01	0.05	0.06	0.04	-0.10	0.10	0.00
B^-C^+	-0.01	0.06	0.01	-0.02	0.13	-0.12	0.00

Table 4.35: Electronic couplings for three naphthalene molecules on a stack in the delocalized description (meV)

	CASSCF			AIFDEM		
	$TT^{(1)}$	$TT^{(2)}$	$TT^{(3)}$	$TT^{(1)}$	$TT^{(2)}$	$TT^{(3)}$
$S^{(1)}$	0.00	5.76	-0.24	2.25	0.00	0.17
$S^{(2)}$	0.96	0.00	0.00	0.00	-35.45	0.00
$S^{(3)}$	0.00	-4.91	0.14	37.63	0.00	-1.18

4.3.6 Overall line results

The overall mechanism of singlet fission plus triplet separation across the line stack can be summarized as

$$A, B, C \xrightarrow{\gamma} AB, BC \xrightarrow{\zeta} AC \tag{4.89}$$

where zeta denotes the triplet separation electronic coupling, of size equal to γ in the benzene stack and half γ in the naphthalene trimer. There may be another possible mechanism, less probable, in which A and C are directly coupled to AC. We denote the coupling which characterized this mechanism as ξ.

$$A, C \xrightarrow{\xi} AC \tag{4.90}$$

which is almost negligible in the benzene stack and can be considered zero in the naphthalene trimer studied. All average values are shown in Table 4.36 in which significant differences between the two materials are observed in the Triplet Separation couplings with respect to those of singlet fission as commented above, making the separation process harder as an extra energy surplus is needed to reach this state. In what refers to charge transfer states, they can highly interact with singlets and coupled triplets and enhance or decrease the electronic couplings, depending of the species at the study. It has been checked that the CT states do not play a relevant role in the benzene according to the CASSCF calculations but can really play an important task in bigger chromophores as seen in the naphthalene.
For further study, the four stack was considered which adds new states BD, AD, enabling the triplet diffusion route from AC and BD to AD with triplet diffusion coupling $\zeta' = 11.76$ comparable to singlet fission and triplet separation in the benzene. The mechanisms can be summarized in the following scheme

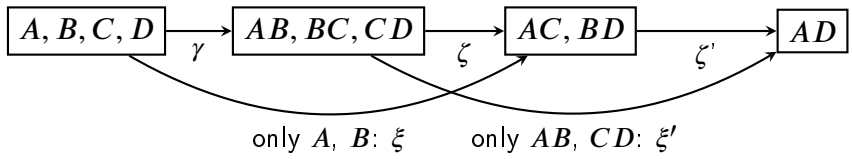

where the direct couplings ξ and ξ' have been proven to be of minor importance. A key characteristic identified in the values of the couplings is that if ζ and γ have similar values then the singlet fission coupled triplets and the triplet separation state are coupled as well as both phenomena, as observed in the benzene stack but not present in the naphthalene as $\zeta \approx \gamma/2$. If ζ' is of the order of ζ then triplet separation and triplet diffusion phenomena are also coupled as observed in the benzene tetramer stack.
Summarizing,

- The study identified three mechanisms for exciton transfer in chromophores, that can be strongly coupled or happening in separate steps, depending on the system:
  - Singlet Fission $A, B, C, D \xrightarrow{\gamma} AB, BC, CD$
  - Triplet Separation $AB, BC, CD \xrightarrow{\zeta} AC, BD$
  - Triplet Diffusion $AC, BD \xrightarrow{\zeta'} AD$
- Charge transfer states can play a fundamental role, enhancing of weakening these mechanisms.
- State AC is very difficult to reach directly from A, B and C in this stack configuration, as well as state AD from AB, BC and CD. Electronic coupling ξ' is very small.

These factors are present in Singlet Fission materials and can enhance or diminish the suitability to build organic solar cells. In particular, charge transfer states have proven to have an important role in pairs of acenes, so the addition of Triplet Separation and Triplet Diffusion states could also be studied as it seems to be reachable from the other excitonic states, which means that simulations should not be restricted to dimer systems only.
The next step is to reproduce the plots obtained from the models. Table 4.37 summarizes the relevant average transition strength values obtained from calculations. The same is done with γ in Table 4.38.
Figure 4.16 recreates the graph 4.4 adjusting the parameters γ_1 and γ_2 by the least-squares method to expression 4.29 . Figure 4.6 was not able to be

reproduced because of two main reasons; 1) the effect of boundaries was neglected in the model while there is an energetic bias towards the innermost fragments in the real calculations; 2) states are nearly degenerated, so the distinction between lowest and highest states is highly arbitrary. Hence, it is very difficult to confirm the difference found in the model calculations between the lowest-to-all and the lowest-to-lowest scenarios using the delocalized description of the states.

Table 4.36: Electronic couplings in the benzene and naphthalene trimer stacks

	Benzene		Naphthalene	
	CASSCF	AIFDEM	CASSCF	AIFDEM
Singlet Fission γ	13.48	12.33	3.51	4.25
Triplet Separation ζ	11.53	9.52	1.20	2.35
Direct Separation ξ	0.09	0.05	0.02	0.01

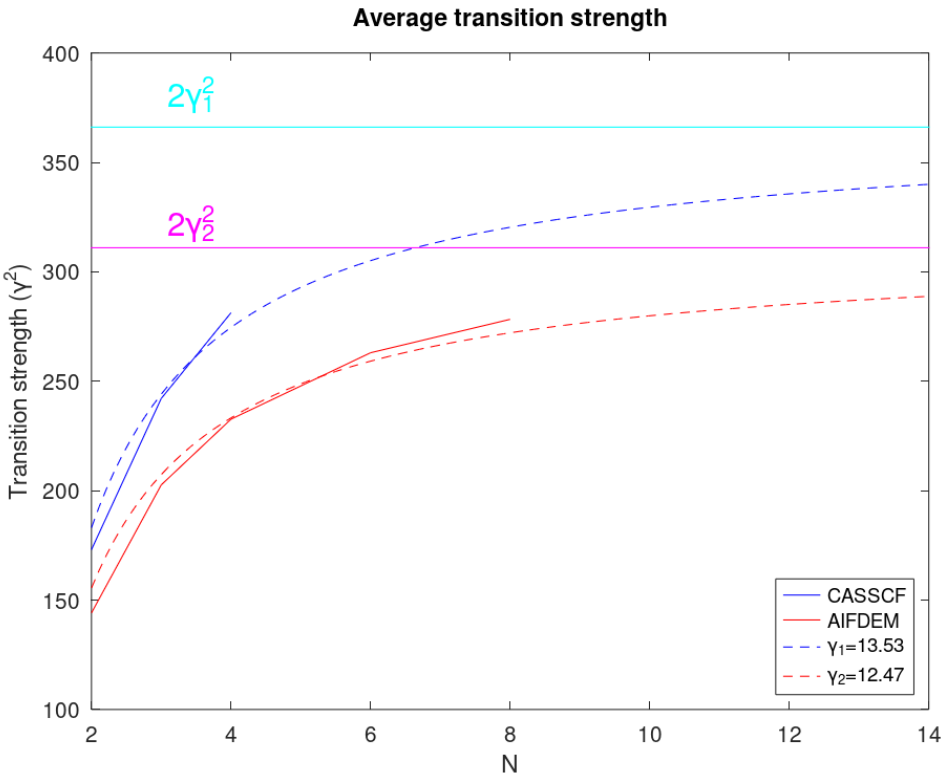

Figure 4.16: Average transition probability for a given number of molecules on a line with CASSCF and AIFDEM inputs for NOCI. Dashed lines are interpolated from the formula 4.29 with γ_1 and γ_2 are adjusted by least-squares method.

Table 4.37: Average transition probabilities obtained with the CAS(6,6)SCF and AIFDEM input wavefunctions. N is the number of molecules on the stack.

N	2	3	4	6	8
CASSCF	175.03	242.12	281.30	-	-
AIFDEM	144.12	202.63	232.66	263.02	278.29

Table 4.38: Average values of γ obtained with the CAS(6,6)SCF and AIFDEM input wavefunctions. N is the number of molecules on the stack.

N	2	3	4	6	8
CASSCF	13.23	13.48	13.69	-	-
AIFDEM	12.00	12.33	12.45	12.56	12.61

4.3.7 Conclusions from METB

A Many Electron Tight Binding (METB) model is proposed in order to understand the effect of delocalization on the $S - {}^1TT$ non-adiabatic coupling. After that, the conclusions drawn from the model study are checked by comparing its results with the ones obtained by a NOCI calculation. The localized description shows a one-to-one correspondence, but the delocalized description is more difficult to reproduce in the NOCI calculations, the neglect of the different environment at the boundaries in the model for the line case obscures the comparison. The choice of the singlet fission chromophore is not optimal, the series of calculations with an increasing number of molecules in the ensembles that is presented here for benzene is not easily done for larger, more realistic SF chromophores. This topic of on-going research and hence the full test of the model for real SF chromophores is still to be done. Full NOCI-F calculations for closed topology have also been carried out, but at the distance where the molecules have significant interaction, it turns out that part of the other molecules in the system start to come unrealistically close.
On the other hand, the validity of the AIFDEM approximation is shown for more qualitative descriptions, which gives similar results as a CASSCF input that is much more expensive to apply. Therefore, for exploration of singlet fission phenomena in bigger clusters of molecules, it can be a good approximation to the full (and computationally expensive) NOCI-F.

4.4 Identification of dark and bright states

Beside the electronic coupling γ can give an insight of the transition probability between states, the oscillator strength is another quantity that can identify the capability of an state to accept or emit a photon and thus to carry more intensity by optical absorption. Those states with high are called bright states in contrast to those that exhibit less sensibility called dark states. In terms of oscillator strength

$$f_{ij} = \frac{2}{3}\left(H_{jj} - H_{ii}\right)|\boldsymbol{\mu}_{ij}|^2 \tag{4.91}$$

where i is the initial state and j is the final state, bright states are those final states that exhibit great values of oscillator strength, while dark states are those whose value is less or almost negligible. An example of this identification is the Perylenediimide dimer system (Figure 4.17) studied in[1] identified as a singlet fission candidate for organic solar panels. The MEBFs of the system are those involved in singlet fission S_0S_0, S_0S_1, S_1S_0, ^1TT, D^+D^-, D^-D^+, where each monomer fulfills the thermodynamic condition $E(S_1) \approx 2E(T_1)$. The calculation and diagonalization of the NOCI Hamiltonian yields the states: S_0S_0 ground state with no mixing, a resonance between the Frenkel excitons $S_0S_1 \pm S_1S_0$ as the first excited state and the triplet coupled singlet state ^1TT, all dressed by the charge transfer states. For an upcoming excitation from the ground-state, $S_0S_1 + S_1S_0$ turns out to be the bright state with an oscillator strength of 1.6 a.u while $S_0S_1 - S_1S_0$ is the dark state with an oscillator strength of $1 \cdot 10^{-5}$. This means that the state with $+$ is the one that is accessed through irradiation from the ground state. On the contrast, this state exhibits a small electronic coupling with the mainly ^1TT state thus not very good for singlet fission. In contrast, the dark state has a big electronic coupling with ^1TT, thus favoring the SF process. However, as in this system both states are close in energy, it expected that both states are accessible from irradiation.

Therefore, oscillator strength incorporation in GronOR can lead to a better understanding of photoexcitation mechanisms and identify allowed transitions in the molecular ensemble.

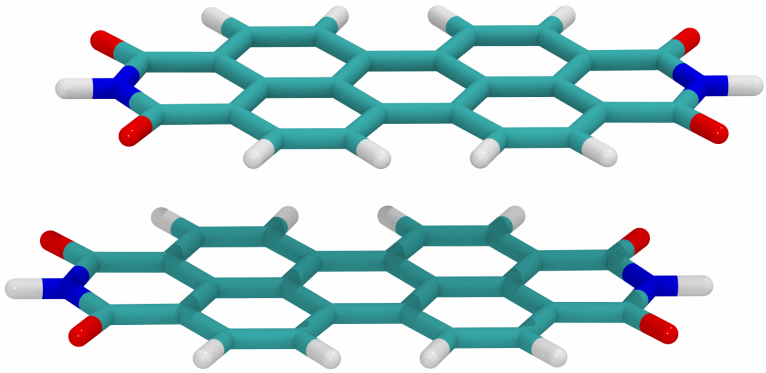

Figure 4.17: Perylenediimide (PDI) dimer.

4.5 Relativistic effects in NOCI

For the test of the spin-orbit coupling features two systems have been used. They are two hepta-coordinated system with a metal in the center, either a Ni or Pd. Both have low-energy triplet configurations and exhibit a high splitting between the M components due to the spin orbit coupling . Both also have a higher in energy singlet configuration that interacts with these via spin orbit coupling, otherwise the interaction would be zero. The calculations have been carried out in OpenMolcas and GronOR by optimizing separately the triplets in one orbital set and the singlet in another, leading to a NOCI calculation. As detailed in Chapter 2 about Electronic Structure Methods, OpenMolcas in its module called RASSI creates a two unique biorthonormal orbital sets for each pair of MEBFs, imposing restrictions on the active space and does not handle the case where there are singularities. On the other hand, GronOR does not impose restrictions with the price to pay of biorthogonalizing the orbitals for each pair of determinants. The consequence of this is that the two methods are in different in essence but their results are comparable.

4.5.1 Hepta-coordinated Ni

For the hepta-coordinated Ni system 4.18, four triplet roots T_1, T_2, T_3 and T_4 lower in energy are considered as long as the first excited singlet S_1. Optimized orbital sets are used for each state being almost identical in the case of the triplets but significantly different for the singlet.
The relative values of the energies for such system are in table 4.39. Tables 4.40, 4.41 show the computed non-zero spin orbit Hamiltonian matrix elements where it can be observed the interaction between different S and M components. Both programs use a slightly different approach explaining the difference in the results specially noticeable in the singlet-triplet matrix elements for which the two set of orbitals are more different. These matrix elements plus the addition of the scalar part 4.39 originate 13 eigenvectors whose relevant information is usually presented in terms of the weights of every multiplicity as shown in tables 4.42 and 4.43. These show some mixing between the triplets and the singlet illustrating the fact that S and M are not "good" quantum numbers when applying a relativistic treatment. Tables 4.44 and 4.45 show the energy splitting between all the energy levels with respect to the lowest spin-orbit level and to the lowest spin free level 4.39.

4.5.2 Hepta-coordinated Pd

The Nickel atom is substituted by Palladium in the center, including three triplet roots in the calculation plus the singlet. The energies of the spin-free states are in table 4.46

Table 4.39: Relative spin-free energies of the hepta-coordinated Ni compound

State	ΔE (eV)
T_1	0.00
T_2	0.35
T_3	0.81
T_4	0.88
S_1	2.13

Table 4.40: Interaction energies (in cm^{-1}) of different states given by OpenMolcas

State 1	S	M	State 2	S	M	Real	Imaginary	Absolute
T_2	1.0	-1.0	T_1	1.0	-1.0	0.00	670.70	670.70
T_2	1.0	1.0	T_1	1.0	1.0	0.00	-670.70	670.70
T_3	1.0	-1.0	T_1	1.0	0.0	-453.12	-0.00	453.12
T_3	1.0	-1.0	T_2	1.0	0.0	0.00	-17.83	17.83
T_3	1.0	0.0	T_1	1.0	-1.0	453.12	-0.00	453.12
T_3	1.0	0.0	T_1	1.0	1.0	-453.12	-0.00	453.12
T_3	1.0	0.0	T_2	1.0	-1.0	0.00	-17.83	17.83
T_3	1.0	0.0	T_2	1.0	1.0	0.00	-17.83	17.83
T_3	1.0	1.0	T_1	1.0	0.0	453.12	0.00	453.12
T_3	1.0	1.0	T_2	1.0	0.0	0.00	-17.83	17.83
T_4	1.0	-1.0	T_1	1.0	0.0	0.00	432.13	432.13
T_4	1.0	-1.0	T_2	1.0	0.0	59.09	0.00	59.09
T_4	1.0	-1.0	T_3	1.0	-1.0	0.00	-545.41	545.41
T_4	1.0	0.0	T_1	1.0	-1.0	0.00	432.13	432.13
T_4	1.0	0.0	T_1	1.0	1.0	0.00	432.13	432.13
T_4	1.0	0.0	T_2	1.0	-1.0	-59.09	0.00	59.09
T_4	1.0	0.0	T_2	1.0	1.0	59.09	0.00	59.09
T_4	1.0	1.0	T_1	1.0	0.0	0.00	432.13	432.13
T_4	1.0	1.0	T_2	1.0	0.0	-59.09	0.00	59.09
T_4	1.0	1.0	T_3	1.0	1.0	0.00	545.41	545.41
S_1	0.0	0.0	T_1	1.0	0.0	0.00	0.00	0.00
S_1	0.0	0.0	T_2	1.0	0.0	0.00	49.55	49.55
S_1	0.0	0.0	T_3	1.0	-1.0	-297.44	0.00	297.44
S_1	0.0	0.0	T_3	1.0	1.0	-297.44	0.00	297.44
S_1	0.0	0.0	T_4	1.0	-1.0	0.00	287.34	287.34
S_1	0.0	0.0	T_4	1.0	1.0	0.00	-287.34	287.34

Table 4.41: Interaction energies (in cm^{-1}) of different states given by GronOR

State 1	S	M	State 2	S	M	Real	Imaginary	Absolute
T_2	1.0	-1.0	T_1	1.0	-1.0	0.00	672.05	672.05
T_2	1.0	1.0	T_1	1.0	1.0	0.00	-672.05	672.05
T_3	1.0	-1.0	T_1	1.0	0.0	-451.93	0.00	451.93
T_3	1.0	-1.0	T_2	1.0	0.0	0.00	-17.44	17.44
T_3	1.0	0.0	T_1	1.0	-1.0	-451.93	0.00	451.93
T_3	1.0	0.0	T_1	1.0	1.0	451.93	0.00	451.93
T_3	1.0	0.0	T_2	1.0	-1.0	0.00	-17.44	17.44
T_3	1.0	0.0	T_2	1.0	1.0	0.00	-17.44	17.44
T_3	1.0	1.0	T_1	1.0	0.0	-451.93	0.00	451.93
T_3	1.0	1.0	T_2	1.0	0.0	0.00	-17.44	17.44
T_4	1.0	-1.0	T_1	1.0	0.0	0.00	431.50	431.50
T_4	1.0	-1.0	T_2	1.0	0.0	59.40	0.00	59.40
T_4	1.0	-1.0	T_3	1.0	-1.0	0.00	-545.97	545.97
T_4	1.0	0.0	T_1	1.0	-1.0	0.00	431.50	431.50
T_4	1.0	0.0	T_1	1.0	1.0	0.00	431.50	431.50
T_4	1.0	0.0	T_2	1.0	-1.0	-59.40	0.00	59.40
T_4	1.0	0.0	T_2	1.0	1.0	59.40	0.00	59.40
T_4	1.0	1.0	T_1	1.0	0.0	0.00	431.50	431.50
T_4	1.0	1.0	T_2	1.0	0.0	-59.40	0.00	59.40
T_4	1.0	1.0	T_3	1.0	1.0	0.00	545.97	545.97
S_1	0.0	0.0	T_1	1.0	0.0	0.00	0.00	0.000
S_1	0.0	0.0	T_2	1.0	0.0	0.00	99.56	99.56
S_1	0.0	0.0	T_3	1.0	-1.0	-276.61	0.000	276.61
S_1	0.0	0.0	T_3	1.0	1.0	-276.61	0.000	276.61
S_1	0.0	0.0	T_4	1.0	-1.0	0.00	298.31	298.31
S_1	0.0	0.0	T_4	1.0	1.0	0.00	-298.31	298.31

Table 4.42: Weights of the spin-orbit-free states for each spin-orbit state given by OpenMolcas

	Energy (eV)	-0.03	-0.03	-0.01	0.35
State	S	1	2	3	4
T_1	1.0	0.91	0.91	0.93	0.05
T_2	1.0	0.07	0.07	0.05	0.95
T_3	1.0	0.02	0.01	0.01	0.00
T_4	1.0	0.00	0.01	0.01	0.00
S_1	0.0	0.00	0.00	0.00	0.00
	Energy (eV)	0.36	0.36	0.77	0.77
State	S	5	6	7	8
T_1	1.0	0.07	0.07	0.01	0.01
T_2	1.0	0.93	0.93	0.00	0.00
T_3	1.0	0.00	0.00	0.66	0.64
T_4	1.0	0.00	0.00	0.34	0.35
S_1	0.0	0.00	0.00	0.00	0.00
	Energy (eV)	0.82	0.89	0.92	0.93
State	S	9	10	11	12
T_1	1.0	0.07	0.07	0.01	0.01
T_2	1.0	0.93	0.93	0.00	0.00
T_3	1.0	0.00	0.00	0.66	0.64
T_4	1.0	0.00	0.00	0.34	0.35
S_1	0.0	0.00	0.00	0.00	0.00
	Energy (eV)	2.13			
State	S	13			
T_1	1.0	0.00			
T_2	1.0	0.00			
T_3	1.0	0.00			
T_4	1.0	0.00			
S_1	0.0	1.00			

Table 4.43: Weights of the spin-orbit-free states for each spin-orbit state given by GronOR

	Energy (eV)	-0.03	-0.02	-0.01	0.37
State	S	1	2	3	4
T_1	1.0	0.95	0.95	0.99	0.00
T_2	1.0	0.04	0.04	0.00	1.00
T_3	1.0	0.01	0.00	0.01	0.00
T_4	1.0	0.00	0.01	0.01	0.00
S_1	0.0	0.00	0.00	0.00	0.00
	Energy (eV)	0.38	0.38	0.78	0.78
State	S	5	6	7	8
T_1	1.0	0.04	0.04	0.00	0.00
T_2	1.0	0.96	0.96	0.00	0.00
T_3	1.0	0.00	0.00	0.72	0.70
T_4	1.0	0.00	0.00	0.28	0.29
S_1	0.0	0.00	0.00	0.00	0.00
	Energy (au)	0.83	0.90	0.93	0.95
State	S	9	10	11	12
T_1	1.0	0.01	0.01	0.00	0.01
T_2	1.0	0.00	0.00	0.00	0.00
T_3	1.0	0.99	0.00	0.28	0.29
T_4	1.0	0.00	0.99	0.72	0.70
S_1	0.0	0.00	0.00	0.00	0.00
	Energy (au)	2.01			
State	S	13			
T_1	1.0	0.00			
T_2	1.0	0.00			
T_3	1.0	0.00			
T_4	1.0	0.00			
S_1	0.0	1.00			

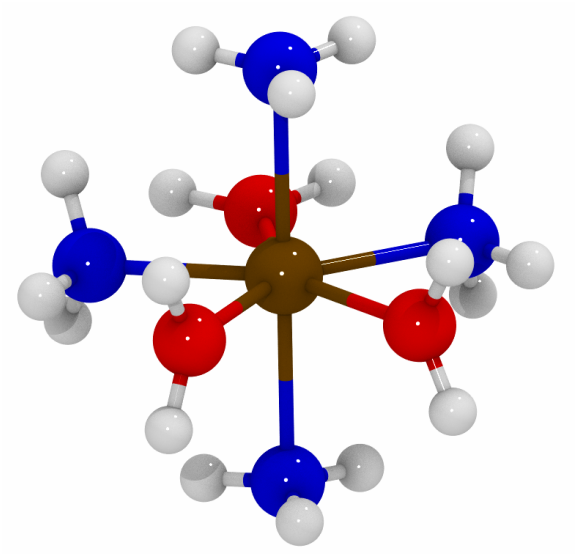

Figure 4.18: Hepta-coordinated nickel compound. Colors; Brown: Ni; Red: O; Blue: N; White: H

Table 4.44: Interaction energies (in cm^{-1}) of different states given by OpenMolcas

State	Relative EMIN(eV)	Rel lowest level(eV)	D:o, cm^{-1}
1	-0.03	0.00	0.00
2	-0.03	0.00	5.09
3	-0.01	0.01	104.53
4	0.35	0.37	2994.97
5	0.36	0.39	3142.57
6	0.36	0.39	3149.32
7	0.77	0.79	6402.14
8	0.77	0.80	6438.12
9	0.82	0.85	6830.83
10	0.89	0.91	7368.50
11	0.92	0.95	7651.24
12	0.93	0.96	7749.89
13	2.13	2.16	17424.05

Table 4.45: Interaction energies (in cm^{-1}) of different states given by GronOR

State	Relative EMIN(eV)	Rel lowest level(eV)	D:o, cm^{-1}
1	-0.03	0.00	0.00
2	-0.02	0.00	5.09
3	-0.01	0.01	98.52
4	0.37	0.39	3147.68
5	0.38	0.41	3289.28
6	0.38	0.41	3295.70
7	0.78	0.80	6476.57
8	0.78	0.81	6514.00
9	0.83	0.86	6904.85
10	0.90	0.92	7447.67
11	0.93	0.96	7729.22
12	0.95	0.97	7827.45
13	2.01	2.03	16385.58

Table 4.46: Relative spin-free energies of the hepta-coordinated Pd compound

State	ΔE (eV)
T_1	0.52
T_2	0.93
T_3	0.46
S_1	0.00

Table 4.47: Interaction energies (in cm^{-1}) given by OpenMolcas for the hepta-coordinated Pd system.

State 1	S	M	State 2	S	M	Real	Imaginary	Absolute
T_2	1.0	-1.0	T_1	1.0	-1.0	0.00	1341.69	1341.69
T_2	1.0	-1.0	T_1	1.0	0.0	4.56	2.90	5.41
T_2	1.0	0.0	T_1	1.0	-1.0	-4.56	2.90	5.41
T_2	1.0	0.0	T_1	1.0	1.0	4.56	2.90	5.41
T_2	1.0	1.0	T_1	1.0	0.0	-4.56	2.90	5.41
T_2	1.0	1.0	T_1	1.0	1.0	0.00	-1341.60	1341.69
T_3	1.0	-1.0	T_1	1.0	-1.0	-0.00	5.79	5.79
T_3	1.0	-1.0	T_1	1.0	0.0	-747.26	-64.27	750.02
T_3	1.0	-1.0	T_2	1.0	-1.0	0.00	-4.27	4.27
T_3	1.0	-1.0	T_2	1.0	0.0	91.14	-619.63	626.29
T_3	1.0	0.0	T_1	1.0	-1.0	747.26	-64.27	750.02
T_3	1.0	0.0	T_1	1.0	1.0	-747.26	-64.27	750.02
T_3	1.0	0.0	T_2	1.0	-1.0	-91.14	-619.63	626.29
T_3	1.0	0.0	T_2	1.0	1.0	91.14	-619.63	626.29
T_3	1.0	1.0	T_1	1.0	0.0	747.26	-64.27	750.02
T_3	1.0	1.0	T_1	1.0	1.0	-0.00	-5.79	5.79
T_3	1.0	1.0	T_2	1.0	0.0	-91.14	-619.63	626.29
T_3	1.0	1.0	T_2	1.0	1.0	0.00	4.27	4.27
S_1	0.0	0.0	T_1	1.0	-1.0	-5.08	27.57	28.03
S_1	0.0	0.0	T_1	1.0	0.0	-0.00	56.20	56.20
S_1	0.0	0.0	T_1	1.0	1.0	-5.08	-27.57	28.03
S_1	0.0	0.0	T_2	1.0	-1.0	-29.11	19.04	34.78
S_1	0.0	0.0	T_2	1.0	0.0	-0.00	23.69	23.69
S_1	0.0	0.0	T_2	1.0	1.0	-29.11	-19.04	34.78
S_1	0.0	0.0	T_3	1.0	-1.0	1089.71	-145.24	1099.35
S_1	0.0	0.0	T_3	1.0	0.0	0.00	-53.25	53.25
S_1	0.0	0.0	T_3	1.0	1.0	1089.71	145.24	1099.35

Table 4.48: Interaction energies (in cm^{-1}) given by GronOR for the hepta-coordinated Pd system.

State 1	S	M	State 2	S	M	Real	Imaginary	Absolute
T_2	1.0	-1.0	T_1	1.0	-1.0	0.00	1341.69	1341.69
T_2	1.0	-1.0	T_1	1.0	0.0	4.56	2.90	5.41
T_2	1.0	0.0	T_1	1.0	-1.0	-4.56	2.90	5.41
T_2	1.0	0.0	T_1	1.0	1.0	4.56	2.90	5.41
T_2	1.0	1.0	T_1	1.0	0.0	-4.56	2.90	5.41
T_2	1.0	1.0	T_1	1.0	1.0	0.00	-1341.69	1341.69
T_3	1.0	-1.0	T_1	1.0	-1.0	-0.00	5.79	5.79
T_3	1.0	-1.0	T_1	1.0	0.0	-747.26	-64.27	750.02
T_3	1.0	-1.0	T_2	1.0	-1.0	0.00	-4.27	4.27
T_3	1.0	-1.0	T_2	1.0	0.0	91.14	-619.63	626.29
T_3	1.0	0.0	T_1	1.0	-1.0	747.26	-64.27	750.02
T_3	1.0	0.0	T_1	1.0	1.0	-747.26	-64.27	750.02
T_3	1.0	0.0	T_2	1.0	-1.0	-91.14	-619.63	626.29
T_3	1.0	0.0	T_2	1.0	1.0	91.14	-619.63	626.29
T_3	1.0	1.0	T_1	1.0	0.0	747.26	-64.27	750.02
T_3	1.0	1.0	T_1	1.0	1.0	-0.00	-5.79	5.79
T_3	1.0	1.0	T_2	1.0	0.0	-91.14	-619.63	626.29
T_3	1.0	1.0	T_2	1.0	1.0	0.00	4.27	4.27
S_1	0.0	0.0	T_1	1.0	-1.0	-6.53	43.46	43.94
S_1	0.0	0.0	T_1	1.0	0.0	-0.00	59.19	59.19
S_1	0.0	0.0	T_1	1.0	1.0	-6.53	-43.46	43.94
S_1	0.0	0.0	T_2	1.0	-1.0	-68.87	46.84	83.29
S_1	0.0	0.0	T_2	1.0	0.0	-0.00	108.97	108.97
S_1	0.0	0.0	T_2	1.0	1.0	-68.87	-46.84	83.29
S_1	0.0	0.0	T_3	1.0	-1.0	1064.62	-321.81	1112.19
S_1	0.0	0.0	T_3	1.0	0.0	0.00	-42.95	42.95
S_1	0.0	0.0	T_3	1.0	1.0	1064.62	321.81	1112.19

Table 4.49: Weights of the spin-orbit-free states for each spin-orbit state given by OpenMolcas

	Energy (eV)	-0.02	0.46	0.46	0.51
State	S	1	2	3	4
T_1	1.0	0.00	0.90	0.89	0.99
T_2	1.0	0.00	0.10	0.11	0.00
T_3	1.0	0.01	0.00	0.00	0.01
S_1	0.0	0.99	0.00	0.00	0.00
	Energy (eV)	0.92	0.96	0.99	1.80
State	S	5	6	7	8
T_1	1.0	0.00	0.09	0.11	0.01
T_2	1.0	0.98	0.88	0.89	0.00
T_3	1.0	0.01	0.03	0.00	0.99
S_1	0.0	0.00	0.00	0.00	0.00
	Energy (eV)	1.82	1.82		
State	S	9	10		
T_1	1.0	0.01	0.00		
T_2	1.0	0.02	0.02		
T_3	1.0	0.97	0.97		
S_1	0.0	0.00	0.01		

Table 4.50: Weights of the spin-orbit-free states for each spin-orbit state given by GronOR

	Energy (eV)	-0.02	0.46	0.46	0.51
State	S	1	2	3	4
T_1	1.0	0.00	0.89	0.89	0.99
T_2	1.0	0.00	0.10	0.11	0.00
T_3	1.0	0.01	0.00	0.00	0.01
S_1	0.0	0.99	0.00	0.00	0.00
	Energy (eV)	0.92	0.96	0.99	1.80
State	S	9	10	11	12
T_1	1.0	0.00	0.09	0.11	0.01
T_2	1.0	0.98	0.88	0.89	0.00
T_3	1.0	0.01	0.03	0.00	0.99
S_1	0.0	0.00	0.00	0.00	0.00
	Energy (eV)	1.82	1.82		
State	S	9	10		
T_1	1.0	0.01	0.00		
T_2	1.0	0.02	0.01		
T_3	1.0	0.97	0.97		
S_1	0.0	0.00	0.01		

Table 4.51: Interaction energies (in cm^{-1}) of different states given by Open-Molcas

State	Relative EMIN(eV)	Rel lowest level(eV)	D:o, cm^{-1}
1	-0.02	0.00	0.00
2	0.46	0.48	3843.26
3	0.46	0.48	3890.06
4	0.51	0.53	4258.56
5	0.92	0.94	7559.61
6	0.96	0.98	7933.21
7	0.99	1.01	8141.92
8	1.80	1.82	14697.05
9	1.82	1.84	14843.77
10	1.82	1.84	14863.45

Table 4.52: Interaction energies (in cm^{-1}) of different states given by GronOR

State	Relative EMIN(eV)	Rel lowest level(eV)	D:o, cm^{-1}
1	-0.02	0.00	0.00
2	0.46	0.48	3854.15
3	0.46	0.48	3899.54
4	0.51	0.53	4267.63
5	0.92	0.94	7574.69
6	0.96	0.98	7943.32
7	0.99	1.01	8151.69
8	1.80	1.82	14704.58
9	1.82	1.84	14853.50
10	1.82	1.84	14876.33

References

[1] C. Sousa et al. “A Nonorthogonal Configuration Interaction Approach to Singlet Fission in Perylenediimide Compounds”. In: *The Journal of Physical Chemistry A* 127.47 (2023). PMID: 37964533, pp. 9944–9958.

[2] P. M. Zimmerman et al. “Mechanism for singlet fission in pentacene and tetracene: from single exciton to two triplets”. In: *Journal of the American Chemical Society* 133.49 (2011), pp. 19944–19952.

Chapter 5

Conclusions

Non-Orthogonal Electronic Structure Methods present a complex but highly interesting topic of research. Removing the restrictions of traditional methods opens a whole new area of study, where the accurate description of the electronic structure of complex materials can be combined with a straightforward interpretation of the results in terms in chemically intuitive concepts. This thesis has dealt with the task of extending the theoretical framework of NOCI with both own and external developments and incorporate them in software production. In the process of testing new ideas, this work has laid the theoretical foundations for further efficiency improvements and implementation of new features in the software in the near future. Especially the formulation of the treatment of excited determinants in second quantization through Wick's Theorem and its extended version can be of great use in this aspect. The following points describe the main conclusions this work has arrived and outlines how the theoretical study can be used to further develop the current NOCI implementation.

1. **Code development:** The two implementations with major impact have been (i) the generalization of the spin coupling in the generation of the many-electron basis functions. The multiplication of fragment wave functions was limited to overall singlet coupling of singlet, doublet or triplet functions, but can now be done for any combination of spin states to any of the physically allowed overall spin couplings; and (ii) the extension of the NOCI-F method to ensembles with an arbi-

trary number of units, either (overlapping) fragments of a molecule or extended structure, or individual molecules found in molecular crystals or self-assembled stacks in solution. These two improvements have made the NOCI-F implementation in GronOR ready for applications other than singlet fission processes, upon which the original code was entirely focused on.

Another significant development that has contributed to the improvement of the method is the possibility of incorporating the contribution of the core orbitals in the nuclear repulsion energy, that is, the frozen core approximation. This has brought important savings to the NOCI-F calculation without significant loss of precision. The code has also been provided with an alternative for cases where the full NOCI-F calculation becomes prohibitive. The implementation of the Ab Initio Frenkel Davydov Exciton Model allows the user to tackle ensembles with a large number of units. The calculation of the natural transition orbitals in GronOR goes beyond the standard procedure as it can be applied to orbital sets that are non-orthogonal and both the initial and the final states can be of multiconfigurational character.

Among the new features that have been added to the code, we can highlight the calculation of the dipole and quadrupole moments of the many-electron basis functions (diabatic representations of the electronic states) and the final NOCI wave functions (the adiabatic representations). Furthermore, the code now also calculates the transition dipole moments among the different MEBFs and NOCI wave functions

2. **Method development:** The addition of the spin-orbit coupling to the NOCI method follows in general the implementation that was adopted in the state-interaction module of OpenMolcas. This implementation is based on a second quantization formulation while the GronOR code has been developed so far in the more traditional first quantization. This first piece of second quantization code in GronOR can be used as template for further extensions of the NOCI implementations such as a perturbative treatment of the dynamic correlation through a Møller-Plesset-like approach. The interaction between one of the MEBFs and

the one created by a two-electron replacement can be calculated in a very efficient way using the extended Wick's theorem. Although not implemented yet, the theoretical foundations described in this thesis can be used as guideline for future work.

3. **Applications:** The main focus of the thesis has been methodological and the subsequent implementation in GronOR to improve the existing NOCI implementation. Apart from the obvious test calculations to verify the new features (frozen core approximation, spin-orbit coupling, general spin coupling, multi fragment ensembles), the thesis also reports the results of a model study focusing on the relation between exciton delocalization and efficiency of the formation of a singlet coupled double triplet, so-called singlet fission. A careful analysis of different model systems shows that the transition probability calculated for a dimer system is proportional to the transition probability calculated for larger systems with a certain degree of delocalization of the excitonic states over the molecules in the ensemble. Furthermore, we have observed that the singlet coupled double triplet state and the triplet separated states are nearly degenerate and have a sizable interaction. This leads to the situation that the final adiabatic description of the electronic states shows a strong mixing of the two electronic configurations. This implies that the singlet exciton created by photon absorption can evolve into a double triplet state which is already delocalized to a certain extent, facilitating the creation of two separated triplet states. The calculations described in the thesis were performed for relatively simple systems and further studies are required to confirm this observation in more realistic singlet fission chromophores.

4. **Limitations:** The parallel efficiency of the GronOR code is based on the fact that the contributions of all the determinants pairs to a matrix element can be calculated independently. The master nodes distributes the tasks over the available workers by broadcasting messages containing information about the determinant pair that need to be handled by a specific worker. This message and the one sent back by the worker with the result is currently very small as it only con-

tains a few integers and a couple of reals. Hence, communication is not the bottleneck in the parallelization process. This has been strictly maintained in implementation of the new features in GronOR in the scope of this thesis. However, when calculating properties than require transferring matrices of certain size between master and workers (or vice-versa), such as the density operator, the parallel efficiency of the code can be significantly affected, especially on massive parallel machines with ten-thousands of workers controlled by a single master. This has been one of the reasons why the implementation of calculating the density operator for the NOCI wave functions has been abandoned during the thesis.

UNIVERSITAT ROVIRA I VIRGILI
INTERMOLECULAR ENERGY AND ELECTRON TRANSFER BY NON-ORTHOGONAL CONFIGURATION INTERACTION
Aitor Maria Sánchez Mansilla

UNIVERSITAT
ROVIRA i VIRGILI